Chapter Seven: Performance Insights for the Injector Array.

Introduction

Though one primary purpose for the present investigation was to test the performance of several new turbulence models, that was not by any means the only reason for performing such extensive and expensive calculations. The nine-hole injector array is a relatively new configuration and must be thoroughly investigated and understood before any attempt is made to judge its value or eventually to incorporate it into practical applications. While wind-tunnel experiments are underway which will accomplish some of the testing required, there is much that wind-tunnel testing has not revealed or cannot reveal in an efficient manner. It is in such cases, when a thorough and fundamental understanding of all aspects the flow is required, that computational fluid dynamics can be an invaluable aid to the design engineer. Not only can CFD be used to measure basic performance parameters such as peak injectant mass fraction, but it can also provide a detailed analysis of the flow structures, providing insight into the interaction of geometry, injectant, and freestream flow. This detailed analysis is often impossible for the experimentalist to accomplish because of the small scale and complexity of the structures involved, but the insight it provides is vital to the design of new, improved injection schemes. Therefore, an attempt will be made to use the data provided by this investigation to gain a more thorough understanding of the injector array, with emphasis on how and why it works. Such analysis is meaningful despite the poor comparison with experiment because the relevant data is of the nearfield, where the flow has been previously identified as dominated by inviscid effects and calculation is more completely resolved. Error in this portion of the calculation is expected to be minimal.

As discussed in Chapter Two, the design of the injector array was chosen with the hope of creating flow structures similar to those

produced by ramp-type injectors. Of particular interest were streamwise vortices, which are believed to play a vital role in the mixing of injectant with freestream fluid in ramp injectors. For this reason our analysis of the performance of the injector array must begin with one question: Does this injector arrangement truly behave like an "aerodynamic ramp," in that it produces streamwise vortices? Once the answer to this question has been established, more detailed issues can be introduced.

Because a detailed analysis of the various solutions revealed in the previous chapter that turbulence model has little or no effect on the mean flow variables for the nine-hole injector array calculations, only one set of data, that produced by the "mixing" RNG $K-\varepsilon$ model, will be presented in this chapter. This data is expected to be representative of all calculations.

Flow Structures

The flowfield associated with the injector array is complex and very three-dimensional, and there is no simple means of accurately and easily presenting all the relevant data about the flowfield in a consistent manner or in one which will be easily understood. Two-dimensional data presentation can at best tell only a portion of the story at a time, and three-dimensional representations, while occasionally useful for computer visualizations, tend to become crowded and confused in hard copy. The approach used in the discussion below is to present data in a series of two-dimensional planes in each logical direction, thereby to attempt to convey information about the overall, three-dimensional flowfield. The primary variables examined are velocity streamtraces, helium mass-fraction contours, and pressure contours, but others are used as necessary to clarify important issues and flow features.

X-Y Planes

Figure 7.1 shows pressure and helium mass fraction contours along z = constant planes in the region of the injectors. Once again

z=0 corresponds to the centerplane, the horizontal (streamwise) point labeled zero corresponds to the center of the first (most upstream) row of injectors, and the freestream flow travels from left to right. Shaded contours outlined in white represent pressure and black lines represent helium mass fraction contours. Figure 7.2 shows the same planes, but with helium mass fraction contours and velocity stream-

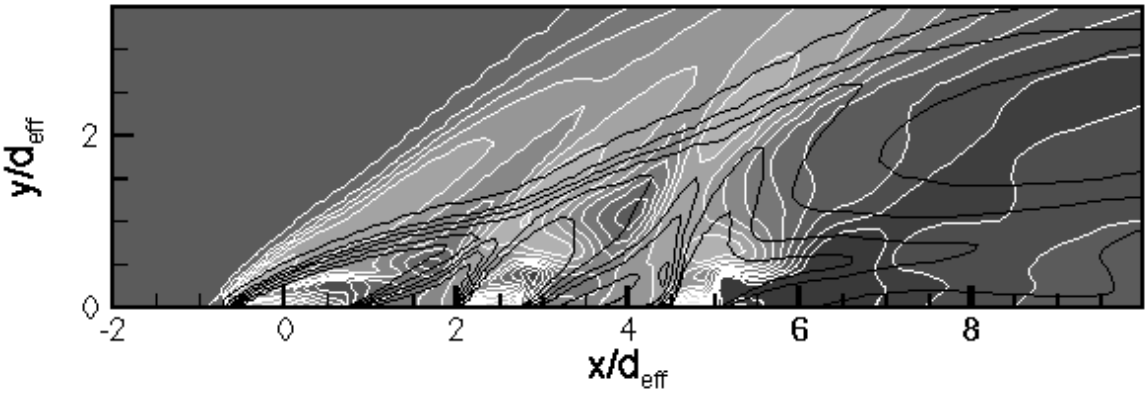

(a) $z/d_{eff} = 0.0$ (Centerplane)

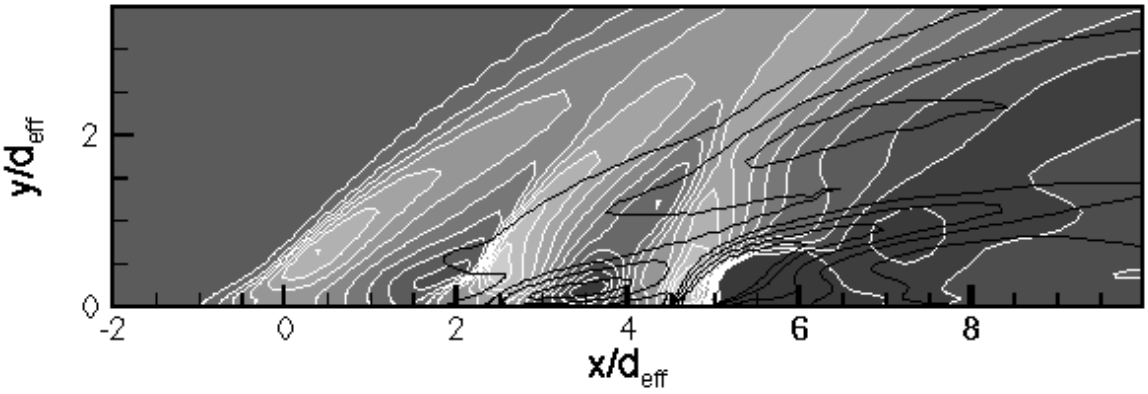

(b) $z/d_{eff} = 0.5$

Figure 7.1. Pressure Contours (shaded with white outlines) with Helium Mass-Fraction Contours (black lines) on Four X-Y Planes for the Nine-Hole Injector Array.

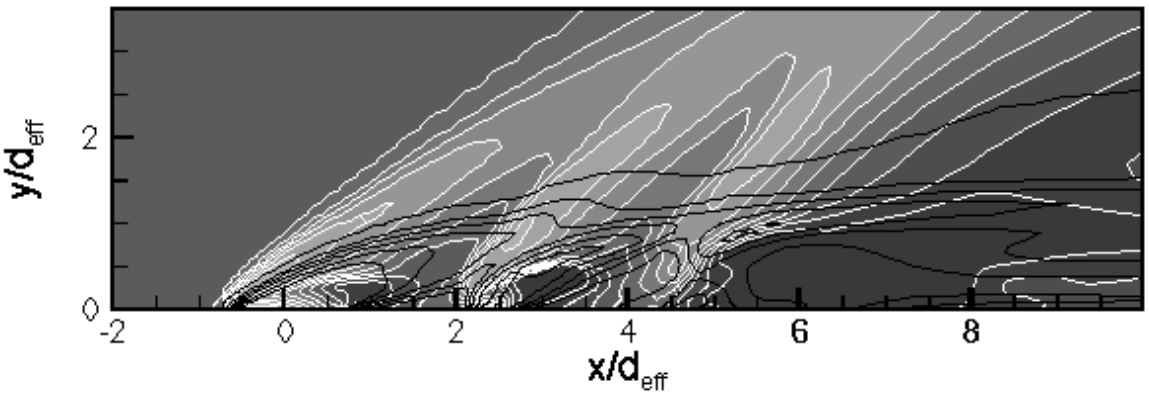

(c) $z/d_{eff} = 1.0$

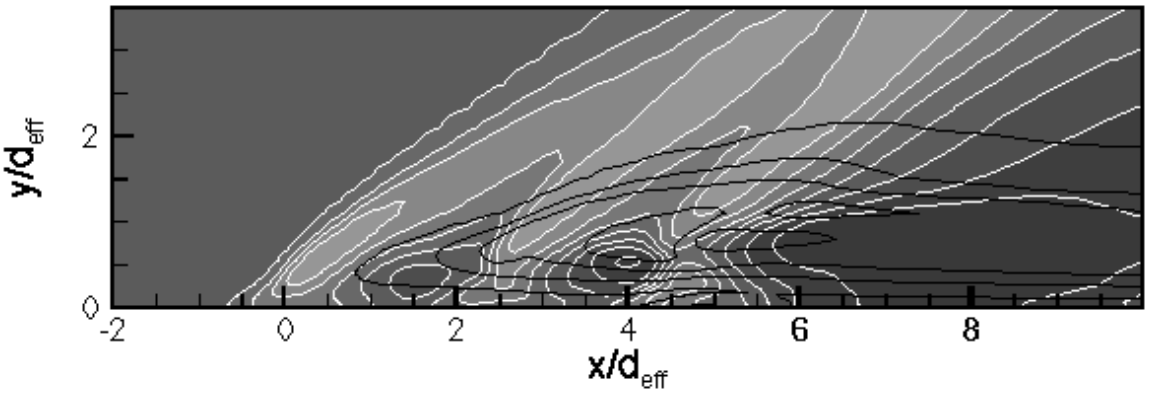

(d) $z/d_{eff} = 1.5$

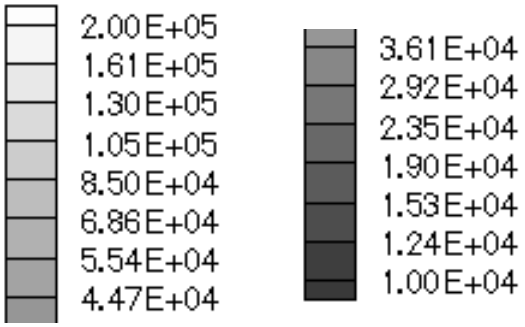

(e) Pressure in Pascals

Figure 7.1 (Continued). Pressure Contours (shaded with white outlines) with Helium Mass-Fraction Contours (black lines) on Four X-Y Planes for the Nine-Hole Injector Array.

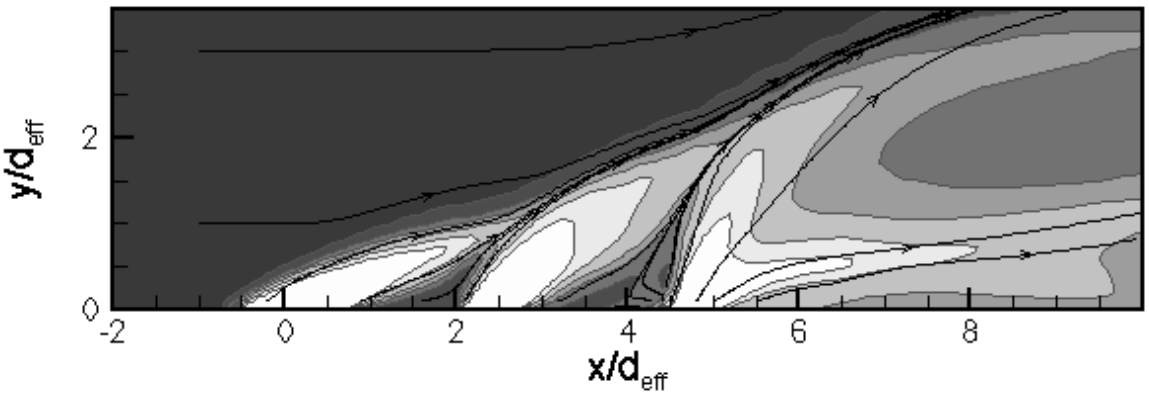

(a) $z/d_{eff} = 0.0$

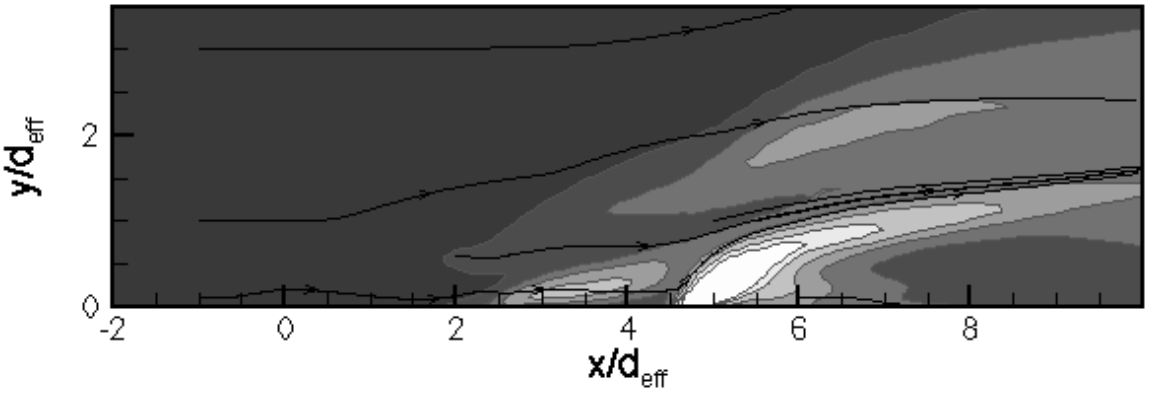

(b) $z/d_{eff} = 0.5$

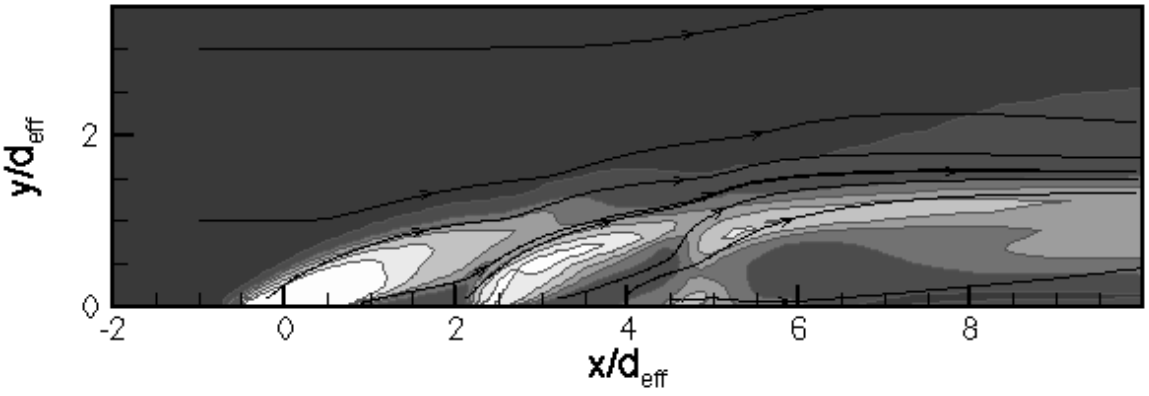

(c) $z/d_{eff} = 1.0$

Figure 7.2. Helium Mass-Fraction Contours with Streamtraces on Four X-Y Planes for the Nine-Hole Injector Array.

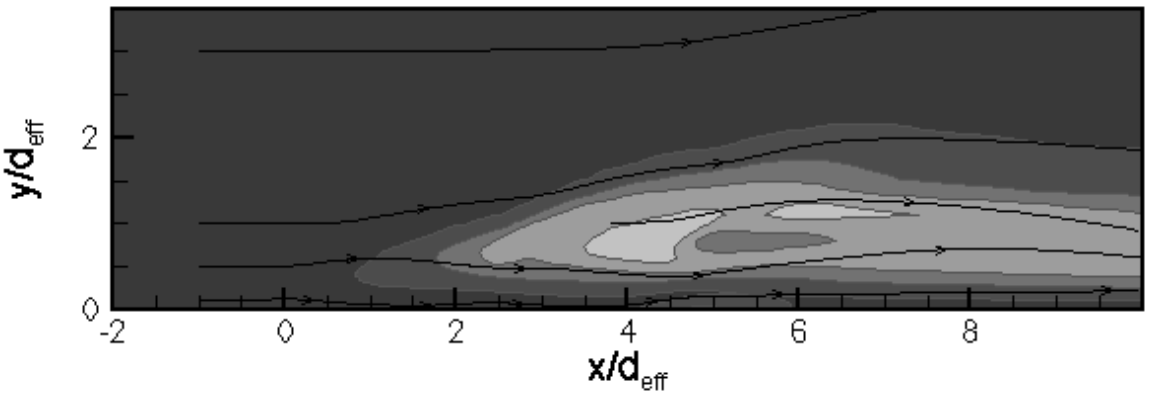

(d) $z/d_{eff} = 1.5$

(e) Helium Mass Fraction

Figure 7.2 (Continued). Helium Mass-Fraction Contours with Streamtraces on Four X-Y Planes for the Nine-Hole Injector Array.

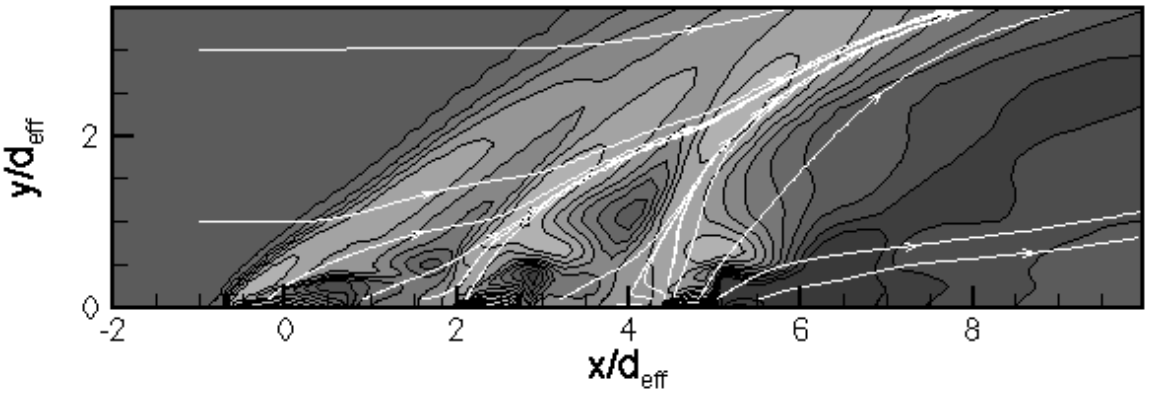

(a) $z/d_{eff} = 0.0$

Figure 7.3. Pressure Contours with Streamtraces on Four X-Y Planes for the Nine-Hole Injector Array.

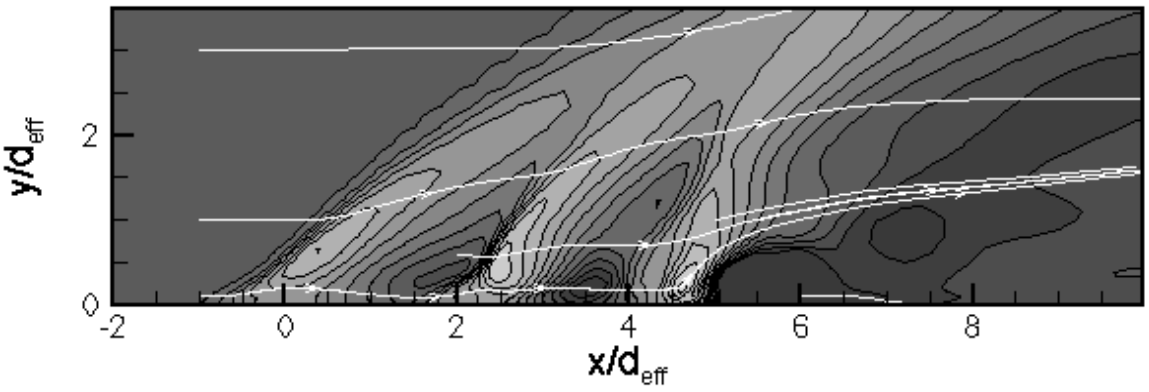

(b) $z/d_{eff} = 0.5$

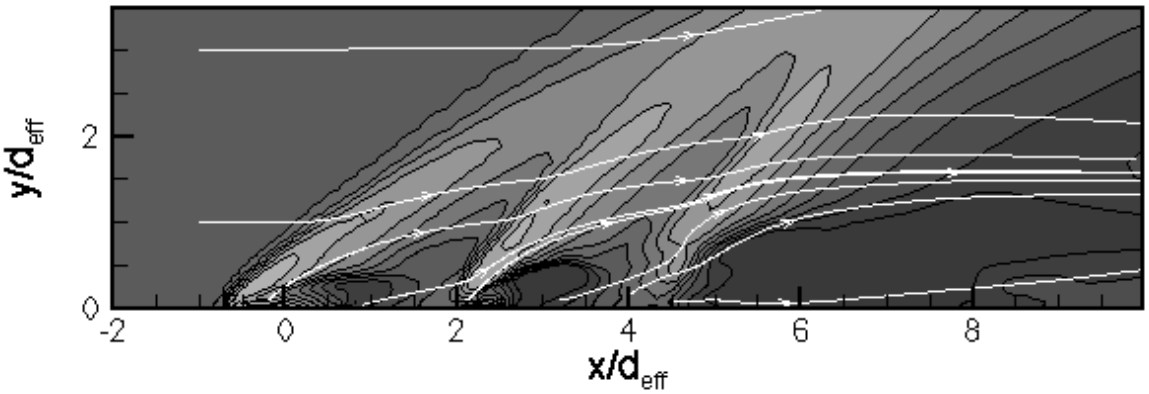

(c) $z/d_{eff} = 1.0$

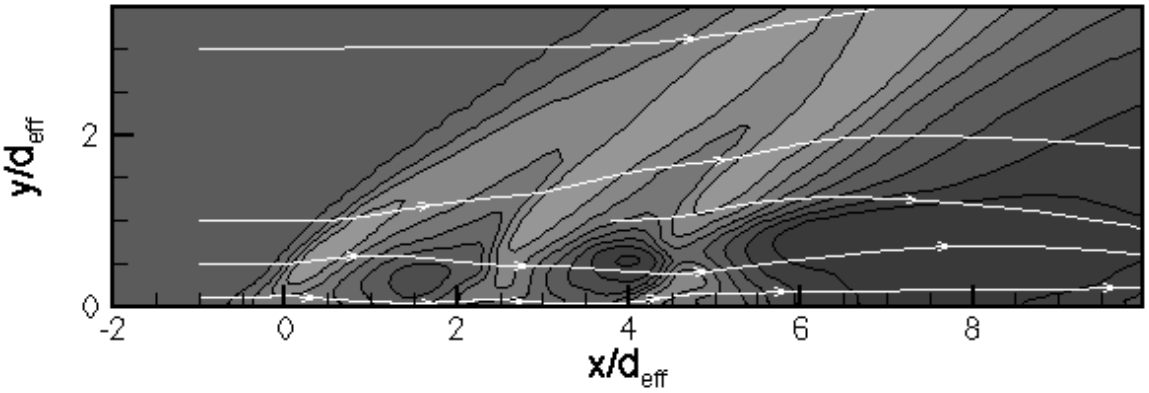

(d) $z/d_{eff} = 1.5$

Figure 7.3 (Continued). Pressure Contours with Streamtraces on Four X-Y Planes for the Nine-Hole Injector Array.

traces instead of pressure. Figure 7.3 completes the set with pressure contours and velocity streamtraces at the same locations. Contour levels for each variable are consistent from figure to figure throughout this chapter.

The analysis will begin with the figures labeled 7.1(a), 7.2(a), and 7.3(a), which present data from the centerplane of the injectors themselves. The first, most noticeable flow feature in all three figures is the bow shock that forms at the leading edge of the first (most upstream) row of injectors. In Figure 7.1 the shock is identified by the steep pressure gradient, and in Figure 7.2 it is most noticeable in the sudden and significant change in the direction of the streamtraces upstream of the mass-fraction contours that mark the edge of the injectant plume. Figure 7.3 combines the pressure and velocity fields, and in that figure one can see that the changes in the two variables are coincident. Artificial dissipation present in numerical schemes tends to broaden and smear the crisp lines of shocks, and to some extent this solution is no exception. Nonetheless, the shock is fairly well resolved, considering the resource limitations inherent in the solution.

Just below and downstream of the bow shock is the first centerline injector. Centered at the point labeled zero, its upstream edge is at $-0.644d_{eff}$ and its downstream edge is at $0.644d_{eff}$. Figure 7.2 shows streamtraces within the injector region, along with the mass-fraction contours that outline the helium plume. The vertical angle of the injector is fifteen degrees, though the plume itself rises somewhat more steeply into the crossflow as the high-pressure injectant helium expands. The vertical expansion of the upper edge of the injectant plume is a bit more constrained than the downstream end, owing to the presence of the bow shock and its high pressure system above. Figure 7.1 shows that near the upstream end of the injector pressures remain relatively high as the bow shock and injector intersect. Downstream there is a wedge of low-pressure fluid between the high pressure coming from the injector itself and the high-pressure fluid immediately behind the bow shock, with the

two areas of high pressure meeting at the upstream point of the wedge and decreasing pressure toward a well-formed low-pressure base downstream. Figure 7.1 shows this area of expansion is well within the purest part of the helium plume, and Figure 7.3 shows that the streamtraces bend inward slightly in the vicinity of the low pressure, as one would expect. Notice that the lowest pressures extend downstream of the injector itself and occur well above the lower wall in roughly triangular contours.

The best explanation of this low-pressure region is that the injectant path represents a real (i.e., viscous, multi-species) flow equivalent of the familiar diamond-shaped shock-expansion pattern of an underexpanded jet, although into crossflow instead of still air. Recall that with this pattern there are a series of overexpansions and recompressions of the injectant plume as it comes into pressure equilibrium with its surroundings. It is proposed that the low-pressure wedge or diamond seen here is the first such overexpansion associated with the first-row centerline injectant jet. In a real flow such as this one the pattern of expansion and recompression will be quickly damped out, especially when represented by a minimally-resolved simulation, but examination of the rest of the injectant plume might reveal a recompression region and perhaps a second overexpansion.

Analysis of the equivalent low-pressure area in Figure 7.2 reveals that the streamtraces at the upper/upstream and lower/downstream edges of the injectant plume run almost parallel to the plume itself, indicating very little diffusion of air into or of helium out of the plume at this point. This conclusion, however, applies only to the present analysis plane. Spanwise diffusion cannot be determined from this figure.

Figure 7.2 shows most clearly the path of the helium as it leaves the high-pressure area associated with the injector. The mass-fraction contours and the streamtraces both level off somewhat and continue downstream with a more modest angle of climb than they showed nearer the leading edge. The co-plotting of mass

fraction and pressure in Figure 7.1 indicates at this point that the helium plume ceases to follow the bow shock and curves instead through the lower pressure region behind it. On the underside of the plume the wedge of low pressure ends only a fraction of an effective diameter downstream of the injector itself, beyond which is a triangular area of slowly increasing pressure and relatively low helium concentration ahead of the second-row injector (Figures 7.1 and 7.3). Figure 7.2 shows that streamtraces in this triangular region are rather horizontal near the wall, but as they rise develop a vertical angle larger than that of the helium mass fraction contours, indicating increased penetration of air into the helium plume, especially as the first-row plume approaches the second-row injector. As a result the inner mass-fraction contours becomes narrower and disappear completely upstream of the second-row injector. This decreasing helium mass fraction at the center of the plume without significant spreading of its outer bounds suggests expansion in the third (out of plane) dimension, a point that will be investigated with cross-flow plots below.

The upper, upstream border of the wedge of low pressure is marked by a narrow, horizontal triangle of sharply higher pressure that extends downstream from the bow-shock high pressure region and appears to be evidence of a recompression or perhaps a weak shock. While this feature is somewhat puzzling, it appears that the low-pressure wedge is actually overexpanded as discussed above and that the recompression or shock is necessary to bring the flow into equilibrium (or closer to equilibrium) with its surroundings, following the diamond shock-expansion pattern. Slightly above and downstream from the recompression region is another area of relatively low pressure, not as neatly shaped as the first but nonetheless enough to suggest that the diamond-shaped expansion/recompression process continues to this point. This second expansion region connects to the outer contours of the first, forming something of a low-pressure wake between the first and second rows of centerline injectors.

The second injector has its center $2.33d_{eff}$ downstream of the origin in the figures and its ends 0.33 d_{eff} upstream and downstream from that point. The presence of the second injector is clearly evident in the pressure, velocity (streamtrace), and helium mass fraction fields in all three figures. Figure 7.2 shows the mass-fraction contour that outlines the fresh injectant plume, along with the streamtraces in the vicinity of the injector itself. Figure 7.3 shows the pressure gradient above the mouth of the injector, along with the small, diffuse band of high pressure at the leading edge. That this high-pressure band cannot properly be called a shock is clear from Figure 7.4, which shows the Mach number in the wake region ahead of the second-row centerline injector to be quite subsonic.

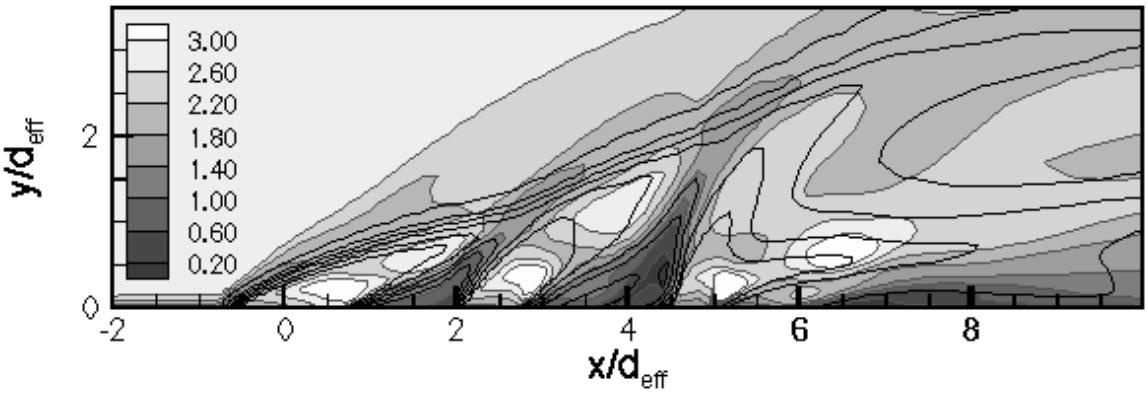

Figure 7.4. Mach Number Contours (Shaded) with Helium Mass-Fraction Contours (Black Lines) Along the Plane at z = 0 (Centerplane) for the Nine-Hole Injector Array.

The plume (as outlined by the helium mass-fraction contours in Figures 7.1, 7.2 and 7.4) passes through this bow shock and rises rather steeply, with very little diffusion or expansion into the low-helium region upstream. The innermost contours are approximately constant in width until they intersect the contours from the previous injector approximately one effective diameter above the lower wall, at which point the vertical component of the velocity decreases and

the plume (and its streamtraces) angle more toward the horizontal. Within this region of constant width is a wedge of low pressure downstream of the leading edge pressure increase and above the high pressure of the injector itself. This low pressure zone extends more than a half of an effective diameter above the surface and almost as far downstream of the injector. At the upper/downstream edge of the low pressure zone is a sharp pressure gradient, leading to a small arm of high pressure diagonally above the low pressure area. The likely explanation is again an overexpansion of the helium in the low pressure region, followed by a recompression. Diagonally above the recompression high-pressure spot is large region of gradually decreasing pressure, perhaps caused by yet another expansion. The theory of expansion and recompression is supported by Figure 7.4, which shows rather high Mach numbers (in excess of the freestream) in the supposed expansion regions and lower Mach numbers where recompression is believed to occur.

Upstream of the low-pressure region, beginning at the point of intersection of the helium mass-fraction contours from the first- and second-row injectors and continuing downstream roughly along the line of intersection between the combined injector plume and the overflowing air, is another, larger band of high pressure. This high pressure is probably created by the lose of vertical velocity (i.e., flow turning) produced by interaction of the second-row plume with the more horizontal flow of the first-row plume and of the air above. (Notice in Figure 7.4 that the flow is supersonic at this height, so shocks are possible.) An alternative explanation is that this may be one last recompression of the first-row injector plume. Supporting such a theory is the fact that this high-pressure region lies approximately in line with the expansion and compression regions previously identified. Supporting the flow-turning theory are the facts that the elevated pressure does coincide with the point of interaction of three separate fluid streams, the primary helium streams from the first- and second-row injectors and the low-velocity, low-helium wake flow between them, and that flow turning

does occur at that location. It is possible that both factors contribute to the pressure field at this location. Additionally, the upper/downstream reaches of these high pressure contours connect with those of the bow shock that formed at the leading edge of the first row of injectors.

Figure 7.2 shows that the streamtraces in flow turning/recompression area are nearly parallel to the upper mass-fraction contours, suggesting a slow rate of diffusion of helium into the air above. Evidence of slow diffusion does not particularly support either theory, however, since movement of low-pressure fluid into a region of higher pressure is expected to be slow no matter what the cause of the pressure fields.

The region of low pressure within the center of the plume (the second expansion region) follows the main channel of the plume diagonally upward from the small spot of high pressure (recompression). The lower helium mass-fraction contours expand somewhat near that spot of high pressure (Figure 7.1), then the innermost contract as out-of-plane mixing appears to accelerate (Figure 7.2). Beneath the primary helium plume is another wake, downstream of the second row of injectors and upstream of the third. The streamtraces in Figures 7.2 and 7.3 clearly show reversed flow in this region, a consequence of a mild adverse pressure gradient. The helium mass fraction is lower here than in the plumes themselves, but as Figures 7.2 shows, the helium mass fraction in a wide path through the wake is greater than 0.25. Because the flow is reversed in the high-helium region, the helium present must originate with the third row of injectors, not the first or second. One interesting feature of this reversed-flow path is the small spot of nearly pure air located downstream and above the reversed flow. The key to understanding this phenomenon is the pressure field. Though the pressure is relatively constant along vertical lines through the wake, downstream of the wake the pressure is considerably higher near the wall. As a result the reversed flow begins along the wall, carrying high concentrations of helium

upstream from the third-row injector. Some distance upstream, near the streamwise position labeled $x/d_{eff}=4$, the reversed flow encounters streamwise flow and turns upward, carrying its helium away from the wall toward the primary helium plume. Downstream of this upward movement is a small pocket of purer air relatively unaffected by the wall-level pressure gradients. The existence of an isolated pocket of nearly pure air in the center of a helium plume again suggests out-of-plane movement of fluid, which will be investigated in later figures.

The third centerline injector is a bit more difficult to identify, in part because of its shorter length and in part because the flow downstream of the injector blends with it in streamtrace and helium mass fraction plots. This injector is perhaps most clearly revealed in the pressure contours of Figure 7.1, where the steep pressure gradients above and just downstream of the injector form an identifiable pattern. The injector itself has its center $4.66d_{eff}$ downstream of the origin and is $0.47d_{eff}$ long. Figure 7.3 identifies the velocity streamtraces associated with the injector and its high-pressure region. This injector has an angle of forty-five degrees, but as the flow leaves the injector and expands it is drawn sharply upward. The plotted streamtraces within the injector itself retain at least a vestige of their downstream angle (see Figure 7.2.), but the streamtraces just ahead of the injector itself are reversed, i.e., facing upstream. As mentioned above, the presence of reversed flow and significant helium concentrations throughout much of the low-helium region ahead of the injector suggest that helium is being drawn from this third injector upstream. Figure 7.3 shows that the pressure structure at the leading edge of this third injector is even weaker and less clearly defined than that of the previous injector, the result of very low Mach numbers upstream (See Figure 7.4.).

Above the high pressure at the injector exit but mostly separate from it is a large, curved bubble of high pressure, which may be evidence of correction for overexpansion, as discussed concerning the previous injectors. The high-pressure bubble's

steepest gradient is on the lower, downstream side, where it gives way to a low-pressure wake region behind the injector. Helium flows almost directly upward from the center of the injector, through the moderate upstream extension of the low-pressure area, and into the front part of this high-pressure region, then continues through it with a strong vertical velocity. Figure 7.3 shows that fluid enters the downstream end of the high-pressure region at a lower angle and disperses widely, traveling downstream as well as vertically.

Figure 7.4 sheds further light on this third-row injector's pressure system. Above and downstream from the injector, a region of high Mach number (M>3) coincides with the upstream portions of the large low-pressure system, suggesting an expansion. Above the high Mach number region is an area of more moderate Mach number, which roughly coincides with the high-pressure region identified as a recompression above. This figure supports that conclusion. Perhaps the most puzzling feature of the Mach number data is the splitting of the next high-Mach number area into two large forks separated by an area of lower Mach number. While a number of explanations might be possible, one should notice that the splitting of the Mach field is matched by a similar splitting of the helium mass fraction field, and any explanation must involve both variables. Such an explanation will be sought in the following analysis.

Figure 7.1 shows that a good deal of the helium misses the high-pressure (presumed recompression) region entirely, creating instead the high helium concentration downstream of the injector in the low-pressure region. Compared to the low-pressure areas behind the other injectors, this one is much more extensive in the streamwise and vertical directions, and aside from the high-pressure bubble dominates the flow downstream of the last injector. It is also unique in that the helium mass fraction remains uniformly high (c_{He}=0.45 or higher) throughout the region and in that the Mach number in the low-pressure region is quite high (Figure 7.4). These three unique features are almost certainly related to each other and to the absence of another injector downstream. With the first two

injectors the next injector downstream served as an obstacle to free movement of the interplume fluid, trapping much of the air between the injectors. The inflow of helium without a sufficient exit path for the air raised the pressure and inhibited travel of additional helium into the region. Downstream of this last injector there are very few obstacles to free movement of the air or helium. There is no downstream obstacle at all, and the higher injection angle means that the high-pressure main helium plume itself is expected to be more removed from the low-pressure region. As the helium moves into the low-pressure region and mixes with the air already present the mixture simply moves downstream. Notice that there is an adverse pressure gradient in this downstream region, which produces a small region of lower helium concentration along the bottom wall between six and eight effective diameters downstream from the origin (Figure 7.1). Though streamtraces in the present figures do not indicate reversed flow in the vicinity of this adverse pressure gradient, the possibility does exist and will be examined in later figures.

Returning to the study of the primary plume, Figures 7.2 and 7.3 show that the flow associated with the leading edge of the plume remains almost vertical until it intersects the primary plume from the previous injectors at a height roughly two effective diameters above the surface. At that point Figures 7.2 and 7.3 show an abrupt turning of the flow, resulting in a more horizontal path and a region of higher pressure at or just above the intersection point. This region of higher pressure is similar to but vertically higher than the one associated with the second injector. Like the other, it could be a result of flow turning, a second recompression, or a combination of the two. Shortly after the inner helium mass-fraction contours of the upstream and third-row plumes merge and turn they cease to exist, with the core of high concentration rapidly decaying, at least in this plane. In its place is a broad area of more thoroughly mixed fluid, which reaches down to the wake-region helium plume and up toward the mainstream. The pressure contours that are the remnants of the first injector's shock structure continue to rise ahead

of the plume into the freestream flow, blended as they now are with the high-pressure structures associated with the intersection and turning of each of the centerline injectors. Downstream of the remnant shock is a gentle favorable pressure gradient as the low-pressure wake grows higher and the pressure dissipates.

The group of figures labeled “b” in Figures 7.1 through 7.3 are similar to those just examined, except that they represent a streamwise, vertical plane half an effective diameter outward from the centerline. (Half an effective diameter places the plane halfway between the centerline and outer injectors in the first row, but the second and third-row outer injectors are more closely spaced.) The values of the contours are the same as those used in previous plots.

Many of the features visible in the present figures are recognizable extensions of the centerline features. Beginning with the leftmost (upstream) edge of the features, one notices the leading-edge bow shock. Notice in Figure 7.1 and 7.3 (parts b) that the well-formed part of the shock is lifted almost half an effective diameter above the lower wall. Because there is no injector in this plane, the shock exists only as a three-dimensional extension of the bow shocks from the centerline and outer injectors in this row. Near the lower wall, Mach numbers are low and the shock is weaker or nonexistent, resulting in a smaller pressure rise and a poorly defined shock. Higher above the wall the Mach number is higher and the shock very well-defined.

Notice also in Figure 7.3 that the flow nearest the wall has almost no vertical component of its velocity, as one would expect given the weak, poorly defined shock at this level. Careful examination reveals a tiny area of reversed flow very close to the lower wall roughly half an effective diameter upstream of the origin of the streamwise axis. This feature, also, is not unexpected given the very high-pressure injectant helium, and simply represents a slight upstream propagation of the effects of its expansion. The coincidence of the area of reversed flow with the first significant levels of helium (seen in Figure 6.7) supports this explanation.

Though very thin, this region of reversed flow does provide an opportunity for information about the shock and its pressure rise to propagate upstream, allowing a gradual adjustment of flow angle and further preventing the shock from completely forming at this level. Alternatively, it is possible that the upstream propagation of information about the shock through the subsonic portion of the boundary layer is primarily responsible for the reversed flow. Reattachment occurs roughly at the center of the first row of injectors (marked zero in the figures). The consequences of this flow reversal and reattachment on wall properties such as heat transfer and skin friction remain to be seen and will be investigated later.

Further from the lower wall the streamtraces develop a more clearly defined vertical component, as is typical of flow passing through an oblique shock. Downstream of the high-pressure shock region the velocity quickly returns to the horizontal, however, as it enters the large, low-pressure wake region that fills the space ahead of the second row of injectors. At the upstream edge of the wake, the streamtraces near the lower wall actually develop a faint downward angle, turning into the region of lowest pressure. See Figure 7.3(b).

The helium concentration throughout this region is very low, with the c_{He}=0.05 contour being the only plotted helium contour that passes through the region at all ahead of the second row of injectors. That contour begins at the wall roughly half an effective diameter upstream from the center of the second-row injectors and climbs only gradually until it interacts with the second-row plume.

The second-row shock structure in Figure 7.1 is much like the shock seen at the first row of injectors, except that the shock is stronger and more clearly defined than either the first-row shock in this plane or the second-row shock on the centerline (seen in Figure 7.1(a)). The explanation for the stronger shock here, half an effective diameter from the centerline, lies with the outer injector in this row. The outer injector in the second row lies only five-sixths of an effective diameter from the centerline, i.e., it is displaced centerward

from the outer injector in the first row by half its own diameter. Due to the displacement, the second-row outer injector will not be sheltered by the injector upstream the way that the second-row centerline injector is, and the bow shock associated with it should be stronger, particularly on the centerward side. This second-row shock will also appear stronger in the present figures than does the first-row shock, because the plotted plane (z/d_{eff}=0.5) is closer to the outer injector (and its shock) than it was to the first-row outer injector, and because the closer spacing allows stronger interaction between the centerline and outer injectors.

One should remember also that the outer injector in the second row is angled centerward by fifteen degrees, so that its upstream end is further from the centerline than its downstream end and the helium injected through it has a fifteen-degree centerward angle. This angle should have consequences on the flowfield, and an attempt will be made to identify features in the present figures that represent the effect.

Figure 7.3 shows that the second-row shock is raised above the lower wall much as the first-row shock was, and undoubtedly for the same reasons. Though this shock is stronger, its associated high pressure region is smaller than the first-row shock and the pressure is lower very near the lower wall. The upstream extension of the high-pressure band along with an apparent weakening of the pressure field suggests the presence of subsonic or even reversed flow, a theory which must be investigated below.

The second-row shock structure itself is sharply vertical, having an angle considerably higher than the second-row injectors' own vertical angle of thirty degrees, as Figures 7.1 and 7.3 show. The velocity field, however, is all but unaffected by the presence of the shock, and the streamtraces in Figure 7.3 continue almost horizontally through it, especially less than two effective diameters above the lower wall. Not far above that point the flow begins to be affected more strongly by the first-row shock and the second-row pressure contours begin to curve downward to match the angle of

the first-row shock. In this region the streamtraces ahead of, within, and behind the shock do have a definite vertical component, though the change in the direction of the streamtraces due to the second-row shock is small. Just downstream of the narrow band of high pressure that follows the shock, the streamtraces return to a more horizontal path, drawn toward the large, low-pressure wake that reaches nearly two effective diameters from the lower wall. Near the lower wall itself, the streamtraces at the upstream edge of the wake develop a downward component, drawn to the lower pressures beneath the shock-induced pressure bands as they were in the previous wake.

Helium mass-fractions first become significant between the first and second rows of injectors, at least near the wall. As briefly mentioned above, the c_{He}=0.05 contour appears along the lower wall roughly two effective diameters downstream of the streamwise origin, several tenths of an effective diameter upstream of the upstream edges of the second-row injectors. Roughly half an effective diameter downstream, coincident with the location of the second-row injectors, the helium concentration begins to show marked increase, with a series of flat, concentric, nearly horizontal contours that extends downstream almost to the third-row helium plume. The origin of this helium cannot be exactly determined by this figure. The absence of a wall-bounded shock suggests that the flow is at least subsonic and possibly reversed at the upstream end of these contours, introducing the possibility that even ahead of the second-row injectors the helium could have its origin with one of the second-row plumes, and the shorter distance from the plotted plane to the outer injector lends credence to the theory that the outer injector is probably the source. The theory will be tested by examination of additional figures below.

The above-mentioned c_{He}=0.05 contour rises gradually above the lower wall for a little more than half an effective diameter of streamwise length, reaching a maximum height of approximately four tenths of an effective diameter, at which point it intersects

another, larger band of helium overlying it. This second band of helium mixture likely has its origin with a different injector than the first (for example, with the first-row centerline injector instead of the first-row outer injector.) It begins at approximately the same streamwise location as the first, but roughly one-half an effective diameter above the lower wall. This larger c_{He}=0.05 contour begins as a fairly narrow, rounded point and grows wider downstream. Figure 7.2 shows that the top and bottom surfaces of the contour away from the upstream edge run roughly tangential to the plotted streamtraces in the area. The bottom of the contour is almost horizontal, and the top of the contour has an upward angle between thirty and forty-five degrees. As the helium field widens downstream, the helium mass fraction increases, reaching 0.45 or higher at heights greater than two effective diameters downstream of the third-row injectors. This large helium mass, well-removed from the surface, is almost certainly the result of outward expansion of one of the first-row helium plumes. Additional plots will be necessary to determine to which plume the helium belongs, but note should be taken of the decreasing helium mass-fraction without vertical spreading of the first-row centerline plume just ahead of the second row of injectors (mentioned above in connection with Figures 7.1(a) and 7.2(a)). The logical conclusion, also mentioned above, is that the centerline plume expands horizontally at that point, and therefore that it could easily produce the contours seen in parts (b) of Figures 7.1 and 7.2. However, no information has yet been presented concerning the first-row outer helium plume, so no conclusions should yet be drawn. The coincidence of the outermost contour in Figure 7.2 with the second-row shock is probably not significant, since a contour of c_{He}=0.10 or c_{He}=0.15 would not coincide with the shock yet would be equally valid as an indicator of increasing helium concentration.

The center of the outer injector in the third row is only two-thirds of an effective diameter from the centerline, it is one third of an effective diameter wide, and it is angled centerward by thirty degrees. Given that the present series of figures present data one

half an effective diameter from the centerline, one expects the figures to capture the centerward portions of this third-row outer injector itself, especially near the downstream edge. In Figure 7.2 the innermost contours and telltale streamtraces reveal exactly that. A full range of helium mass-fraction contours (with contoured values as high as 0.95) outline the primary injector plume, which includes not only the flow directly above the injector itself but also a region roughly an effective diameter long downstream of the injector. Though the streamtraces at the front of the injector have a very large vertical component, they quickly level off, so that the upper edge of the innermost contours rise only one and a half effective diameters by the downstream edge of the figure (ten effective diameters downstream of the streamwise origin, and more than three effective diameters downstream from the center of the third-row injector). The outer contours on the upper side of this helium plume blend with those of the large, upper helium band discussed previously. The lower edge of the contour rises sharply from the wall approximately six effective diameters downstream of the streamwise origin (a little more than one effective diameter downstream of the end of the injector), then turns and becomes nearly parallel to the upper edge of the contour. Notice that this portion of the outer injector lacks the vertical penetration of the centerline, third-row injector, but other portions may not. Notice also that helium concentration within the center of the plume decays rather rapidly with axial distance, but vertical spreading of the outer contours is only moderate, especially in the nearfield. As with the centerplane data, this phenomenon suggests out-of-plane mixing. Further figures will be needed to address both these issues.

The c_{He}=0.25 contour upstream of the third-row, outer injector blends smoothly with those identified and discussed in association with the second-row area, without showing any change in shape or location as a result of the third-row injector. There is a separate bubble of lower helium concentration below and downstream of the third-row injector's helium contours. It begins near x/d_{eff}=7.0 with a

height of roughly three quarters of an effective diameter and widens gradually downstream. It attains a maximum width near $x/d_{eff}=9.0$, beyond which the spreading of the third-row plume increases the concentration of helium in the near-wall region.

The pressure field associated with the third-row, outer injector and its surroundings is quite complex, as Figure 7.1 and 7.3 reveal. There is a sudden increase in pressure just ahead of the injector, as comparison with the helium mass-fraction contours in Figure 7.1 reveals, but the pressure rise is not so sudden as to appear as a fully formed shock. In particular, the presence of strongly elevated pressures a significant (though small) distance upstream of the source of the flow disturbance rules out the possibility of a shock caused by the downstream disturbance. One possible explanation would be the existence of a bow shock at the most upstream part of the third-row outer injector, located further from the centerline than this plane, which could propagate downstream and centerward to elevate pressures in this plane. However, the relatively weak pressure gradient at the upstream edge of this high-pressure region, best seen in Figure 7.3, does not support the theory of a three-dimensional shock. A more likely explanation is that the flow ahead of the injector is subsonic in this plane as it is on the centerline, allowing a more gradual increase in pressure ahead of the injector itself. The sharpest pressure gradient associated with this injector occurs downstream of the injector itself and bends slightly upstream above it before angling back downstream to become nearly horizontal. As it turns toward the horizontal it falls in line with the helium mass-fraction contours that outline the third-row injector in Figure 7.1. There, as all along its length, it separates very high pressures upstream from the low-pressure wake downstream. This structure is very similar to that identified in part (a) as part of the expansion/recompression pattern. Streamtraces in Figure 7.3 show flow near the upstream end of the injector skirting the pressure gradient as it moves upward and downstream, through the high-pressure area (which extends through the injector itself, as seen in

Figure 7.1) and into the lower-pressure region downstream of this last injector. The wall-region streamtrace in Figure 7.2 shows helium leaving that portion of the injector plume through a horizontal extension of the primary injector plume (just above the lower wall, mostly between the 5.5 and 6.5 ticks on the streamwise axis) and remaining quite close to the lower wall. Thus portions of the flow move directly along a high pressure path that follows the upstream/upper edge of the injector, and others pass into the low-pressure region just downstream of the injector, within the plume itself. This region of low pressure within the helium plume could represent an overexpansion, but if a pattern of expansion and recompression exists, it is not as clear here as it was in the centerplane flow. One should remember, however, that this injector and its expansion/recompression pattern are misaligned from the current plane by thirty degrees, and a textbook-perfect pressure field should not be expected in this figure.

Downstream a distance from the purest portion of the third-row wake, near $x/d_{eff}=7$ and a little more than one effective diameter above the lower wall, a contour of low pressure exists in an area of otherwise higher pressure. Though insufficient data exists in this series of figures to explain this pressure contour, it could possibly represent another expansion. Alternatively, the contour of lower pressure could simply the upper portion of the third-row wake, separated from the lower portion by some, as yet unidentified pressure elevation mechanism.

The next plane of data continues the established pattern of streamtraces and helium mass-fraction and pressure contours in a plane parallel to the centerplane. All figures labeled “c” in Figures 7.1 through 7.3 represent data in a plane one effective diameter from the centerplane, which coincides with the center of the first-row, outer injector. Contour levels are consistent with those in other figures. Flow is again from left to right.

One of the features most readily identifiable in the first-row portion of the pressure field in parts (c) of Figures 7.1 and 7.3 is the

degree to which it resembles the corresponding centerplane pressure field in parts (a) of the same figures. This is not at all remarkable, since the injectors themselves are identical, with differences arising only in their spanwise and downstream surroundings. The centerplane injector is surrounded by symmetric pressure and concentration fields caused by symmetric outer injectors, and is followed by a second, centerplane injector directly downstream. The outer injector has no injector at all on its outer side, which dramatically changes the nature of the pressure and concentration fields which influence it. Furthermore, the second-row, outer injector is not directly downstream from the first-row, outer injector, but is displaced and yawed inward, and though the flowfield is primarily supersonic there is nonetheless a slight upstream influence on the first-row, outer injectant plume.

The leading-edge bow shock that forms ahead of the first-row, outer injector is clearly seen in Figures 7.1 and 7.3. It very much resembles its centerplane counterpart, except that the pressures in the shock are somewhat lower, the innermost helium mass-fraction contours are shorter and thicker (more bluntly shaped), and helium concentration in general decays a bit more quickly. The lower pressure is most likely caused by the increased opportunity for expansion present in this outer row, where there is very little to oppose spanwise expansion in the direction away from the centerline. A similar argument applies to helium mass-fraction. As with the centerplane shock, the streamtraces in Figure 7.3 show turning at the first sign of increased pressure, though Figure 7.2 indicates that the helium concentration in this region is relatively low (but rapidly increasing downstream). In this respect the shock is like that created by supersonic flow over a wedge or cone, with the helium plume playing the role of the obstacle.

As with the centerplane plume, the streamtraces in part (c) of Figure 7.2 run nearly parallel to the helium mass-fraction contours, suggesting little diffusion of fluid into or out of the first-row helium plume, at least in the plane of the present figures. Within the plume

itself is the pattern of decreasing pressure downstream along the lower wall, with which the reader is now familiar. Above and downstream of the high-pressure region associated with the injector itself is the region of low pressure expected by expansion/compression analysis. The pressure here is lower over a wider area than the corresponding low-pressure area in the centerplane, probably because the centerward displacement of the second-row, outer injector leaves room for a larger wake and a more unrestrained expansion of the injectant helium. (Notice that the streamtrace that follows the lower/downstream side of the first-row helium plume through the wake has a more horizontal path in part (c) than in part (a), indicating weaker opposition to the streamwise movement of fluid.)

Above the low-pressure expansion region, the diamond-shaped recompression pattern is less clearly defined in the outer row than on the centerline. No definitive explanation is immediately forthcoming, but it is probably related to the overall lower pressures and asymmetric spanwise pressure field associated with this outer injector.

The helium contours for the first-row, outer injector are shown with streamtraces in Figure 7.2. Though virtually identical to the centerplane data in and above the injector region itself (ending approximately six and a half tenths of an effective diameter downstream of the streamwise origin), the helium contours marking the path of the outer injector take quite a different shape in the wake between the first and second rows of injectors. Overall penetration is somewhat lower, and helium concentration in the near-wall region is considerably higher, due to the lower wake pressures downstream of the outer injector. The primary helium plume itself is thicker and more horizontal than the centerplane plume, as indicated by the shape and path of the innermost helium contours. The contours on the lower/downstream side of the plume remain within half an effective diameter of the lower wall until they end or reach the second injector plume, depending upon the value of

the contour in question. The lowest levels of helium mass-fraction occur just above the wall in the region of low-Mach-number flow (See Figure 7.5), where the velocity appears close to stagnation.

The second-row, outer injector shown in Figure 7.1 part (c) appears much the same in the pressure contour plots as the second-row, centerplane injector, though the outer injector is displaced centerward by one sixth of an effective diameter and yawed centerward by fifteen degrees. The pressure field that outlines the injector is well formed, with a pressure rise at the leading edge (which is not exactly a shock because the Mach number is less than one for some distance above the wall ahead of this injector. See Figure 7.5.) and the closely-spaced pressure contours that indicate the rapid expansion of high-pressure helium as it leaves the injector. The pressure outline of the outer injector is somewhat shorter than its centerplane equivalent because the streamwise cross-section of the yawed injector is smaller.

The pressure rise ahead of the second-row, outer injector actually is much better formed and has higher pressures than its centerline equivalent. The reason is the centerward displacement: the second-row, centerline injector lies directly downstream from the first-row, centerline injector and its bow shock and is sheltered by them, but the second-row, outer injector is displaced centerward from the first-row, outer injector and is incompletely sheltered, so that a second-row bow shock might form centerward of the first-row injector and even in the present plane the pressure field is stronger. In addition, the yaw of the second-row, outer injector increases the size of the cross-section around which the shock can form and creates the possibility of a larger shock. The innermost (highest-valued) pressure contour associated with the outer pressure occurs roughly one effective diameter from the lower wall, as seen in Figure 7.3. This feature is probably the result of the intersection of the first-row helium plume with that of the second row, or with the absorption into the primary helium stream of the thin layer of purer air (helium mass fraction less than .65) trapped ahead of the second-

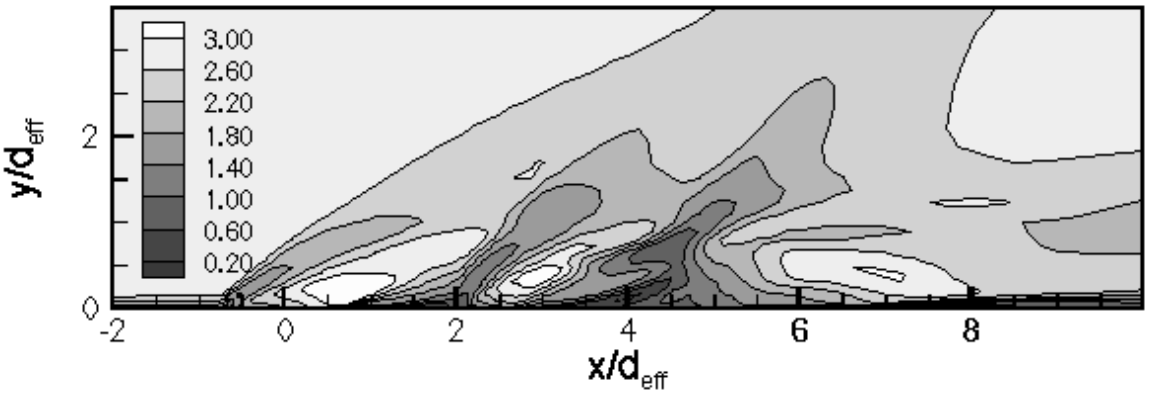

(a) Shaded Mach Contours

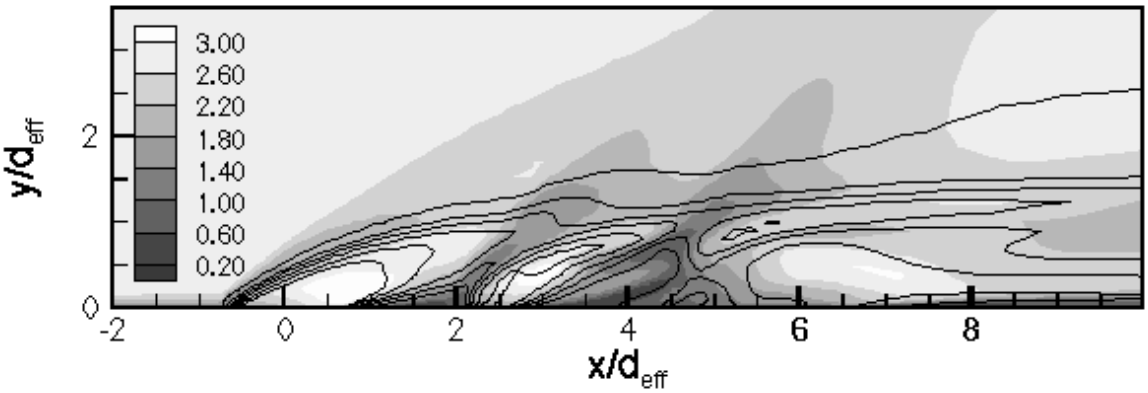

(b) Shaded Mach Contours with Black Helium Mass-Fraction Lines

Figure 7.5. Mach Number Contours Along the Plane at z = 1.0 for the Nine-Hole Injector Array.

row plume. (See Figure 7.1) It is also possible that the second-row bow shock does form on the centerward side of this outer injector, and that it propagates inward and upward to intersect the first-row helium plume.

Downstream of the high pressure region is a roughly diamond-shaped low-pressure contour that marks the first expansion of the injectant helium. As with the low-pressure region downstream of the first outer injector, the pressures are considerably lower than

those on the centerline and the low-pressure region is much larger. Once again this is a consequence of the centerward displacement of the downstream injector, but in this case the centerward yaw of the second-row injector also plays a part. That yaw causes the diamond-shaped expansion/recompression pattern to lie in a plane out of alignment with the current figures, so that first recompression appears weak and poorly formed, and the second expansion blends into the general low-pressure wake downstream of the second-row, outer injector.

The helium mass-fraction contours that outline the second-row, outer injectant plume are radically different from those in the centerplane, as Figure 7.2 shows. Vertical penetration is much lower, with the highest point of the inner contours little more than one effective diameter above the lower wall. The highest penetration of the c_{He}=0.45 contour occurs at the upstream end of the plume at the intersection of the first-row and second-row plumes. (Higher-valued contours do not intersect their first-row equivalents at all, because the latter have ceased to exist in this plane before they reach the second-row injector.) Downstream of that intersection, the upper edge of the c_{He}=0.45 contour is nearly horizontal. This compares to a sharply climbing centerplane contour, which reaches twice as far from the lower wall at x/d_{eff}=4 than does the outer contour. The lower/downstream edge of the second-row, outer c_{He}=0.45 contour rises gradually from the wall just downstream of the first expansion, then turns ever so slightly toward the horizontal near the following recompression. The contour contracts gradually for nearly an effective diameter, then blends into the third-row plume. The point of intersection coincides with a small contour of higher pressure, which may represent the outer remains of the third-row bow shock, since the third-row injector itself is well centerward of this streamwise plane.

The innermost helium mass-fraction contour, c_{He}=0.95, has an interesting shape in this second row. Figure 7.2 shows it to have the shape of a narrow, slanted “figure eight”, or as two elongated

contours that connect at a single point. It is possible that this shape is related to the entrainment of air into the plume, but the streamtraces in Figure 7.2 do not support such an hypothesis. A more likely explanation is some out-of-plane effect, which must be investigated in later figures.

Beneath the helium plume in the low-pressure wake between the second and third rows of injectors, the helium concentration drops rather low. This represents another deviation from the centerplane pattern, where the helium concentration was considerably higher. Streamtraces in this region roughly parallel the helium mass-fraction contours, moving into the plume itself only at the intersection of the second and third-row injectors' plumes. (One streamtrace seems to penetrate directly into the third-row plume itself, a matter which must be studied below.) The Mach number field in this wake is quite complex, as Figure 7.5 shows. The subsonic region is rather extensive, reaching at least an effective diameter above the lower wall to the point of intersection between the second and third-row plumes. Most puzzling is a narrow, diagonal extension of higher-Mach flow into this subsonic region from the vicinity of the second-row injector. This extension of sonic or supersonic flow into the subsonic wake may be the result of some out-of-plane activity, or perhaps two out-of-plane activities, a separate one responsible for each subsonic region. Note should be taken of the low helium mass fractions in the separating, supersonic region, seen in Figure 7.5 part "b". Attention will be directed to this phenomenon in later figures.

Above the innermost helium contours, the c_{He}=0.25 contour reaches a vertical peak roughly $1.5d_{eff}$ above the lower wall and a little more than three effective diameters downstream from the streamwise origin, then drops significantly. One and a half effective diameters downstream from the vertical peak the same contour is only an approximate $1.2d_{eff}$ above the lower wall. The cause of the peak seems to be the interaction of the helium plume from the first outer injector with that from the second. The dropping of the c_{He}=0.25 contour along with the contraction of the inner contours

suggest a strong out-of-plane mixing or translation mechanism. The c_{He}=0.05 contour shows only a slight peak nor drop, and continues to climb very gradually downstream. Streamtraces in the vicinity roughly parallel this outer injector, which path carries them through higher-valued helium contours upstream and into more diffuse parts of the plume, indicating that a significant degree of mixing may be occurring along this path.

As mentioned above, the third-row, outer injector has its center only two-thirds of an effective diameter from the centerline and is not shown in the present series of figures. Its influence is shown, however, through the pressure and helium mass-fraction contours and through the streamtraces.

The pressure influence of the third-row, outer injector in the present plane is relatively weak, as Figures 7.1 and 7.3 indicate. There is one band of elevated pressure just upstream of the main helium plume, but it is far too diffuse and the Mach number far too low to be properly called a shock. Instead it may be the three-dimensional extension of a more centerward bow shock, weakened by interaction with the wake upstream. The very low Mach number in the wake downstream of the second-row injector creates an opportunity for upstream propagation of information about the third-row injector and its shock, lowering wall pressures in the path of the shock and preventing the complete formation of the shock itself. Within the band of elevated pressure and roughly one effective diameter above the lower wall, there is a sudden widening of the pressure band coincident with a slight horizontal turn. It lies very close to the intersection of three separate streams of fluid: the second-row helium plume, the third-row helium plume and the wake flow of purer air. (See Figure 7.1.) At that point the nearly vertical flow of wake fluid meets the two helium plumes and must turn to follow their more horizontal paths, as the streamtraces in Figure 7.2 indicate. The resulting momentum loss may create the region of elevated pressure. The general shape of the outer pressure contour

is consistent with such an explanation, with the sudden widening of the area of elevated pressure very near the intersection.

Downstream of the high-pressure region, the pressure decreases to form a very large wake, which spreads rapidly upward and downstream. There is a relatively large band of very low pressure downstream of the third-row helium plume. The shape of this low-pressure band suggests higher pressures along the lower wall both upstream and downstream of its center, as one might expect, with pressure information propagating through the boundary layer. The presence of higher pressures below the wake but above the lower wall roughly $8.5d_{eff}$ downstream of the origin suggests a different process, however, and will be investigated in later figures.

The helium mass fractions in Figures 7.1 and 7.3 are unique to this plane. There is a distinct band of helium-rich flow that outlines the upper portions of the injectant plume, or at least the outer edge thereof. It does not, however, directly contact the contours of helium along the lower wall. These lower contours reach significant levels (greater than c_{He}=0.45) at the lower wall approximately $4.5d_{eff}$ downstream from the streamwise origin, a location that happens to nearly coincide with the streamwise center of the third-row injector. The outer contour reaches another half an effective diameter upstream, reaching further upstream than the third-row injector itself. The contour lines are concave upward and counterclockwise (bending upstream) for a distance of approximately half an effective diameter, then reverse their curvature and bend downward and downstream, so that the c_{He}=0.45 contour returns to the lower wall near x/d_{eff}=5.25. The outer contour remains just above the lower wall another three-quarters of an effective diameter downstream. Within this wall-bounded helium plume the innermost contour corresponds to c_{He}=0.65.

The c_{He}=0.25 contour of this wall plume extends upward to blend with the upper-level plume associated with the third-row injector. The upper plume is nearly horizontal, beginning roughly half an effective diameter above the lower wall and tapering upward

and downstream. The upper edge rises slightly then becomes increasingly horizontal beyond $x/d_{eff}=6$, and exits the figure (at $x/d_{eff}=10$) less than two effective diameters above the lower wall. The downstream/lower edge of the inner contours follow a very similar pattern, at least in the nearfield. It tapers upward as it moves downstream, narrowing the plume gradually and becoming nearly horizontal by $x/d_{eff}=7$. Near $x/d_{eff}=8.5$ the $c_{He}=0.45$ contour completely changes shape, as a distinct, lower contour appears and merges with the main plume. Clearly this represents an out-of-plane effect that must be studied in later figures.

The unique shape of this third-row plume is more difficult to explain than previous injectant plumes. The presence of helium upstream of the third-row injector in the near-wall region indicates out-of-plane movement of helium, a phenomenon not at all unlikely given the complex three-dimensional nature of the flowfield and the low pressure in the wake upstream of this third injector. The extension of the helium downstream along the wall simply indicates flow into the large, low-pressure wake, as the streamtraces in Figures 7.2 and 7.3 show. The separation of the wall-bounded and upper plumes is more puzzling. Notice the streamtrace in Figure 7.2 that indicates the penetration of nearly-pure air from the wake region upstream into the space between the upper and lower helium contours. Such penetration could result in a decreased helium concentration and a separation of the third-row plume into parts, but a separation of this type has not been identified in association with any other injector plume and the indicated inflow is unlikely to have sufficient momentum to break the plume. Given the fact that the injector itself lies centerward of the present plane, a more plausible explanation is that the upper and lower helium contours visible in this plane are outward extensions of the actual third-row plume, carried outward to this plane by separate and distinct mixing mechanisms. Supporting this theory is the fact that Figure 7.5 shows the wall-bounded helium plume to be in a region of relatively low Mach number, while the upper one is in a region of higher Mach

number. Similarly, the lower plume is part of the low-pressure wake but the upper plume lies at the edge of the high-pressure band that overspreads the wake. This helium pattern will be further investigated in later figures.

For the most part the lowest-concentration helium contours are easier to understand. Above the plume the c_{He}=0.05 contour continues to rise gradually, a smooth continuation of the second-row plume's contour. It exits the figure (at x/d_{eff}=10) approximately two and a half effective diameters from the lower wall. This is much lower than the equivalent for the centerline plume. Beneath the third-row plume, the c_{He}=0.25 contour begins downstream of the wall-bounded plume, as mentioned above, roughly one and a half effective diameters downstream of the c_{He}=0.65 contour as helium travels downstream through the boundary layer, then doubles back along the wall and runs nearly parallel to it before turning upward. This contour connects with the upper plume, curving first toward it then away, and dropping again toward the lower wall. By x/d_{eff}=8 it levels off again, flowing horizontally and without contour change around the second c_{He}=0.45 contour. The rest of the space underneath the third-row plume is filled with fluid of c_{He}=0.05 or higher, except for a very narrow, nearly horizontal band that begins on the wall near x/d_{eff}=7 and ends only a small fraction of an effective diameter above it near x/d_{eff}=10. The band of lower helium concentration must indicate a change in the source of the wall-region helium. Upstream of the break, it seems to flow downstream from the wall-bounded plume. Downstream, the adverse pressure gradient visible in Figures 7.1 and 7.3 could be responsible for a thin layer of reversed flow along the wall. Alternatively, there could be simply one more out-of-plane phenomenon to investigate in later figures.

The plots labeled “d” in Figures 7.1 through 7.3 show data in a k=constant one and a half effective diameters from the centerline. This distance is half again further from the centerline than the center of any outer-column injector, and experiences the effects of the

injectors only through the three-dimensional propagation of information and injectant.

Parts “d” of Figures 7.1 and 7.3 show that the bow shock at the leading edge of the first-row outer injector does extend outward to this location, though significant concentrations of helium are identified only well downstream of the shock and lower pressures with a more gradual increase near the lower wall suggest the shock itself may be lifted above the wall somewhat, as was the case in the channel between the centerplane and outer rows of injectors (seen in parts “b” of Figures 7.1 and 7.3). Pressures just behind the shock are somewhat lower than those in the plane of the injector, but the angle the shock makes with the horizontal is essentially unchanged. Streamtraces in Figure 7.3 are nearly horizontal through the first-row bow shock, with any upward momentum the shock might impart quickly decaying, except near one effective diameter from the lower wall, where higher pressures below do encourage a slight upward turn.

Downstream of the shock is a large wake of moderately low pressure, which extends nearly two effective diameters above the lower wall and pulls streamtraces wallward once more. The downstream end of the wake is lifted off the wall, as the wake appears to “ride above” the pressure field of the second-row injector.

The first evidence of helium penetration to the present plane begins at the downstream edge of the leading-edge bow shock, coincident with the beginning of the wake. Helium concentrations are low, with mass fractions remaining below 0.25 throughout all but a small downstream portion of the large wake region. Moreover, the mass fraction contour corresponding to c_{He}=0.05 remains nearly half an effective diameter above the lower wall and practically parallel to it throughout this region, suggesting virtually no helium is present along the lower wall itself. Because the streamtraces in this region are also practically parallel to the lower wall, little downward diffusion of helium is indicated. The upper edge of this outermost helium contour roughly parallels the upper/upstream edge of the

wake, angling upward with a nearly constant rate from its beginning near $x/d_{eff}=1$ through this wake, the next high-pressure pattern, and the wake beyond, by which location it extends nearly two effective diameters above the lower wall. The higher-valued contours which begin near $x/d_{eff}=2$ run nearly parallel to this outer one, especially on the upper edge.

Streamtraces in the wake region itself flow from regions of nearly-pure air into the helium plume, as Figure 7.2 shows. From the data presented in the current figures this would seem to be a region of signicant mixing, but the planar nature of the data could be deceptive, and confirmation of this mixing must be sought in other figures. Downstream of the wake, traces of particles within the helium plume follow the plume's contours rather closely, at least in this plane.

The pressure rise associated with the second row of injectors is far too diffuse to be considered a shock, though it probably represents the spanwise propagation of shock located closer to the centerline. The high pressure system along the lower wall is quite long, extending nearly an effective diameter downstream from its beginning at the point labeled $x/d_{eff}=2$. Despite this extensive high pressure region the lower streamtraces in Figure 7.3 remain parallel to the lower wall, seeming uninfluenced by the pressure increase. At higher levels, where the pressure gradient is steeper and the flow is more likely to be supersonic, the streamtraces do bend upward abruptly as they pass into higher pressure. Notice that the innermost pressure band is far more extensive in this second-row formation than it was in the first, indicating higher pressures. This is not an intuitive development, since the all the second-row injectors are at least partially sheltered by their first-row equivalents and might be expected to produce weaker shocks.

This second pressure band is nearly vertical for nearly an effective diameter above the lower wall, but then bends downstream and eventually merges with the first-row pressure band. Beneath and downstream is another wake, slightly larger and with lower

pressures than the first and again roughly triangular. Streamtraces drop minutely toward the wall as they enter the low-pressure region, but remain almost perfectly parallel. Helium concentration again increases in this region, with the innermost mass-fraction contour corresponding to c_{He}=0.65. Like the others it is roughly arrow-shaped, coming to a rounded point upstream near x/d_{eff}=3.5 and y/d_{eff}=1, with a lower edge that is nearly flat and an upper edge that rises gradually before it ends in the next region of high pressure. The downstream edge is slightly indented and seems to follow the line of the third-row high pressure band. This second significant increase in helium concentration in wake regions is significant but not unexpected, as the lower pressures create natural opportunities for spanwise expansion.

The pressure and helium patterns associated with the third row of injectors are perhaps even more complicated than in previous planes. The high-pressure field is split into two parts, with a large (nearly two effective diameters long and roughly half an effective diameter high), roughly triangular region along the lower wall and a familiar, elongated band angling downstream from a location just above the wall region. The pressure gradient at the upstream edge of the wall high-pressure region is one of the steepest in this plane, suggesting the possibility of a shock. (A shock is more likely in this spanwise plane, since there is no real obstacle to reduce the Mach number upstream to subsonic levels.) The streamtraces in Figure 7.3, however, are virtually uninfluenced by this wall-bounded high-pressure field. The pressures within the upper band are high and approximately uniform over a long distance. This band rises slightly more steeply than the second-row pressure band, and their respective highest-valued contours merge only above the bounds of the present figure, if at all. Downstream of both parts of the third-row high-pressure field and extending upstream to fill the space between them is a very large wake. In the wake region the streamtraces that rose slightly in the high-pressure fields become horizontal then begin to drop again as they exit the figure.

The outermost mass-fraction contours in Figure 7.2 follow a familiar pattern, remaining virtually parallel to each other and the lower wall on the underside for the length of the figure. There are deviations from the parallel, especially between x/d_{eff}=4 and x/d_{eff}=6, where the c_{He}=0.45 contour rises slightly to avoid the higher pressures near the wall and where a separate, wall-bounded contour of c_{He}=0.05 appears, grows to just connect the equal-valued, overlying band, then shrinks to nothing once more. A similar effect was identified in part "c", one effective diameter from the centerline, and there as here spanwise movement of helium is indicated. Evidence of such movement will be sought in later figures. On the upper side of the helium plume the story is equally familiar. The mass-fraction contours follow the streamtraces upward through the high pressure area, then drop slightly toward the low pressures of the wake. At its highest point the c_{He}=0.05 contour reaches just more than two effective diameters above the lower wall, but it leaves the figure roughly half an effective diameter lower.

It is within the c_{He}=0.45 contour that the helium pattern becomes puzzling. Near the point of separation of the two parts of the third-row pressure field and just downstream of the end of the previously-discussed c_{He}=0.65 contour (near x/d_{eff}=5) is an elongated, almost airfoil-shaped contour of low helium concentration (mass fraction less than 0.45). (See Figure 7.1.) One effective diameter downstream and half an effective diameter higher is another mass-fraction contour of similar size and shape, but Figure 7.2 identifies this one as an area of higher helium mass fraction (c_{He}>0.65). As with the rest of the helium plume in this spanwise plane, it is difficult to determine exactly which injector is the source of this last, high-valued contour. Clearly the phenomenon is three-dimensional and must be investigated with additional figures.

Streamtraces in Figure 7.2 run roughly parallel with the helium contours until the beginning of the last, large wake. In the wake region the streamtraces seem more confluent than the helium contours. One possible explanation is that the helium field could be

undergoing constant replinishment from a centerward source. As with most other theories expounded in this section, additional data from other planes will be necessary to test this explanation.

X-Z Planes

The next series of figures represent y=constant planes (parallel to the lower wall) in the flowfield of the injector array, from which knowledge can be gained about the spanwise variation of the flow. In each figure the computed data is mirrored about the symmetry axis, so that more data can be presented and so that it will be presented more clearly. Figure 7.6 is a series of plots that show pressure and helium mass fraction contours at five vertical locations throughout the interaction area. Pressure is represented by shaded contours, with white streamtraces on the upper side of the centerline and black helium mass-fraction contours on the lower side. The variable values of each contour are consistent with those used in Figures 7.1 through 7.5, facilitating easy comparisons. Flow is once again from left to right. Figure 7.7 is similar, with shaded helium mass-fraction contours on both the upper and lower halves of the figure and black streamtraces superimposed on the lower side. In both these figures the symmetry plane is labeled $z/d_{eff}=0$ and lies in the center of the plot, with the computed solution mirrored to reveal the entire flowfield. As in previous figures, the center of the most upstream row of injector is labeled $x/d_{eff}=0$.

The first plot in Figure 7.6 (part “a”) shows the flow pattern at a vertical position one third of an effective diameter above the lower wall. The bow shock associated with the first (most upstream) row of injectors is clearly visible in the pressure contours. The shock from each injector is curved like a hyperbola around the elliptical upstream ends of the injector plumes, and the two shocks intersect and are drawn into the open space between them. The penetration of the interacting shocks into the space between the injectors elevates the pressure, so that there is a long strip of high pressure that extends almost to the downstream end of the first injectors.

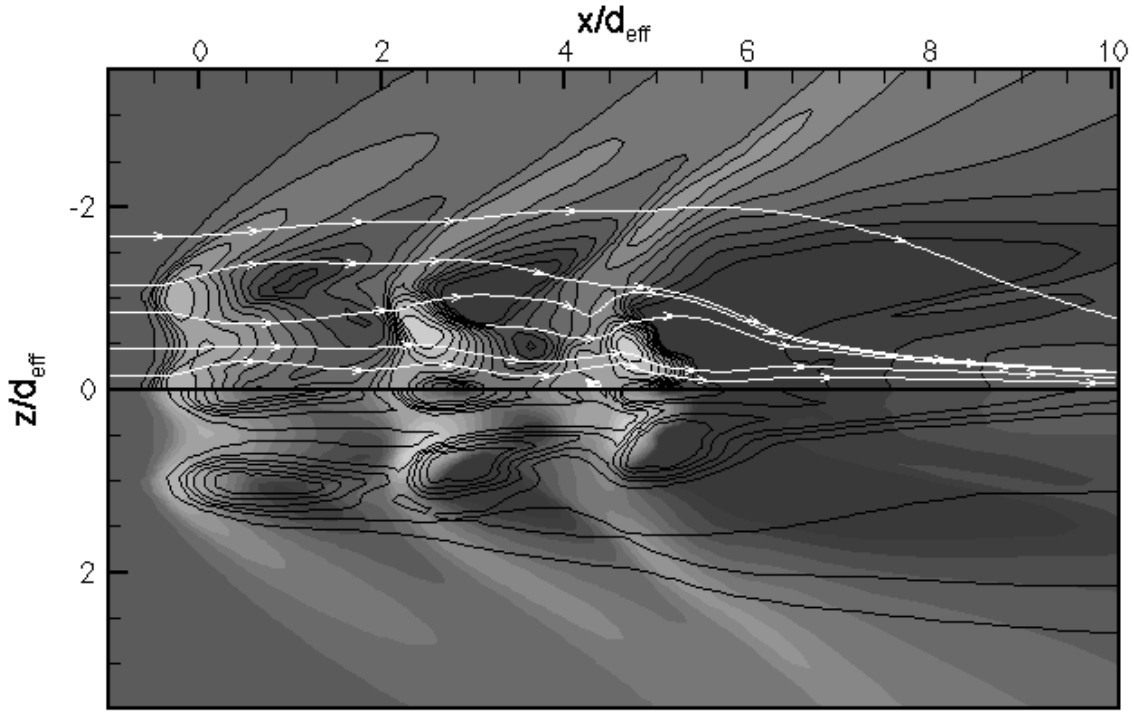

Figure 7.6(a). Pressure Contours (shaded) with Streamtraces (white lines on upper half) and Helium Mass-Fraction Contours (black lines on lower half) on Plane y/d_{eff}=0.33 for the Nine-Hole Injector Array.

Within the helium plumes themselves the pressure contours are quite complex, as parts "a" of Figures 7.6 and 7.7 both reveal. Where the helium injectant plumes intersect the high pressure region behind the shock there is an extended region of high pressure within the plume itself, followed by lower pressures in a wake region downstream. Neither the pressure nor mass fraction contours associated with the outer injector are symmetric. The shock interaction centerward of this injector makes a stronger pressure field than the already-weakening shock on the outside, so the pressures are considerably lower and the wake longer and larger on the outside. The helium mass fraction contours are almost symmetric for much of the plume, but become clearly asymmetric a little more than an effective diameter upstream from the next row of

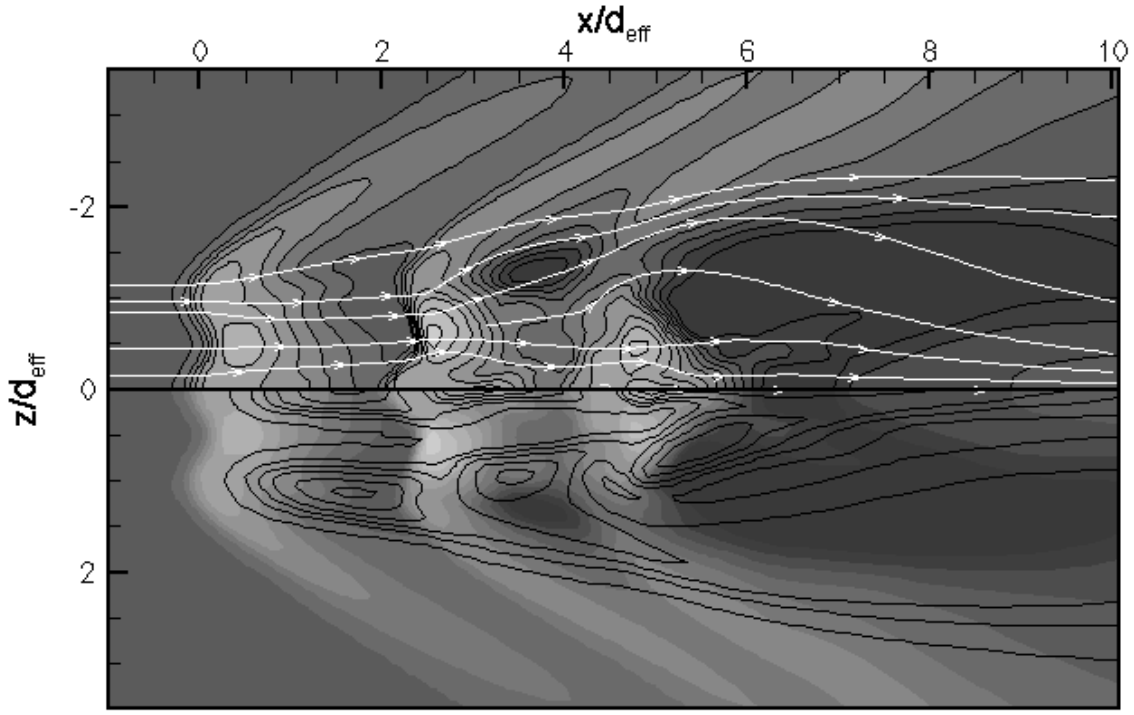

Figure 7.6(b). Pressure Contours (shaded) with Streamtraces (white lines on upper half) and Helium Mass-Fraction Contours (black lines on lower half) on Plane y/d_{eff}=0.66 for the Nine-Hole Injector Array.

injectors. Figure 7.6 suggests that the increasing pressure ahead of the second outer injector creates an obstruction around which both the low-pressure wake and the injectant plume must bend, but the sharp curvature and faintly notched pattern of the inner mass fraction contours suggest a more complicated, perhaps three-dimensional explanation. Furthermore, the highest concentrations of helium in the downstream part of the first-row, outer plume fall in a line that leads toward, not away from, the high pressures of the second row. This feature will be considered again in combination with data from later figures. Notice all but the lowest-valued mass fraction contours associated with the first-row injectors do not connect with those of the second-row injectors at this horizontal plane.

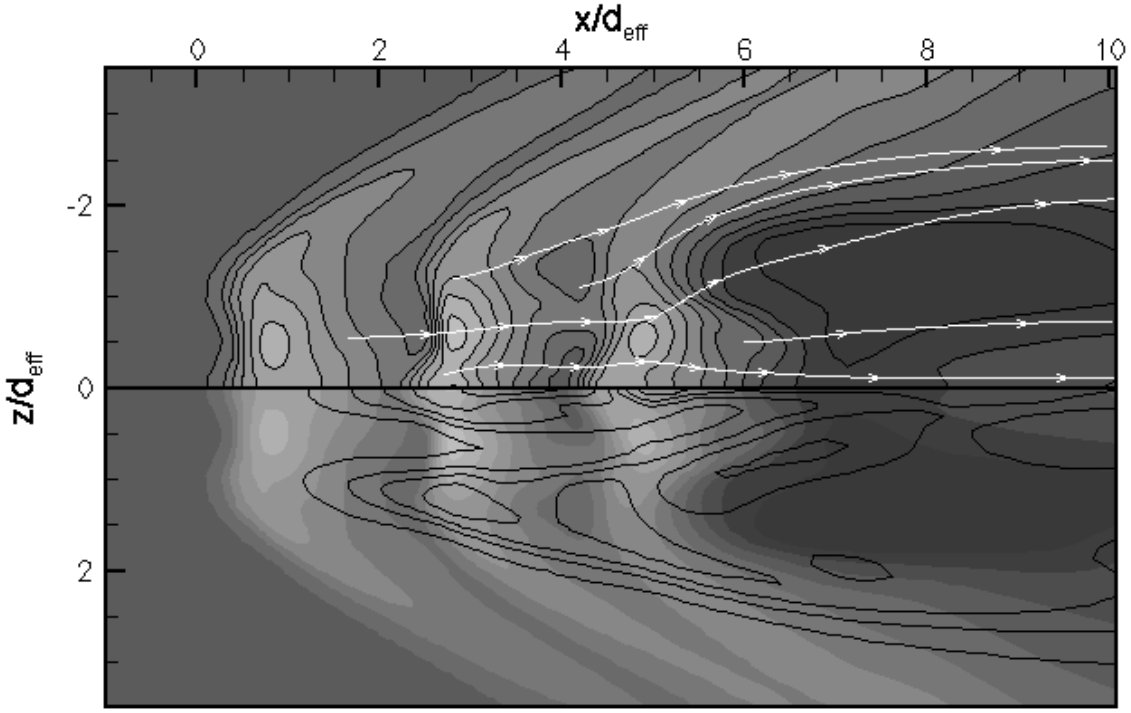

Figure 7.6(c). Pressure Contours (shaded) with Streamtraces (white lines on upper half) and Helium Mass-Fraction Contours (black lines on lower half) on Plane y/d_{eff}=1.00 for the Nine-Hole Injector Array.

The pressure and helium contours associated with the centerline plume are of course symmetric, but they, too, show the effects of increasing pressure ahead of the second-row injector. Because the pressure is highest on the centerline, the helium concentration decreases along that line, so that at least one mass-fraction contour (the one corresponding to c_{He}=0.25, according to Figure 7.7) pulls away from the centerline and forks ahead of the second injector. Along with the inner tail of the outer injector's helium plume, it is drawn toward the space between the outer and centerline injectors, which before the second-row pressure field is an extension of the overall low-pressure wake behind the first-row bow shock.

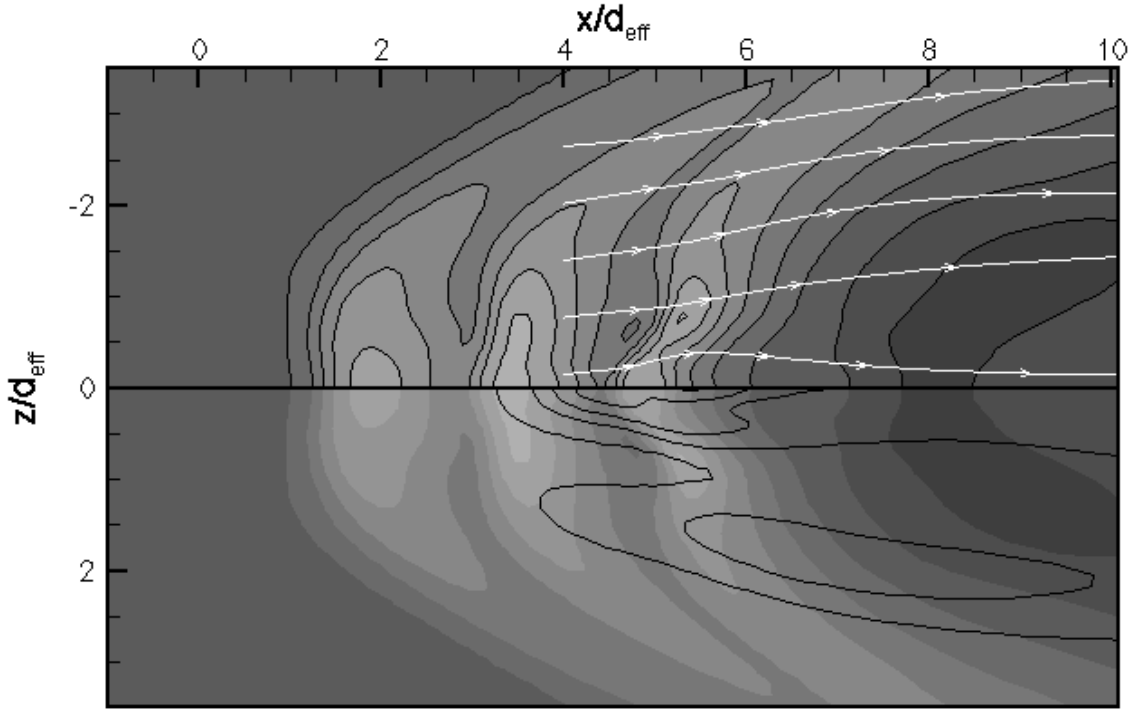

Figure 7.6(d). Pressure Contours (shaded) with Streamtraces (white lines on upper half) and Helium Mass-Fraction Contours (black lines on lower half) on Plane y/d_{eff}=1.66 for the Nine-Hole Injector Array.

Streamtraces in this plane are relatively straightforward ahead of the second row of injectors. Those which encounter injector plumes bend neatly around them, following the helium contours almost perfectly, and those that do not encounter helium plumes continue along essentially straight lines downstream.

The second row of injectors differs from the first in two important ways: first, the flow ahead of it is already disturbed by the previous injectors, and second, the outer injector is yawed inward by fifteen degrees. This second difference results in the outer injector of the second row presenting a larger spanwise cross-section than the first-row injectors or the centerline second-row injector, even though it has the same diameter. In addition, this outer injector is displaced centerward by one sixth an effective diameter (one half its

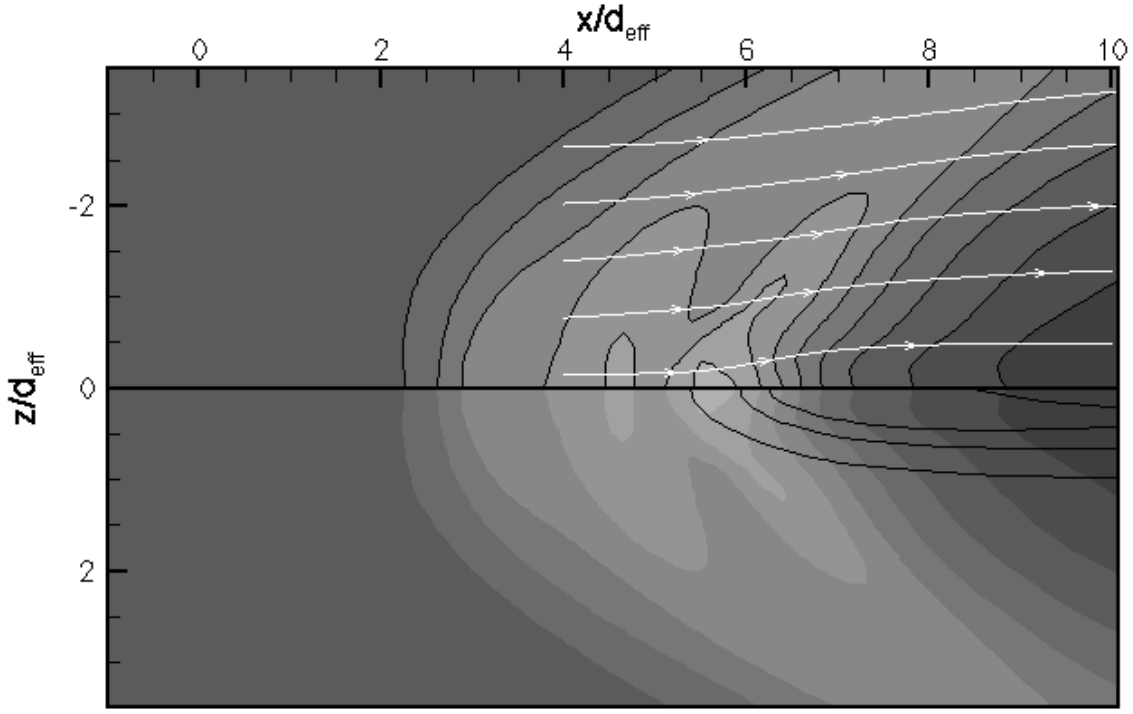

Figure 7.6(e). Pressure Contours (shaded) with Streamtraces (white lines on upper half) and Helium Mass-Fraction Contours (black lines on lower half) on Plane y/d_{eff}=2.66 for the Nine-Hole Injector Array.

own diameter) from the outer injector of the first row, reducing the sheltering effect of the first injector. The consequence is shown in Figure 7.6 part "b", in which the bow shock that forms at the leading edge of the second row of injectors is similar to that at the first row of injectors, except that the region of highest pressure is no longer at the leading edges of the two injectors but on the centerward side of the outer injector. The peak pressure within this second-row shock is also considerably higher than that of the first row, indicating a stronger flow disturbance as a result of the increased blockage. There may still be some contortion of the high-pressure pattern due to interaction of the helium plume with the shock-induced high pressures, but any such effect is rendered more obscure by the asymmetric shape of the shock itself. Notice that the outer bands of

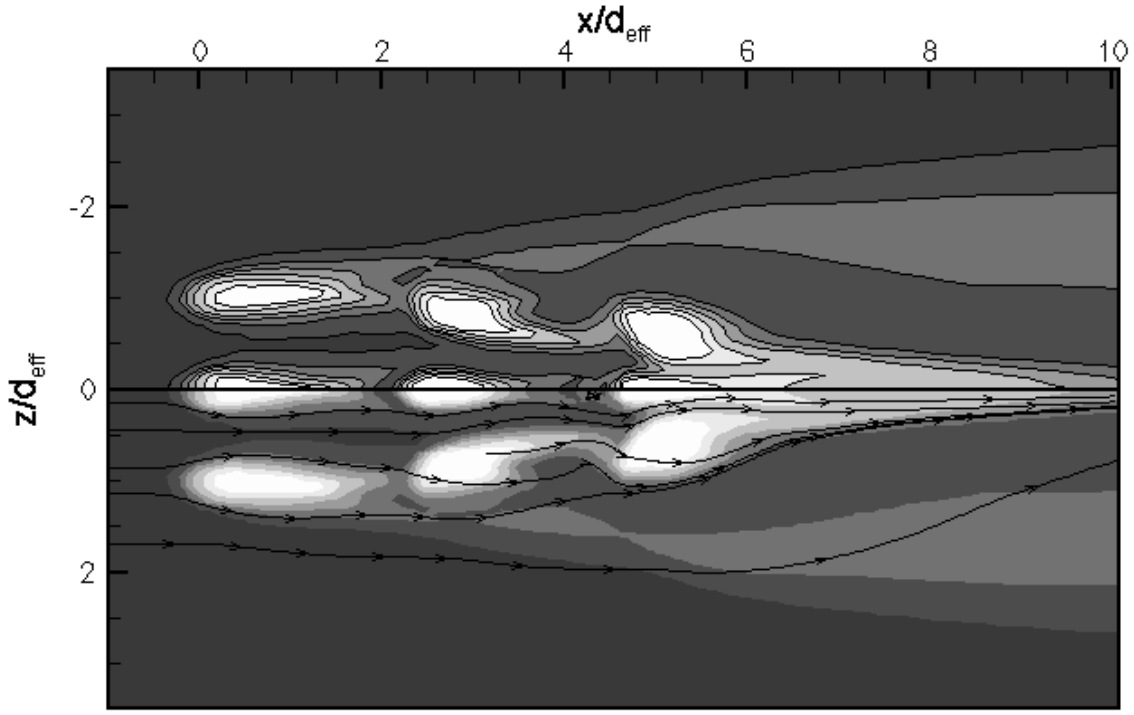

Figure 7.7(a). Helium Mass-Fraction Contours with Streamtraces on Plane y/d_{eff}=0.33 for the Nine-Hole Injector Array

pressure that mark the second-row bow shock do not intersect those of the first row at this horizontal plane, suggesting the shock begins to weaken before merging can occur, at least at this vertical location. The pressure gradient ahead of the shock at the outer injector is for the most part smooth and steep, and it does flow smoothly into the low-pressure wake behind the first injector. However, the pressure gradient alone does not provide a ready explanation of all of the kinks in the helium mass-fraction contours associated with the downstream end of the first injector's plume. Again more data will be needed for a thorough understanding of the flow. The pressure gradient ahead of the centerline injector is much shallower and the centerline pressures lower, and the pressure contours do generally share the shape of the helium mass-fraction contours in that area.

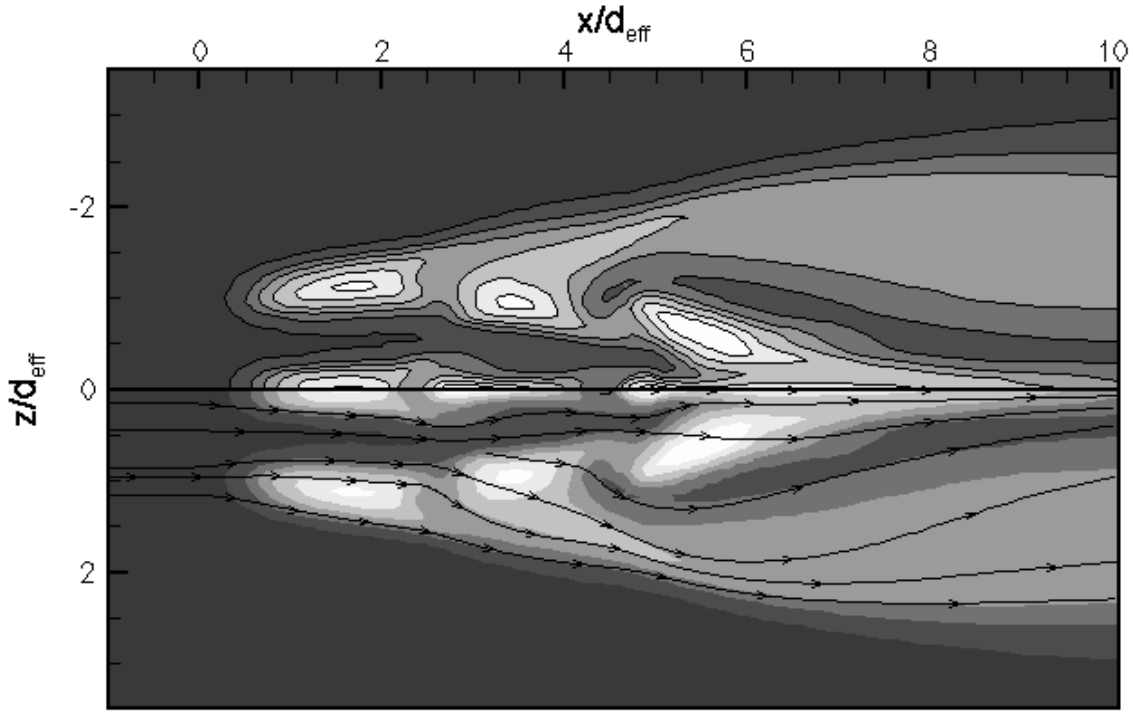

Figure 7.7(b). Helium Mass-Fraction Contours with Streamtraces on Plane y/d_{eff}=0.66 for the Nine-Hole Injector Array

Behind the regions of high pressure in each injector plume is another low-pressure wake, as suggested in Figure 7.3. Figure 7.6 shows that the wake is much larger than the centerline data would suggest, as the pressures are lowest and the wake contours largest behind the outer portion of the shock structure. Indeed, Figure 7.4 shows that the flow downstream of the second centerline injector is quite subsonic at this level, and the formation of the wake is prevented by the upstream propagation of the influence of the third-row pressure system. By contrast, the low pressure region downstream of the outer portions of the second-row shock are much more extensive and may be more properly called a wake. Away from the centerline the low-pressure wake generally follows the shape of the combined centerline and outer bow shocks that shelter

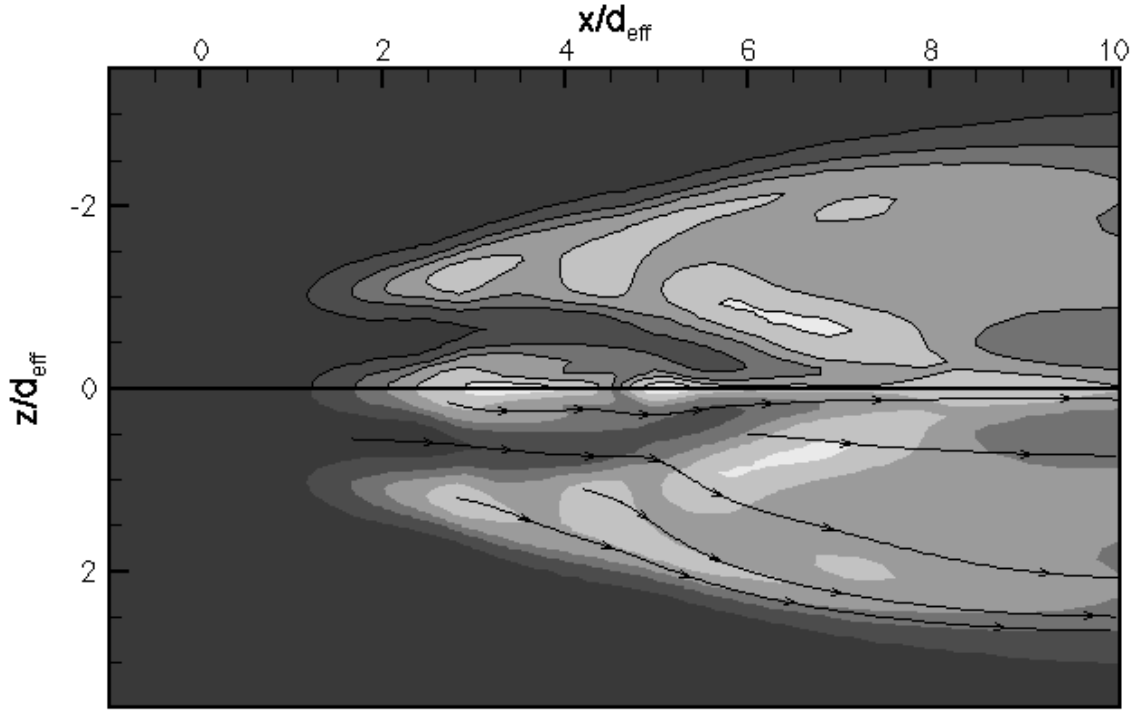

Figure 7.7(c). Helium Mass-Fraction Contours with Streamtraces on Plane y/d_{eff}=1.00 for the Nine-Hole Injector Array

it from the upstream flow. One exception is the separation of the outer wake into a very large portion outward of the center of the outer injector and a smaller portion centerward of the same injector. The narrow band of more moderate pressure that separates the two portions is not aligned with any shock or with the helium mass-fraction contours, though it does seem to be aligned with the series of notches that mark the downstream edge of the second-row, outer helium plume. (See the lower half of Figure 7.6.) A weakened form of this pattern, particularly in the pressure field, has already been identified in association with the first-row wake.

Behind the regions of high pressure in each injector plume is another low-pressure wake, as suggested in Figure 7.3. Figure 7.6 shows that the wake is much larger than the centerline data would

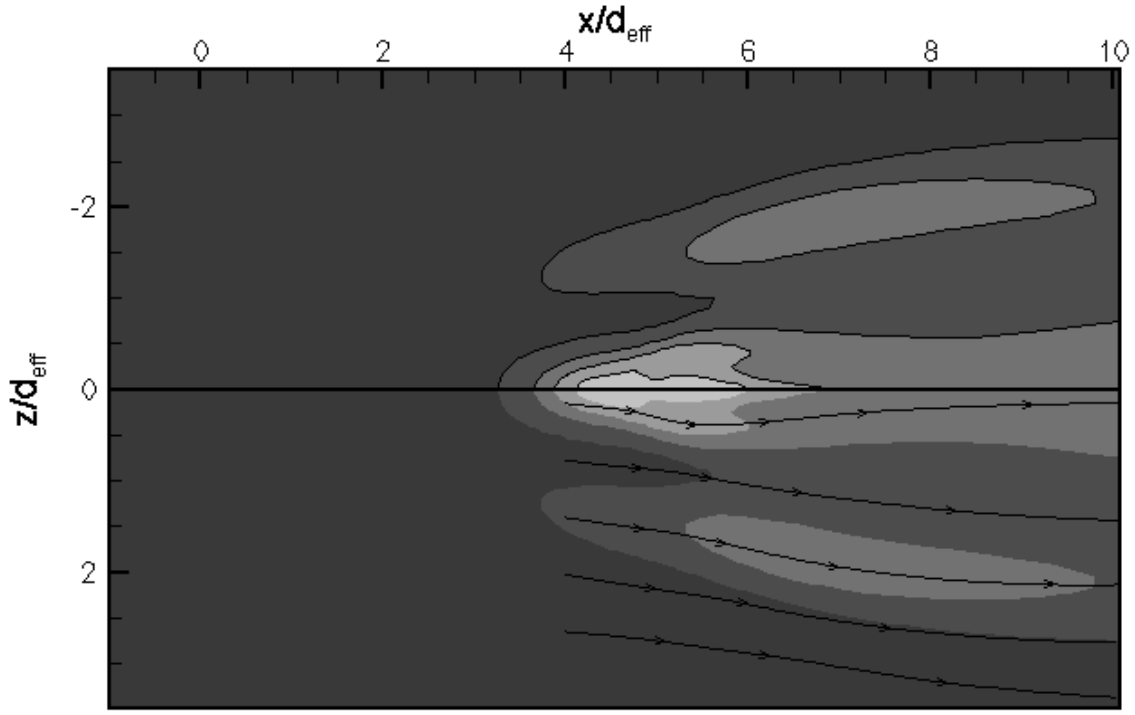

Figure 7.7(d). Helium Mass-Fraction Contours with Streamtraces on Plane y/d_{eff}=1.66 for the Nine-Hole Injector Array

suggest, as the pressures are lowest and the wake contours largest behind the outer portion of the shock structure. Indeed, Figure 7.4 shows that the flow downstream of the second centerline injector is quite subsonic at this level, and the formation of the wake is prevented by the upstream propagation of the influence of the third-row pressure system. By contrast, the low pressure region downstream of the outer portions of the second-row shock are much more extensive and may be more properly called a wake. Away from the centerline the low-pressure wake generally follows the shape of the combined centerline and outer bow shocks that shelter it from the upstream flow. One exception is the separation of the outer wake into a very large portion outward of the center of the outer injector and a smaller portion centerward of the same injector. The narrow

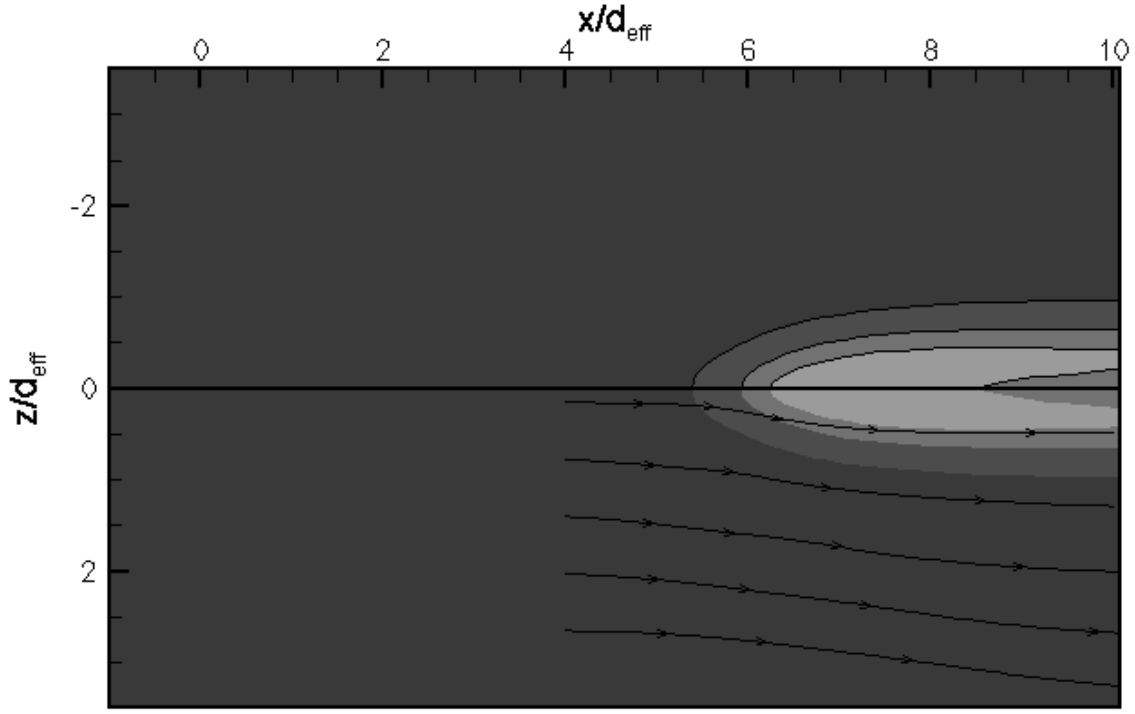

Figure 7.7(e). Helium Mass-Fraction Contours with Streamtraces on Plane y/d_{eff}=2.66 for the Nine-Hole Injector Array

band of more moderate pressure that separates the two portions is not aligned with any shock or with the helium mass-fraction contours, though it does seem to be aligned with the series of notches that mark the downstream edge of the second-row, outer helium plume. (See the lower half of Figure 7.6.) A weakened form of this pattern, particularly in the pressure field, has already been identified in association with the first-row wake.

(As mentioned in the preceding paragraph, the "wake" downstream of the second, centerline injector has been previously identified as a region of subsonic and even reversed flow. Note in Figure 7.6 the pinpoint streamtrace near the centerline at x/d_{eff} just greater than four, indicating flow with essentially no streamwise velocity component. This feature is consistent with the reversed flow identified in Figures 7.2 and 7.3. A better indication of the

extent of the reversed flow is given by Figure 7.8, in which the streamwise component of velocity is plotted on an x-z plane just above the lower wall. This figure reveals three distinct regions of reversed flow. The first lies between the centerline and outer injectors of the third row, roughly aligned with the high pressure region behind the shock at the leading edge and confirming the theory first presented in association with the "b" parts (z/d_{eff}=0.5) of Figures 7.1 and 7.3. The second lies in the region of the present discussion, along the centerline upstream of the third row of injectors. Figure 7.8 shows that the reversed flow close to the wall here is larger in magnitude than the first reversed-flow region and more widespread than the streamtraces in Figure 7.6 indicate. The third region occurs as part of the outer, second-row wake, which was identified as a subsonic region in Figure 7.5 but is now identified as reversed. Here the reversed flow forms a large, "L"-shaped pattern that surrounds the path of the outer, second-row injectant plume.)

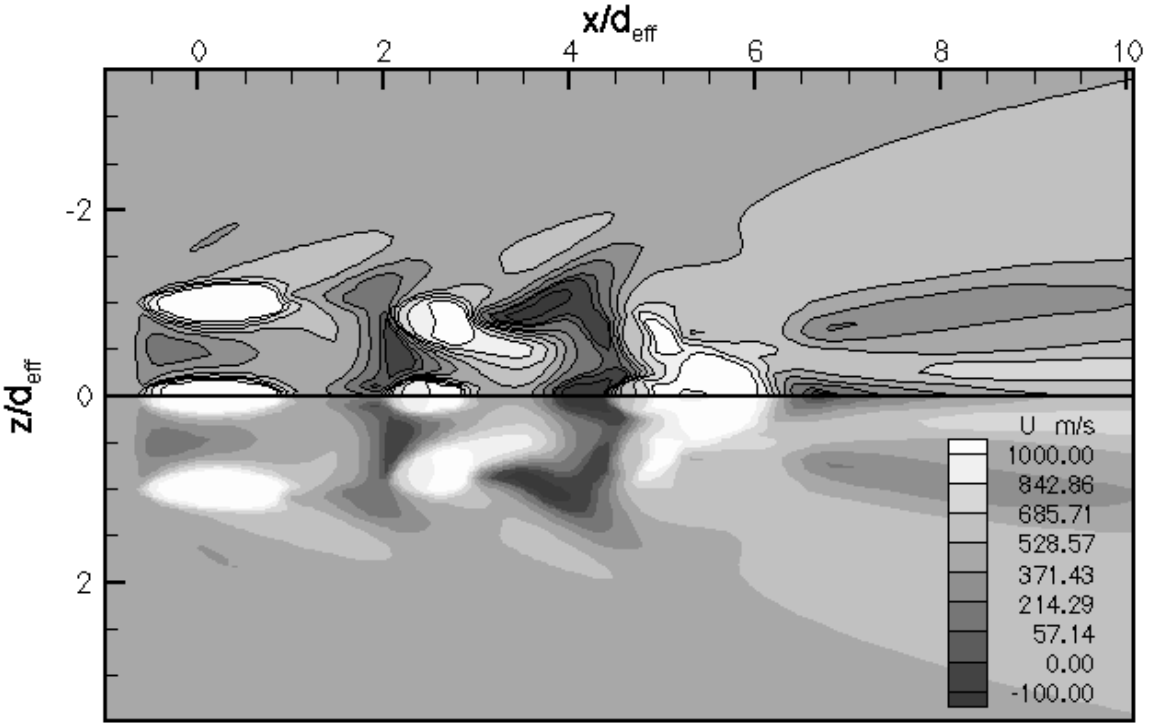

Figure 7.8. Streamwise Velocity Components on a X-Z Plane at y/d_{eff}=0.05.

The helium mass-fraction contours associated with the second-row injectors have largely the same shape as those associated with the first-row injectors, as Figure 7.7 indicates. The line of peak concentration of the centerline plume leaves the centerline as the pressure increases downstream and the c_{He}=0.25 contour widens considerably, but the mass fraction on the centerline drops below 0.25 only in one narrow band ahead of the third-row injector. The reason is that the reversed flow brings helium from the third injector upstream, increasing helium concentration in this area. The c_{He}=0.25 mass-fraction contours of the centerline and outer plumes do meet at this injector, just ahead of the third-row bow-shock, though they intersect only at one tiny point. All the mass-fraction contours of the outer injector are much more sharply notched than were their counterparts in the first row, though as mentioned above the pressure contours do not provide a clear explanation and further study is required. The inner "tail" of this outer helium plume is considerably longer than the first, curving downstream to connect with the third-row outer plume. Even more interesting than the pattern of notches and tails is the narrow, isolated bubble of moderately high helium concentration (c_{He}=0.25 or higher) that sits outside the primary plumes and close the outer edge of the low-pressure wake. (See Figure 7.6.) There is a much shorter but similar feature just upstream of the second-row outer injector, and placement suggests that the two are connected. Almost certainly it is a three-dimensional phenomenon that merits closer investigation in other figures.

Streamtraces in the vicinity of the second-row injector and plume are only slightly different from those of the first-row area. Near the centerline the streamtraces parallel the helium mass-fraction contours almost perfectly (Figure 7.7), but toward the outside the streamtraces move from contours of higher helium concentration into the purer air of the wake, as comparison between Figures 7.6 and 7.7 reveals. Far from the centerline, flow seems

quite unaffected by either the pressure or helium fields, at least in this plane.

The outer injector of the third row is angled inward by thirty degrees, twice the angle of is predecessor, and displaced inward by another one sixth effective diameter, so that the bow shocks of the outer and centerline third-row injectors completely merge. (See the lower half of Figure 7.6.) The highest pressure again occurs on the angled, centerward side of the outer injector and roughly equals that of the second row. It extends downstream in a short band of elevated pressure roughly coincident with the space between the injectors, though there is only partial separation of the helium plumes from each injector in this row, as identified by their plotted mass-fraction contours. There is a long band of moderately high pressure indicating the outward and downstream extension of the "bow shock" (using quotation marks because the flow ahead of the injectors themselves is subsonic at this level and cannot form a shock), but this pressure field does not completely merge with that of the previous injectors at this level. The unique feature of this "bow shock" is that the outer extension is separated from the central shock by a small area of lower pressure between one and one and a half effective diameters from the centerline.

The low-pressure wake behind the shock structure is much larger at this row of injectors, extending more than three effective diameters downstream from the center of the third row of injectors before reaching a maximum width. The extent of the lowest-level pressure contour is several times larger in this third wake than at either of the previous ones, though the lowest pressures seem to occur near the outer edge of the outer injector, or downstream therefrom. The lower half of Figure 7.6 shows that much of the outer helium plume lies within this low-pressure region; it is possible that the low pressures of an injectant-plume expansion are blending with those of the wake proper in this figure. In this case the slight recompression near the downstream end of the outer injector would correspond to a recompression of the injectant plume. The increase

in pressure that occurs along the centerline near $x/d_{eff}=7$ probably corresponds to the interaction of the centerline and outer plumes as they converge, but it could also be related to another injectant recompression following a presumed expansion in the intervening low-pressure region. There is one, very narrow, nearly streamwise band of higher pressure just outward from the centerline band and merging with it downstream. This is a most unique development and must be investigated in later figures.

As mentioned above, all but the highest-valued contours of helium mass-fraction in this row merge immediately and follow the centerline downstream, contracting markedly. Unlike the contours of previous rows, the outer-injector contours are not notched in the direction of the wake extension. This lends credence to the theory that the notches seen in previous mass-fraction contours are in some way dependent upon the presence of downstream injectors, though the closer spacing and joined plumes of the third row may also be responsible, especially for changes in the outer plume shape. At least one of the centerline-injector contours does separate from the centerline itself, indicating that the peak helium mass fraction has left the centerline. Streamtraces in the vicinity of the plumes themselves generally parallel them, converging at the centerline as they more downstream. The outermost contour, $c_{He}=0.05$, continues to spread in expanding scallops from the injector plumes, joining the plumes from all three rows. By the downstream edge of the figure, ten effective diameters downstream from the center of the first injector, the $c_{He}=0.05$ line is more than two and a half effective diameters from the center symmetry line. The unexpected “ribbon” of purer helium identified outward from the second-row outer injector persists throughout the rest of the figure, reaching a minimum width where it crosses the third-row bow shock (Figure 7.6) and widening considerably downstream. At the downstream edge of the figure the “ribbon” is nearly an effective diameter wide and reaches two effective diameters from the centerline. The streamtrace that existed beyond the reaches of any helium plume

upstream of the third-row injectors moves into the c_{He}=0.05 near the third-row bow shock and then into the helium "ribbon", crossing centerward to exit the figure little more than half an effective diameter from the centerline. Clearly some three-dimensional mixing mechanism is at work.

Figures 7.6 and 7.7 parts "b" correspond to data $0.66d_{eff}$ above the lower wall, and generally resemble plots at the lower level. Figure 7.6 part "b" shows the bow shocks of the two first-row injectors merging, as before, though the shocks are sharper at this level and the highest pressures occur within the plumes themselves. Pressures in the shock interaction between the injectors are somewhat lower, though this interaction region is more clearly defined at this level than before. Pressures within the helium plumes themselves are somewhat lower as the helium begins to expand. Pressures associated with the outer plume are particularly low, as noted in the discussion of Figure 7.3 part "c". These expansions blend into the wake downstream, which is also larger and more clearly formed than at the lower level. The separation of the outer wake into two parts at the notch in the outer helium plume is more clearly formed than it was closer to the wall, and cannot yet be completely explained. Streamtraces throughout this first-row area continue to move almost directly downstream, being deflected only by the presence of the injectors and, outward from the injectors, the bow shock.

The helium mass-fraction contours in part "b" of Figure 7.7 have changed little from their appearance in part "a", except that they are displaced slightly downstream, the contours are more rounded, and the outermost (lowest-level) contours blend together more extensively than at the lower level. Both the centerline and outer plumes have split trailing edges as before, but this time the three lowest-level contours (up through and including c_{He}=0.45) have no trailing edges at all but flow smoothly into the second-row plumes. Even the lowest-level contours from the centerline and outer injectors in the first row remain separate until x/d_{eff}=2.5,

downstream of the centers of the second-row injectors (though not downstream of the centers of the second-row injectant plumes).

The changes in the second-row pressure data are much like the first. The second-row bow shock is stronger at this height, owing to the higher Mach numbers away from the wall. Pressures behind the shock are higher, but the helium plumes themselves show the low pressures of an expansion. The wakes are more clearly formed and larger. The separation of the outer wake into parts is more distinct at this level and corresponds even more clearly to a decrease in helium concentration (notch) within the outer helium plume.

As mentioned above, the three lowest-level helium mass-fraction contours of the first and second-row outer injectors blend together virtually without distinction, as do the corresponding centerline contours. On the centerline, however, the transition from first-row helium to second-row helium is marked by an increase in plume width, which quickly decays as the contours return very close to the centerline. This may be the beginning of the out-of-plane expansion at the intersection of the first and second-row centerline plumes, predicted in association with Figure 7.2. Downstream of the helium bulge, the centerline plume is only a small fraction of an effective diameter wide. The outermost (c_{He}=0.05) contour connects the second-row, centerline plume both to the second-row, outer plume and to both third-row plumes. The c_{He}=0.25 contour connects only to the third-row centerline injector, and the c_{He}=0.45 contour decays without connecting to any downstream injector at all. The second-row outer injector is separated from the first by a distance of some quarter to half an effective diameter. Though this outer injector fits for the most part within the boundaries of the first-row plume, the shape of its higher-level contours is very different. At this level the second-row outer injector's outer tail is long and rich in helium, extending outward more than two effective diameters from the centerline and forming a wide, upper-level extension of the mysterious "ribbon" of helium identified in part "a". It would seem, then, that helium rises at least to the current level, two thirds of an

effective diameter above the lower wall, is by some means drawn outward from the centerline, leaving a band of purer air centerward and below, then drops again toward the lower wall. This is an interesting fluid formation that could be quite significant for mixing and will be studied extensively below. The centerward tail of the second-row, outer plume is much shorter, flowing smoothly into the third-row plume. Between the centerward and outer plumes the helium mass fraction drops below 0.25 just ahead and outward from the outer, third-row helium plume.

Streamtraces in this second-row area follow the helium mass-fraction contours almost perfectly. Away from the centerline, most of the streamtraces are swept into the outer "ribbon", converging as the contours narrow, then separating downstream as the remaining contours widen.

The third-row pressure field remains largely unchanged from part "a". The pressure rises associated with the centerline and outer injectors are still quite merged, with the maximum pressure higher than at the lower level but still occurring on the centerward side of the outer injector. The presence of an extended region of high pressure upstream of the injector plumes, along with the virtually zero-length streamtrace near the centerline, suggest that the flow in the wake ahead of the third-row injectors is subsonic and possibly reversed. The high pressures still penetrate into the narrow channel between the centerline and outer injectors, though the pressure band is not as long as at the lower level. The outer, downstream extension of the bow "shock" has a noticeable division, a significant drop in pressure almost one and a half effective diameters from the centerline, beyond which the pressure increases again to the previous levels. Careful comparison of Figures 7.6 and 7.7 indicate that the pressure drop occurs in a region of low but increasing helium concentration, as the second-row outer plume bends around the third. Additional insight into this phenomenon will be sought in later figures, but the pressure drop could simply be the effect of the second-row outer wake penetrating into the shock downstream.

Downstream from the third row of injectors is the large wake identified in part “a”. The wake is somewhat smaller than at the lower level, and lacks the narrow band of elevated pressure that extends downstream of the injector plumes’ high pressure in part “a” of Figure 7.6. Instead there is an increase in pressure along the centerline at the downstream end of the region of lowest pressure, possibly caused by the centerline confluence and resulting turning of helium from the third-row outer injector (See the paragraph below.). In addition, a separate, narrow, almost streamwise spike of higher pressure begins near the centerline at the downstream end of the third-row injectors and penetrates roughly an effective diameter spanwise into the wake itself. Its position between the downstream end of the outer injectors and the centerline suggests a flow turning mechanism, but the separation of the elevated pressures from the centerline itself invites a more complicated explanation, which will require further study with additional figures.

The helium plumes of the third row are relatively simple in this plane. The centerline plume is narrow almost to the point of oblivion, existing only as a thin strip along the centerline with a slight widening at the upstream end. The outer plume is essentially an oval, just brushing against the second-row injector’s outer “ribbon” on the upstream, outer end and angling centerward to blend with the centerline plume near $x/d_{eff}=6$. Once merged, the helium plume continues to narrow, so that it exits the figure only a fraction of an effective diameter wide, as it did in part “a”. The “ribbon” produced by outward movement of a portion of the second-row outer plume continues to expand outward but turns centerward as well, so that by the edge of the figure it spans a width of more than two effective diameters and reaches roughly three effective diameter from the centerline. Helium mass fraction on the centerward side of the ribbon drops below 0.25 but remains above 0.05. Throughout the “ribbon” region streamtraces follow the expansion of the helium plume, but closer to the centerline they do not. One streamtrace seems to outline the centerline plume, but another cuts through the

center of the outer third-row plume before turning toward the centerline.

Figure 7.6 part “c” shows the pressure and helium fields $1.00d_{eff}$ above the lower wall. The bow shock from the leading edges of the first row of injectors crosses this plane just downstream of the streamwise center of the injectors themselves (the origin of the horizontal axis), and retains almost no evidence of the indention that separated the shocks of the centerline and outer injectors at lower levels. There are two processes that may influence the decay of the high-pressure indention. First, as the strength of the plume decreases with height the high-pressure air mixture from the channel may simply expand into the plumes themselves, thereby relieving the pressure. This theory is supported by the presence of broader, spanwise bands of high pressure and a much smaller wake region. Second, as the bow shock climbs, expands and moves downstream it may absorb the high-pressure indention into itself. It is possible that these two explanations are in fact different statements of the same physical process. The contours of highest pressure are no longer small, separate spots directly tied to interaction of the bow shocks with the helium plumes; instead, there is one oval centered in a broad, spanwise band of high pressure which shows only faint coincidence or interaction with the helium plumes. This change indicates a spreading of the shock structure as it progresses downstream. The outer contours are much straighter and smoother than they were at lower levels and show only faint curvature changes as they interact with the helium plumes. The outermost pressure contour of the shock structure (which encounters the purer parts of the helium plume) does retain a noticeable lobe of elevated pressure as a result of its interaction with the outer helium plume, though careful examination of the lower half of Figure 7.6 is necessary to identify the interaction.

The interplume wake is almost nonexistent at this point, being marked not by contours of low pressure but instead by a narrow region of no pressure contours at all ahead of the second-row shocks.

This is consistent with expectations, since the second row of injectors have a vertical injection angle of thirty degrees, twice that of the first-row injectors, and will penetrate more directly into the flow with less downstream travel, causing the plumes and shocks from the first two rows to approach each other and leaving little room for a wake. The wake region is broadest away from the centerline, probably because the intersection of the first and second-row centerline plumes elevates pressure.

Most of the helium mass-fraction contours that identify the paths of the first-row injectant plumes are quite different at this horizontal plane than they were closer to the lower surface, though a few have generally the same shape. The outermost contour, the c_{He}=0.05 contour, shows little change from its shape, form, and position at the lower level, except that it is shifted downstream as expected and that it is broader spanwise. This outer contour extends more-or-less smoothly from the leading edges of the first row of injectors downstream around the outsides of all three rows of injectors, and crosses the downstream edge of the figure (ten effective diameters downstream of the origin) approximately three effective diameters away from the centerline, indicating little spreading from its position in the previous plane. The innermost mass-fraction contours on the centerline in the first row of injectors have an arrow shapw at this point, as the first-row plume with its off-the-centerline “tails” intersects the second, narrower center plume. The point of intersection can be identified in Figure 7.6 as a region of high pressure, which is consistent with Figures 7.1 through 7.3 as they show intersection of the helium plumes at this location and higher pressures as a result.

The separation between the centerline and outer helium plumes in the first row is greater at this height than it was at the lower plane, as the outer plume appears to be drifting outward. The low-level contours associated with this outer plume retain the basic shape they had at the lower level but in general the helium concentrations are lower. None of the contours are notched in this

plane, but either flow smoothly into the second-row plume or take a simply, teardrop shape. All the contours flow slightly toward the outside as they move downstream, apparently influenced by the centerward band of high pressure that dominates the region at lower levels.

The only identifiable shock left intact one effective diameter above the second row of injectors is centered in the low-helium region between the outer and centerline injectors, and it is quite well formed. Just ahead of the are the lowest pressures of the interplume wake region. Behind the shock is a small bubble of high pressure, which gradually expands into a lower pressure region. There are still areas of elevated pressure associated with the leading edges of each second-row injector, but at this height they are too weak and diffuse properly to be called shocks. (The high pressures associated with the centerline plume have already been identified as the product of interaction and turning with the first-row helium plume.) The band of pressure that marks the outer extent of the outer injector and the spanwise/downstream extension of the high-pressure region (elsewhere identified a shock) is lower in magnitude than the centerline pressure band but is connected more directly to the pressure contours that outline the actual shock. Downstream of this band of higher pressure is a bubble of low pressure that marks a wake-like, interplume region. This outer wake remains separate from the centerline portion of the wake as it has at lower level, separated as before by a band of moderate pressure. At lower levels this moderate pressure coincided with a notch in the second-row, outer helium plume, but careful comparison of Figures 7.6 and 7.7 show that no such notch is present at this level. Instead the pressure band lies in a region of low helium mass fraction, between the centerline and outer plumes. One possible explanation is suggested by Figure 7.1, which shows that the low pressures along the centerline are more a region of “diamond-shaped” injectant expansion than a wake proper, and thus have a different nature and origin than the outer low-pressure contour.

The helium mass-fraction are somewhat simple to discuss in the vicinity of this second row of injectors. Along the centerline the helium plume is completely engulfed by the first-row plume, as has been discussed. The lowest-level contours (c_{He}=0.05) of the centerplane and outer injectors merge near x/d_{eff}=3, but the inner contours of the centerline plume do not extend more than half an effective diameter from the centerline. One of these contours, c_{He}=0.25, takes the shape of a long oval and surrounds all three centerline injectors, but the higher-valued centerplane contours of the first plumes end just upstream of the third-row plume. The separation between the helium mass-fraction contours of the centerline and outer second-row plumes is smaller than that of the first-row plumes, but is still larger than the corresponding separation in lower planes closer to the lower wall. The highest-level helium contour visible in the outer row has a mass-fraction value of 0.65 and the shape of an exaggerated airfoil (or perhaps a paisley), with a thick, curved upstream end, a much narrower, tapered outer/downstream extension, and a flatter underside. This is the only contour present in the second-row, outer plume as a distinct entity, separate from those of the first and third-row plumes. The lower-valued contours continue their smooth expansion around it, with no noticeable change in shape or curvature. The centerward edge does angle a bit more steeply toward the center as it approaches and then connects with the third-row plumes. The outer edge curves more gently under the influence of the pressure field, reaching downstream past the outside of the third row of injectors to the edge of the figure, ten effective diameters downstream of the origin, where it still reaches three effective diameters from the centerline.

The pressure field that outlines the third row of injectors is unexpectedly well defined. The region of reversed flow ahead of the injectors allows upstream travel of the high pressures associated with the injectors, resulting in a “shock” structure that is poorly defined for some distance above the surface. At this level, however,

there is a steep pressure gradient marking the transition from low pressure in the region ahead of the third row to the high pressure of the injectors' leading edge. While it is tempting to think of the pressure gradient as a shock, Figure 7.1 part "a" shows that, at least on the centerline, the pressure gradient marks the transition from an expansion of the second-row helium plume to an interaction region, where the second and third-row plumes meet and turn. (Most of the interaction takes place at levels just above the present plane, as Figure 7.1 shows. Figure 7.1 part "c" also shows that the interaction region exists not only in the center plume but in the outer one as well.) Downstream of the interaction region the third-row centerline plume experiences recompression, which maintains a high pressure. Though it is difficult to exactly determine from the plotted data, the outer injector may undergo recompression as well.

Downstream of the pressure gradient is a familiar pattern of high pressure. Along the centerline injectant recompression creates quite a long but narrow high pressure area (reflecting the long but narrow shape of the third-row centerline plume itself, as Figure 7.7 indicates.) The slightly higher pressures located between the centerline and outer plumes, near $x/d_{eff}=5$ and $z/d_{eff}=0.5$, probably represent the upper-level expansion of the formation identified in this area in lower planes of the present figure. At this level the formation might perhaps exist in a supersonic state and thus be considered a proper shock. Outward the end of this "shock" curves ahead of the outer, third-row injector and angles downstream. Unlike the shock extensions from other rows, this pressure band maintains a constant width. It also approaches its second-row counterpart, though they do not merge within the confines of this figure. Downstream of the entire high-pressure area is a large wake of relatively low pressure, with a gradual increase in pressure on the centerline beginning eight effective diameters downstream from the origin.

The helium mass-fraction contours are somewhat simpler at this third row. As mentioned above, the centerline plume exists only

as a narrow bubble and tail that begins near x/d_{eff}=4.5 and merges with the outer plume roughly two effective diameters further downstream. The outer plume begins at least half an effective diameter downstream and angles centerward. It is longer and much wider, with a nearly oval c_{He}=0.65 contour as the primary outline and a thin line of higher contour (c_{He} =0.85) at its center. This contour approaches but does not quite reach the centerline near x/d_{eff}=8, instead allowing a slight decrease in helium concentration to separate it from the third, long, narrow c_{He}=0.65 contour that forms on the centerline. Despite the separation it is likely that the third contour is composed of helium from both the centerline and outer plumes. There is one other, small band of c_{He}=0.65 flow quite separate from the others and more than two effective diameters from the centerline. Though it lies within a thick blanket of helium associated with the "ribbon" identified in the outer reaches at lower planes, this formation does not appear to be a part of the same phenomenon. Clearly this is evidence of a three-dimensional behavior of the flow, and it must be investigated in other planes. The aforementioned blanket of moderately mixed helium does surround the entire third-row region, except for a narrow channel just outside the centerline injector, so that the outer reaches of the outer, third-row plume are indistinguishable from those of the second-row plume. The helium mass fraction in this blanket is generally above 0.45, though downstream of the third-row injectors the concentration begins to decrease, particularly just outward from the last, centerline helium plume. By the downstream edge of the figure, x/d_{eff}=10, approximately half the plume (which has a width of approximately three effective diameters) has a helium mass fraction lower than 0.45.

The streamtraces in part "c" of Figures 7.6 and 7.7 show that along the centerline, flow is still largely streamwise, with little spanwise expansion. For the most part these streamtraces outline the centerline helium plumes. Away from the centerline, within the joined outer plume, a different pattern is seen. Here the

streamtraces sweep gradually outward from the centerline, turning streamwise to parallel the outer edge of the plume. This suggests a large flow formation of which the outer helium plume is an vital part, which is responsible for movement of the helium away from the centerline and into the freestream air. Clearly such a formation could be important for mixing enhancement.

Part "d" of Figure 7.6 is another horizontal cut through the flowfield, this one $1.66d_{eff}$ above the lower wall. The pressure and especially the mass-fraction contours are rather simpler at this location, as most of the complexity of the flowfield occurs at a lower level. The bow shock that forms at the leading edge of the first row of injectors is still fairly well developed in this figure, though the band of highest pressure is smaller and contours of high pressure slightly more expanded. One noticeable change from the lower horizontal planes is that there is no longer any separation between the high pressures of the first row of injectors, be they bow shocks, injectant recompressions, or something different, and those of the second row. Instead the two merge, with only a small area of lower, though still somewhat high, pressure between them. Figure 7.1 identifies this lower pressure as the uppermost extent of the wake that separates the first and second-row high pressure areas at lower levels. As at lower levels, pressures are lower and the wake better formed outward from the centerline.

The pressure elevation in the second row along the centerline itself can be compared with Figures 7.1 and 7.3, which reveal that it is neither the bow shock from the second row of injectors nor the expansion/recompression pattern which is the cause of pressure elevation, but the point of intersection between the plumes from the first and second-row injectors. Outward from the centerline, the pressure probably has the same origin as at lower levels, namely, the presence of a shock on the leading edge of the outer, second-row injector. This shock extends outward and downstream in the familiar manner, though it is more diffuse and poorly formed in this high plane.

Behind the second-row high pressure system is a relatively large region of lower pressure. On the centerline the low pressure is the uppermost reaches of the second expansion of the second-row centerline helium plume, as illustrated in Figures 7.1 and 7.3. The rest of the low pressure region appears to be a simple wake, the result of the sheltering effect of the high pressure area upstream. As usual, this outer portion of the wake is large and is marked by lower pressures. Downstream of the region of lower pressure is a band of moderately high pressure, the remains of the pressure system associated with the third row of injectors. Though the pressure in this third-row system is weaker, the pressure gradients are steeper, suggesting shocks that have not yet diffused. Along the centerline the source of the elevated pressure is again the interaction of present-row helium with that from the previous-row plume, as Figure 7.1 shows. Outward from the centerline such an explanation is not valid and the best explanation is that the pressures represent a shock; however, the lack of alignment of the presumed shock with the third-row outer plume suggests that the shock formed elsewhere (at a lower level) and propagated upward to this location. Whatever its origin, the shock propagates outward and downstream as well, as it has in other figures. Downstream from it all are a series of contours of lower pressure, smooth except for slightly higher pressures along the centerline, another feature carried over from lower levels. The wake is much shorter and horse-shoe shaped at this level, as pressure begins to build along the centerline almost immediately.

The helium mass-fraction contours are more easily described in this plane. The centerline and outer plumes each have only one set of concentric mass-fraction contours, indicating that plumes from all three injectors in each column have merged. The first indication of the presence of significant helium is along the centerline near $x/d_{eff}=3$, where the pressure field has already indicated interaction between the first and second-row plumes. Helium mass fraction increases steadily and the contours expand downstream for

approximately two effective diameters, until they encounter the third-row plume. This transition to the third-row plume is marked in the innermost contour (c_{He}=0.65) by a faint notch and by a much deeper one in the c_{He}=0.45 another effective diameter downstream. These two contours taper centerward and soon end, but the c_{He}=0.25 contour shows neither a notch nor a taper, instead reaching a maximum width of approximately one effective diameter near x/d_{eff}=6 and holding it very nearly constant downstream. The lowest-level helium contour deviates from the others at this same location, connecting with that the outer column. The outer column's mass-fraction contours themselves are simple elongated shapes. The outermost begins approximately one effective diameter from the centerline at x/d_{eff}=4 and expands slowly outward, encountering the second and innermost contour visible at this location, corresponding to c_{He}=0.25, roughly one and a half effective diameters downstream. As the outer plume moves downstream its outward expansion slows and the edges of the contours become more streamwise, so that the c_{He}=0.05 exits the figure less than three effective diameters from the centerline. (This distance is slightly smaller than in lower planes, suggesting the present plane is above the location of the plume's maximum width.) The c_{He}=0.25 contour tapers to an end just upstream of the edge of the figure, indicating a decrease in helium mass fraction in this plane.

Plane "e" of Figure 7.6 is a horizontal plane $2.66d_{eff}$ above the lower wall of the wind tunnel. At this height even the bow shock associated with the first row of injectors is displaced downstream by more than two and a half effective diameters, and most of the shock structure is dissipated beyond recognition. As in plane "d" there is a broad arcing band of moderately high pressure that marks the outer extent of injectors' influence on the freestream, and just downstream within it (near x/d_{eff}=4) is a band of high pressure. The centerline portion of high-pressure band is the expanded, weakened remnant of the leading-edge bow shock. Just downstream of the bow shock is another broad, weak region of high pressure, though this one is

larger and broader than the bow shock itself. Comparison with Figure 7.1 indicates that this region of high pressure is the remnant of the interaction zone between the first and second-row centerline plumes. Downstream another effective diameter is a second region of high pressure, this one corresponding to the interaction of the third-row plume with the second-row plume and the air just upstream (the flow turning mechanism, with which the reader is by now familiar). The narrow, outer reaches of the high pressure system may simply indicate a spanwise continuation of this flow turning effect or a propagation of its associated pressure rise, or they could correspond to some flow feature from the outer row of injectors. There is not enough information to reach definite conclusions at this time. All but the innermost pressure contour of this system have a very rectangular downstream edge in the vicinity of the centerline. This slight downstream extension of elevated pressure overlaps the helium plume and is probably yet another example of the shock/injectant interaction that was present at lower levels, noticeable although the shock is much weaker and dissipated at this point. Beyond the high pressure system the pressure drops rather rapidly, especially on the centerline, where the helium concentration also falls rapidly. (Notice that this figure does not show pressure recovery along the centerline, as data in lower planes did.) Away from the centerline the lower-pressure contours move diagonally downstream, with generally higher pressures further from the centerline as the dissipated shocks continue to move outward and downstream.

The helium mass-fraction contours at this highest horizontal plane are extremely simple. On the centerline there are three nested contours, with the centermost (c_{He}=0.45) beginning more than five effective diameters downstream from the origin. The downstream end of this contour is forked, with the peak helium concentration leaving the centerline. This is the first time a forked shape has appeared on the most downstream helium plume, and it is somewhat surprising, because Figure 7.6 shows that the separation of peak

helium mass fraction from the centerline occurs in the wake region, where the lowest pressures lie along the centerline itself. However, the data presented in plane "d" of Figure 7.7 show that the c_{He}=0.45 was significantly notched at that level, one effective diameter lower, where the pressure was higher along the centerline. It is possible that the forking is the result of pressure gradients at lower levels and has simply propagated to the present plane. Furthermore, at the lower levels the first and second-row plumes have been the only ones to show any kind of forking or notching at all. If the forking in this plane is the result of upward propagation of a lower-level phenomenon, it is possible that the both the forking and the helium at this level are more closely related to the plumes from the first two rows than to the plume from the third.

The two lowest-level mass-fraction contours wrap around this inner plume but extend beyond it so that they cease spanwise expansion and exit the downstream edge of the figure without beginning to contract at all. Every plotted streamtrace in this plane seems to parallel these helium mass-fraction contours, angling gradually away from the centerline as they move downstream.

Y-Z Planes

Examination of Figures 7.1 through 7.8 has provided invaluable insight into the detailed workings of the injector array and its flowfield. More information is needed, however, to complete the understanding. That information will be drawn from Figures 7.9 through 7.11, which show spanwise (x=constant) cuts of the flowfield in the vicinity of the injectors. Seven such cuts are examined, beginning at the center of the first row of injectors. In each plot data is presented so that the reader looks into the page as though looking upstream. The calculated half-flowfield is mirrored about the y (vertical) axis, so that the entire flowfield is shown. For clarity the vertical axis is then displayed on the left-hand side of the figure. Figure 7.9 presents shaded pressure contours on both sides of the symmetry axis at each of the seven axial stations. The contours are

outlined in black on one side of the figure and not outlined on the other, to suit the particular circumstances of the different plots and the preferences of the reader. Figure 7.10 repeats the pressure data, but overlays additional data for comparison purposes. On the left sides of these figures, helium mass-fraction contours are shown as black lines overlaying the pressure field. On the right sides, black lines outline and clarify the pressure contours themselves, and white lines represent planar velocity streamtraces. Figure 7.11 is similar, with shaded helium mass-fraction contours on both sides, black helium mass-fraction lines overlaid on the left for clarity, and black planar velocity streamtraces overlaid on the right. Contours of both pressure and helium mass fraction are plotted at the same values used in Figures 7.1 through 7.7, and are consistent throughout Figures 7.9 through 7.11 as well.

The spanwise cut labeled Station 1 in Figures 7.9 through 7.11 lies exactly at the center of the first row of injectors. The injectors each have a diameter of one third an effective diameter, and the outer injector has its center one effective diameter from the centerline. Figure 7.9 shows the tiny bubbles of elevated pressure outlining the helium that enters the flow from the injector ports. The pressure of the helium at the injector exit is lower than specified at the upstream end of the injector, because this first row of injectors enters the flowfield at a very acute angle (fifteen degrees) and the incoming helium begins to lose pressure before it exits the injector ports. Above each injector's pressure bubble is an area of lower pressure, as the helium expands further. Notice that the pressure field corresponding to the outer injector is not symmetric, but has lower pressures on the outside. This is expected, since the presence of the centerline injector and the streamwise extension of the bow shock high-pressure region between the two injectors serve to elevate the pressure on the centerward side. Above the overhead expansion-layer of lower pressure is the bow shock from the leading edges of the injectors. At this location and in this plane it has a shape like two intersecting semicircles, though on the outside the

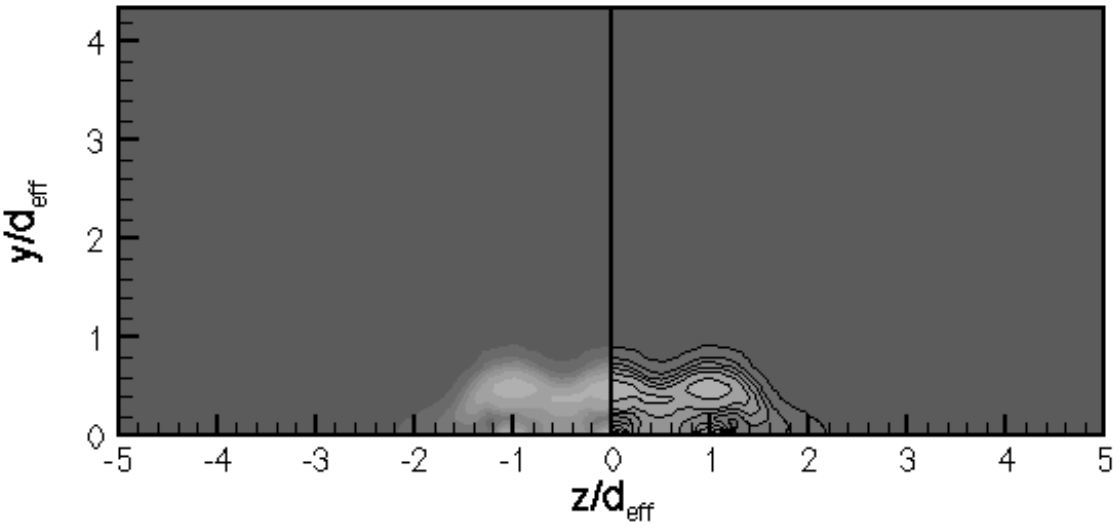

(a) Station 1, $x/d_{eff} = 0.00$

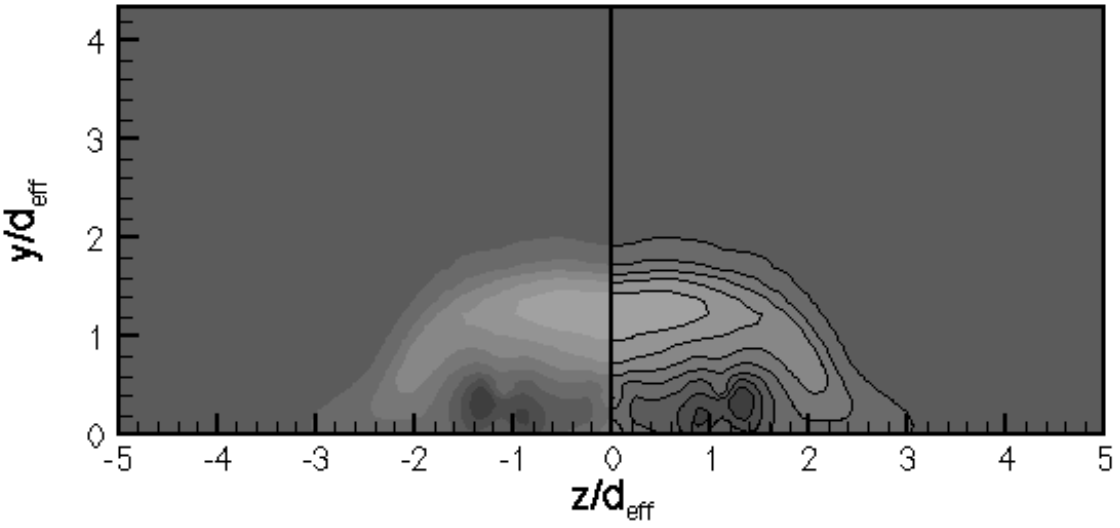

(b) Station 2, $x/d_{eff} = 1.32$

Figure 7.9. Pressure Contours (with and without black outlines) for Seven Different Crossflow Planes for the Nine-hole Injector Array.

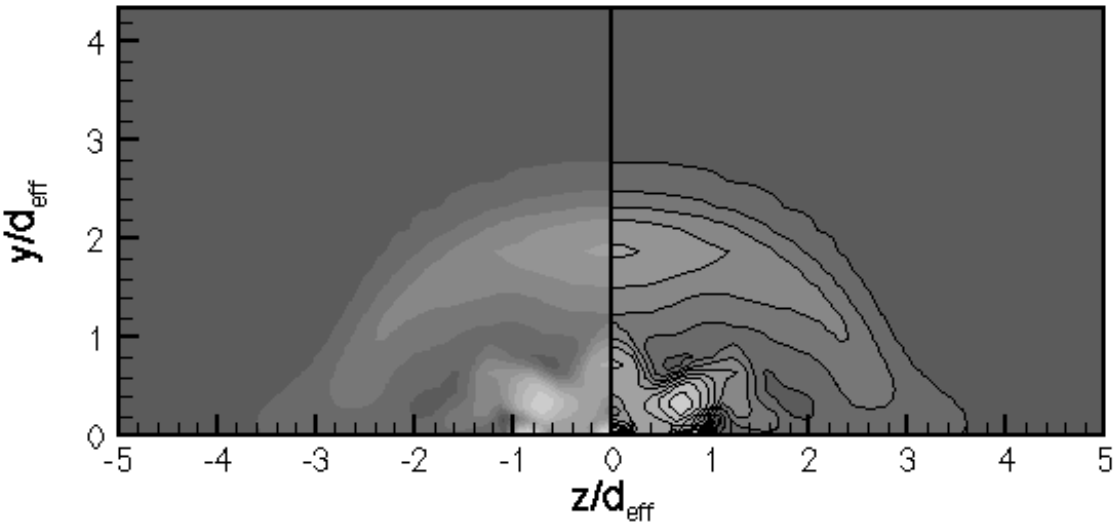

(c) Station 3, $x/d_{eff} = 2.33$

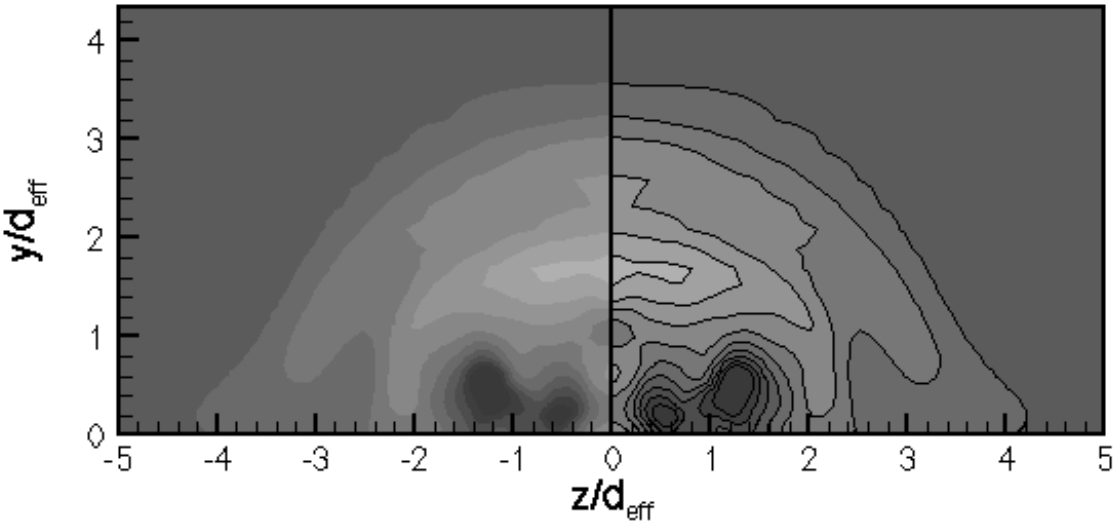

(d) Station 4, $x/d_{eff} = 3.55$

Figure 7.9 (Continued). Pressure Contours (with and without black outlines) for Seven Different Crossflow Planes for the Nine-hole Injector Array.

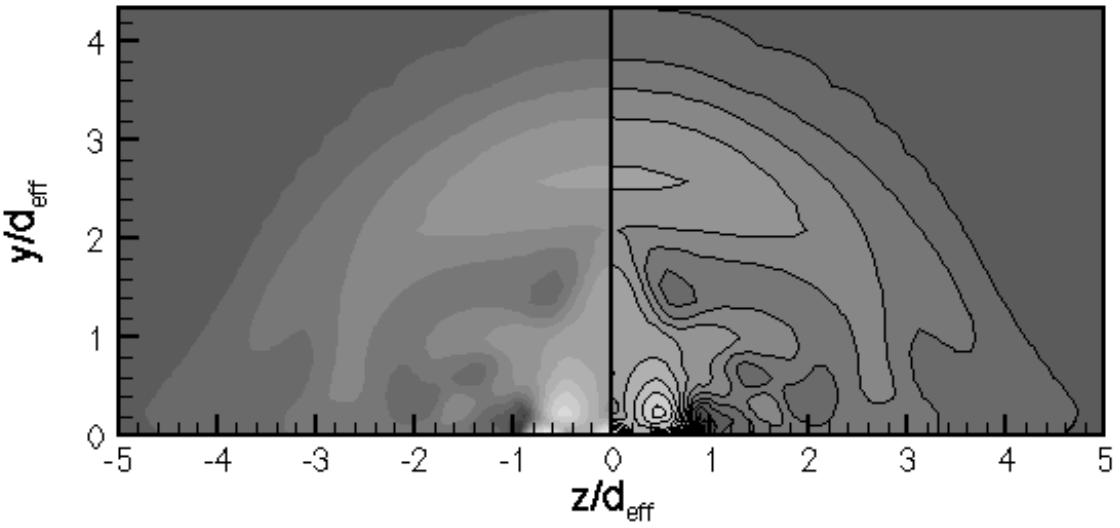

(e) Station 5, $x/d_{eff} = 4.66$

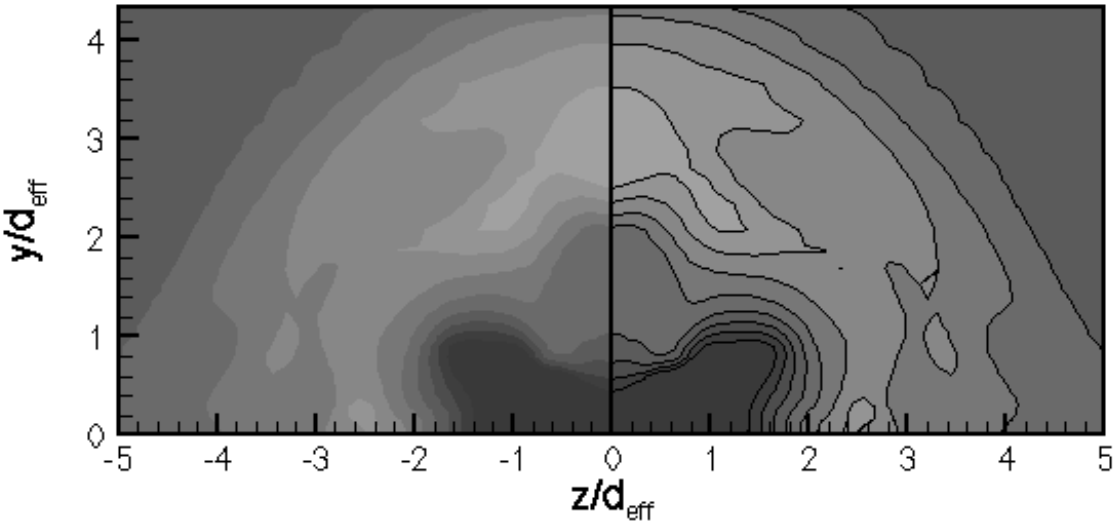

(f) Station 6, $x/d_{eff} = 6.00$

Figure 7.9 (Continued). Pressure Contours (with and without black outlines) for Seven Different Crossflow Planes for the Nine-hole Injector Array.

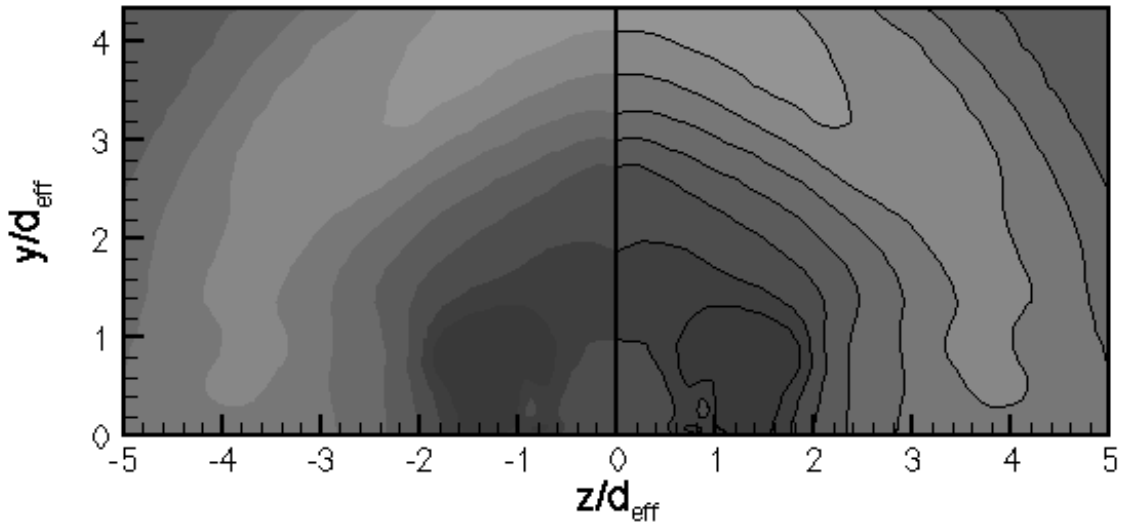

(g) Station 7, $x/d_{eff} = 8.00$

Figure 7.9. (Continued.) Pressure Contours (with and without black outlines) for Seven Different Crossflow Planes for the Injector Array.

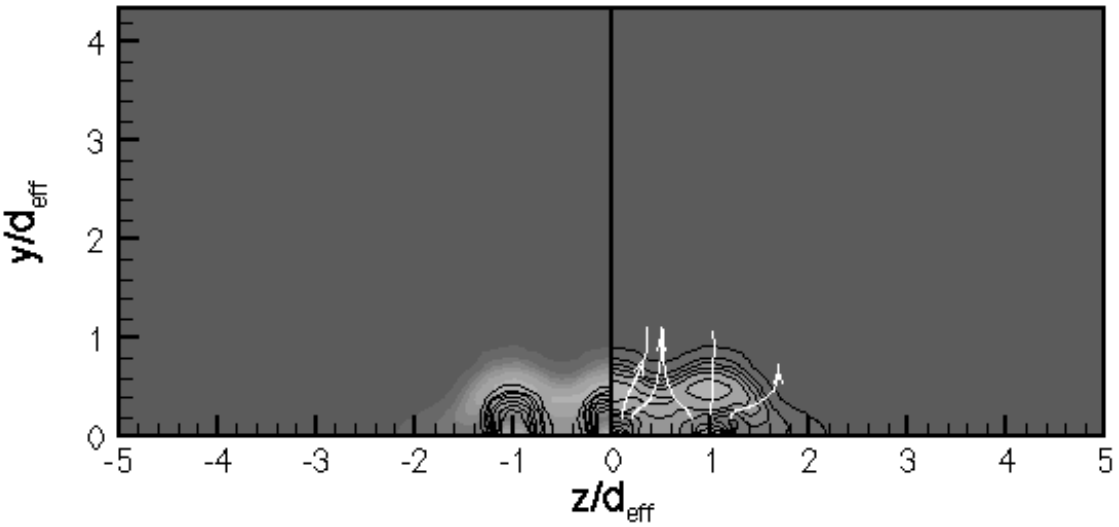

(a) Station 1, $x/d_{eff} = 0.00$

Figure 7.10. Pressure Contours (shaded) with Helium Mass-Fraction Contours (black lines on left) and Velocity Streamtraces (white lines on right) for Seven Different Crossflow Planes for the Injector Array.

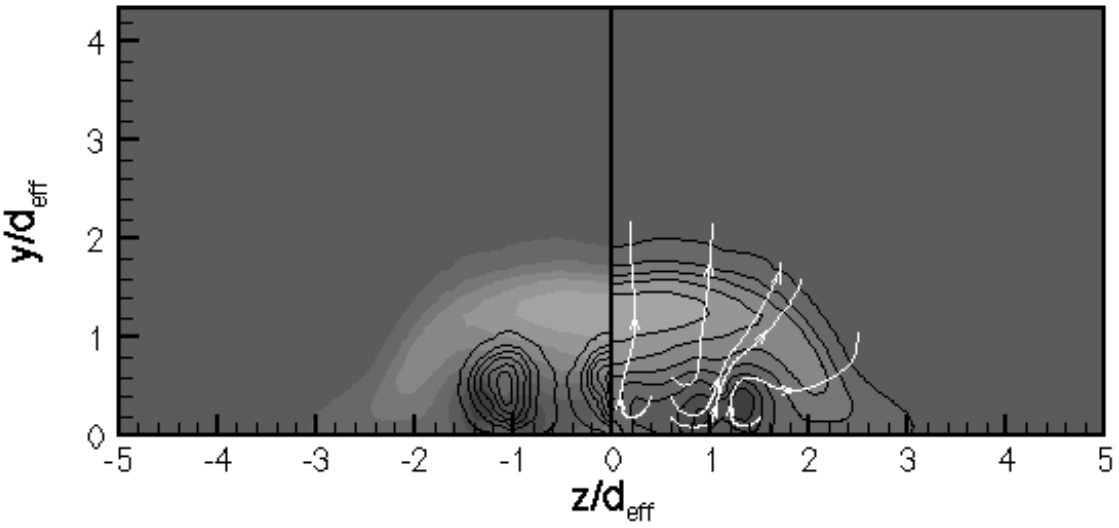

(b) Station 2, $x/d_{eff} = 1.32$

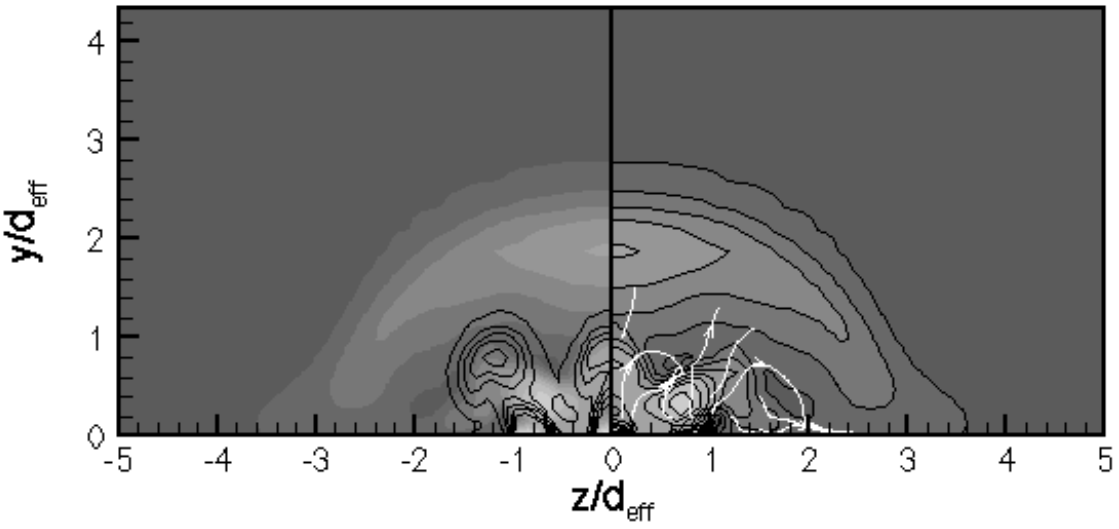

(c) Station 3, $x/d_{eff} = 2.33$

Figure 7.10 (Continued). Pressure Contours (shaded) with Helium Mass-Fraction Contours (black lines on left) and Velocity Streamtraces (white lines on right) for Seven Different Crossflow Planes for the Nine-hole Injector Array.

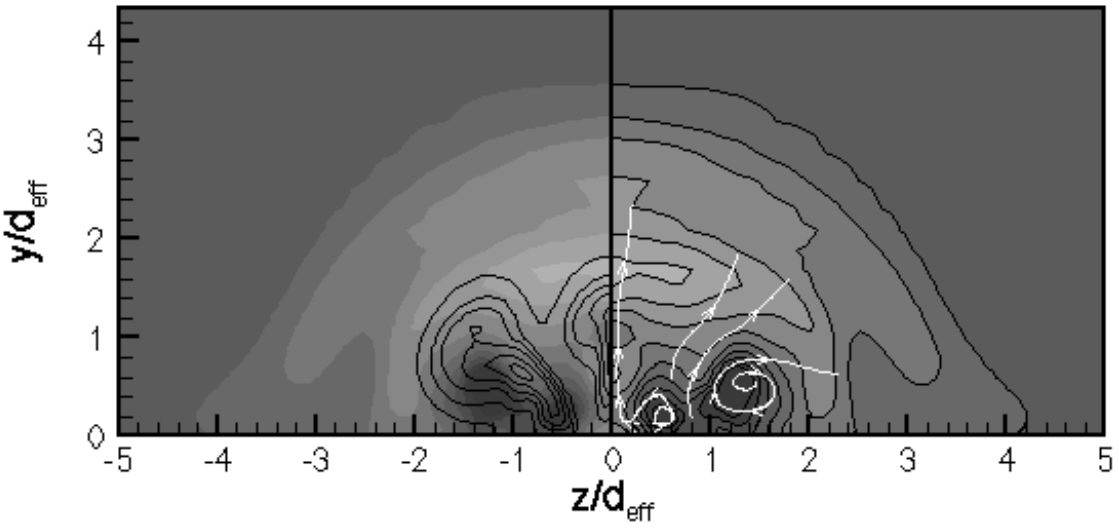

(d) Station 4, $x/d_{eff} = 3.55$

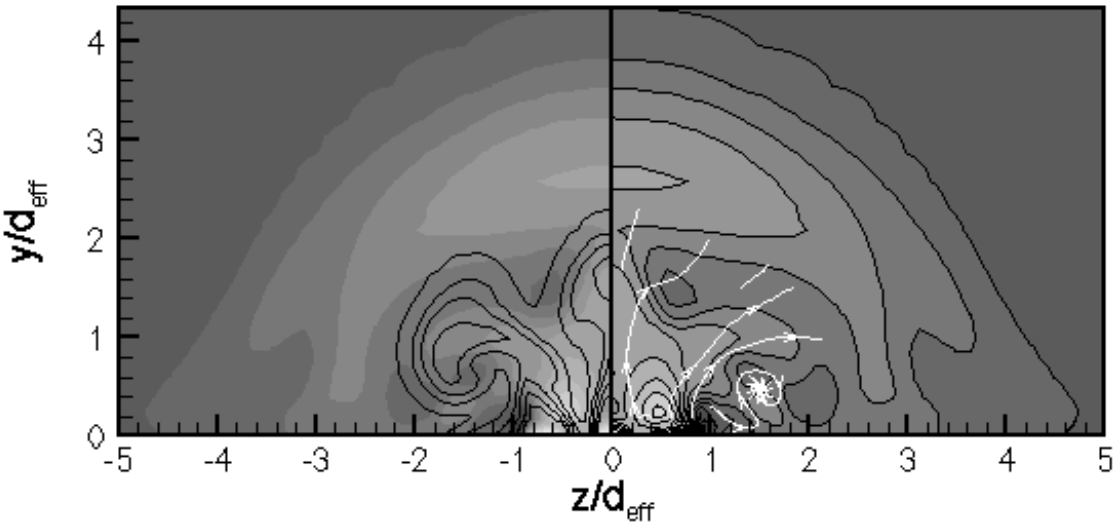

(e) Station 5, $x/d_{eff} = 4.66$

Figure 7.10 (Continued). Pressure Contours (shaded) with Helium Mass-Fraction Contours (black lines on left) and Velocity Streamtraces (white lines on right) for Seven Different Crossflow Planes for the Nine-hole Injector Array.

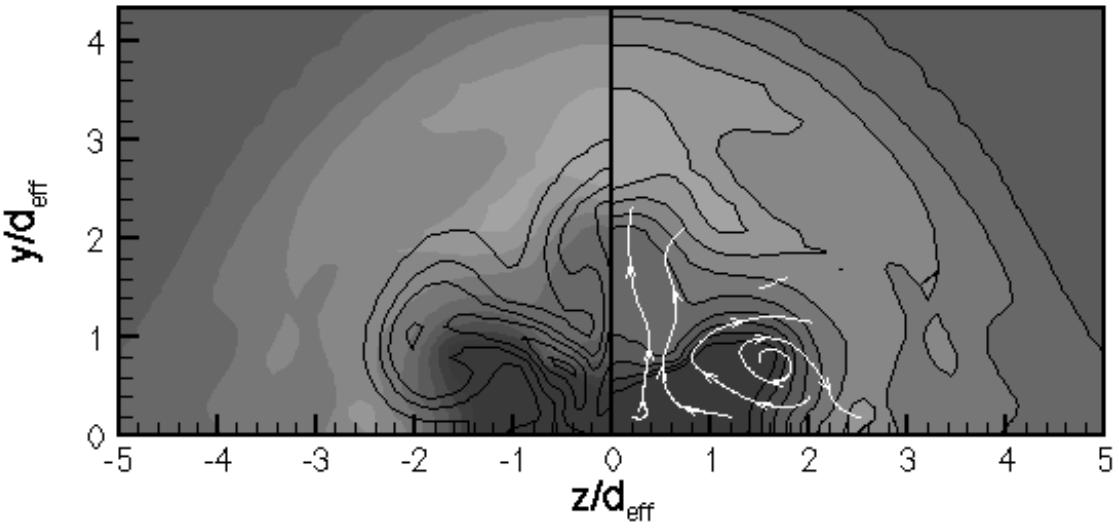

(f) Station 6, $x/d_{eff} = 6.00$

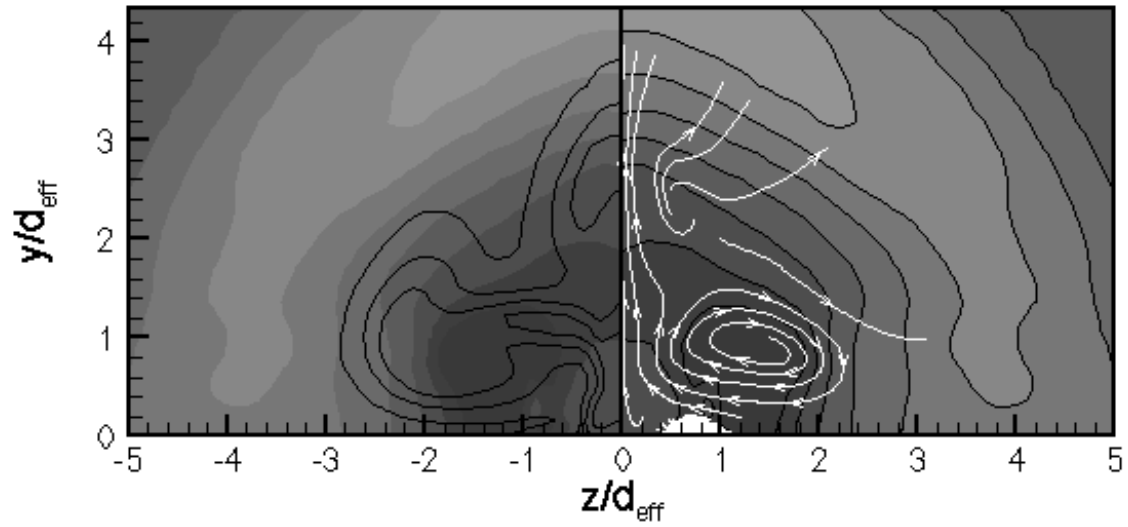

(g) Station 7, $x/d_{eff} = 8.00$

Figure 7.10 (Continued). Pressure Contours (shaded) with Helium Mass-Fraction Contours (black lines on left) and Velocity Streamtraces (white lines on right) for Seven Different Crossflow Planes for the Nine-hole Injector Array.

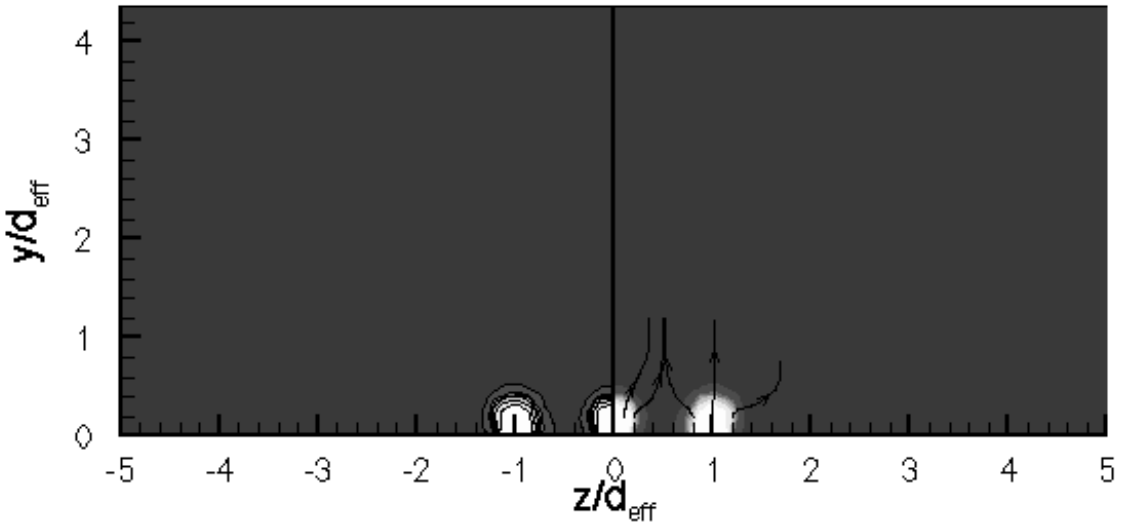

(a) Station 1, $x/d_{eff} = 0.00$

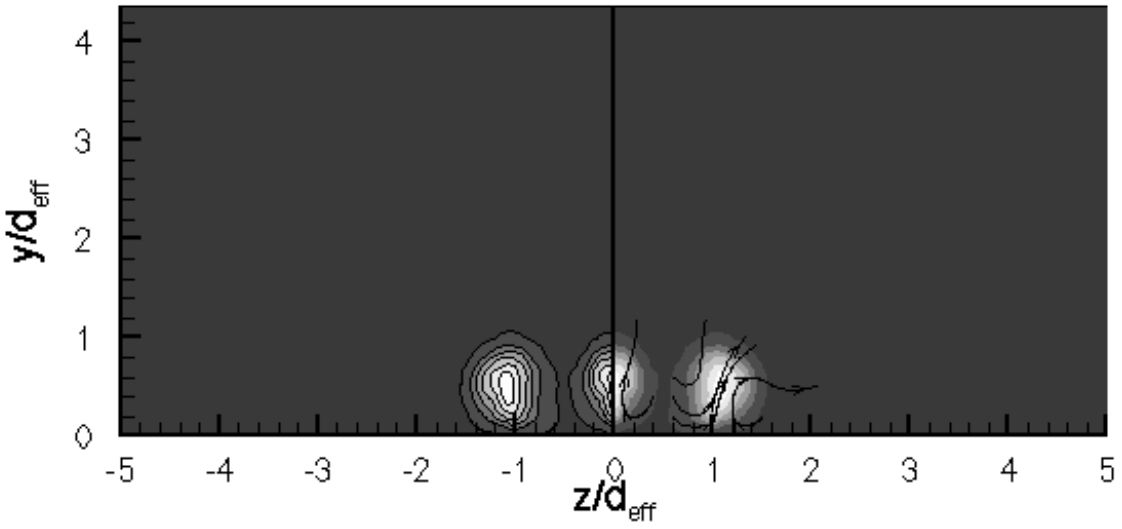

(b) Station 2, $x/d_{eff} = 1.32$

Figure 7.11. Helium Mass-Fraction Contours (shaded) with Helium Mass-Fraction Contours (black lines on left) and Velocity Streamtraces (black lines on right) for Seven Different Crossflow Planes for the Nine-hole Injector Array.

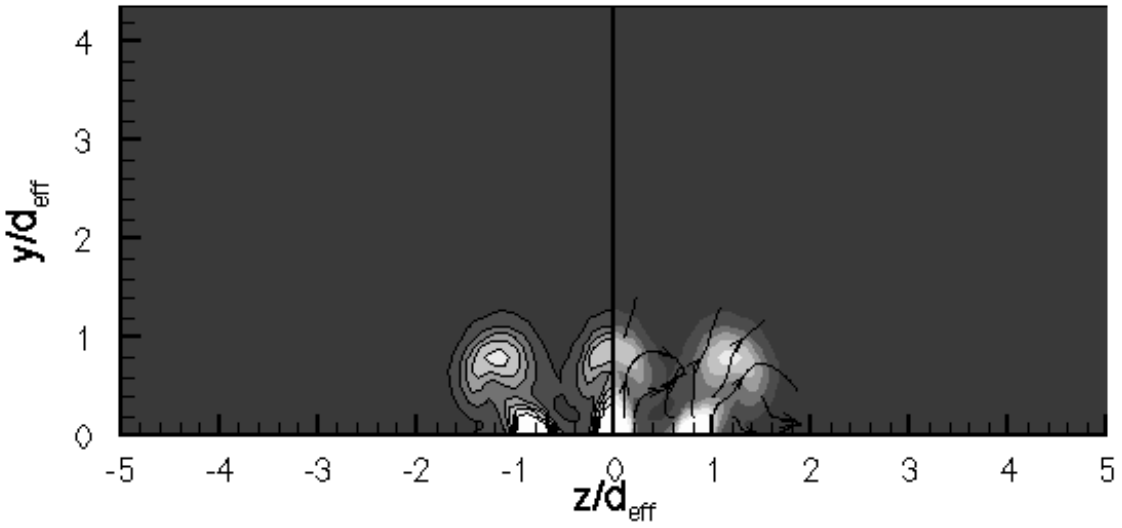

(c) Station 3, $x/d_{eff} = 2.33$

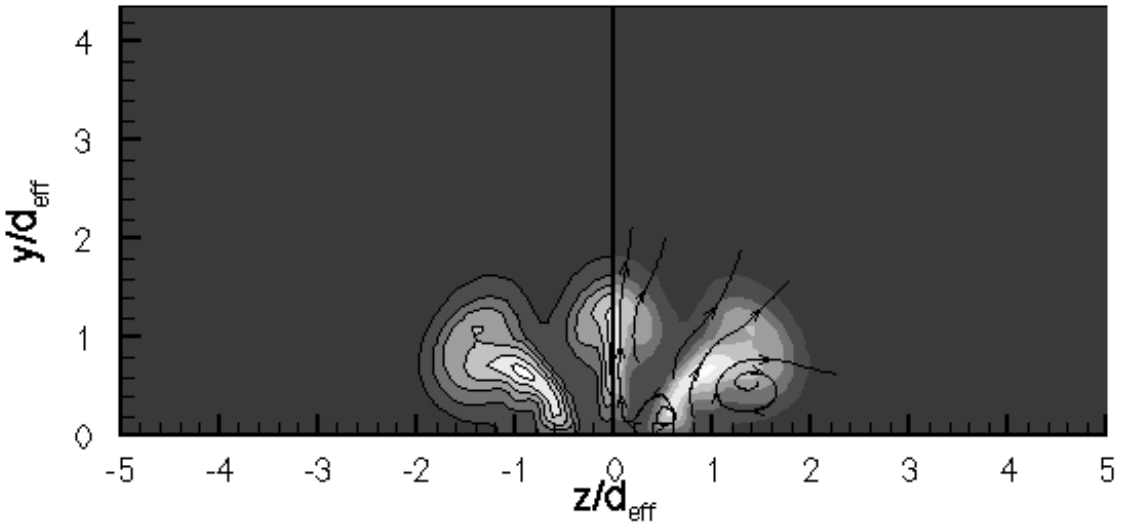

(d) Station 4, $x/d_{eff} = 3.55$

Figure 7.11 (Continued). Helium Mass-Fraction Contours (shaded) with Helium Mass-Fraction Contours (black lines on left) and Velocity Streamtraces (black lines on right) for Seven Different Crossflow Planes for the Nine-hole Injector Array.

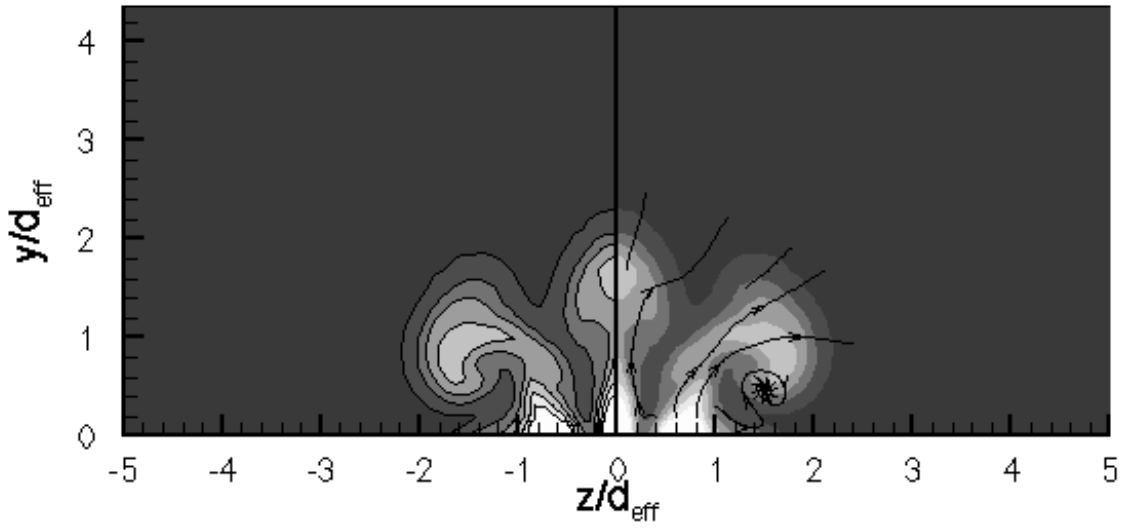

(d) Station 5, $x/d_{eff} = 4.66$

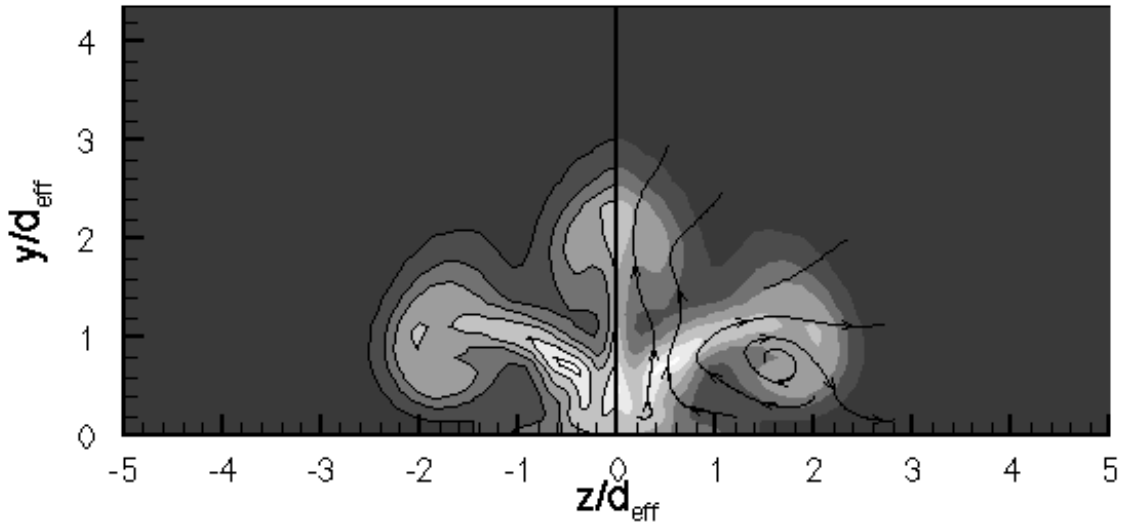

(f) Station 6, $x/d_{eff} = 6.00$

Figure 7.11 (Continued). Helium Mass-Fraction Contours (shaded) with Helium Mass-Fraction Contours (black lines on left) and Velocity Streamtraces (black lines on right) for Seven Different Crossflow Planes for the Nine-hole Injector Array.

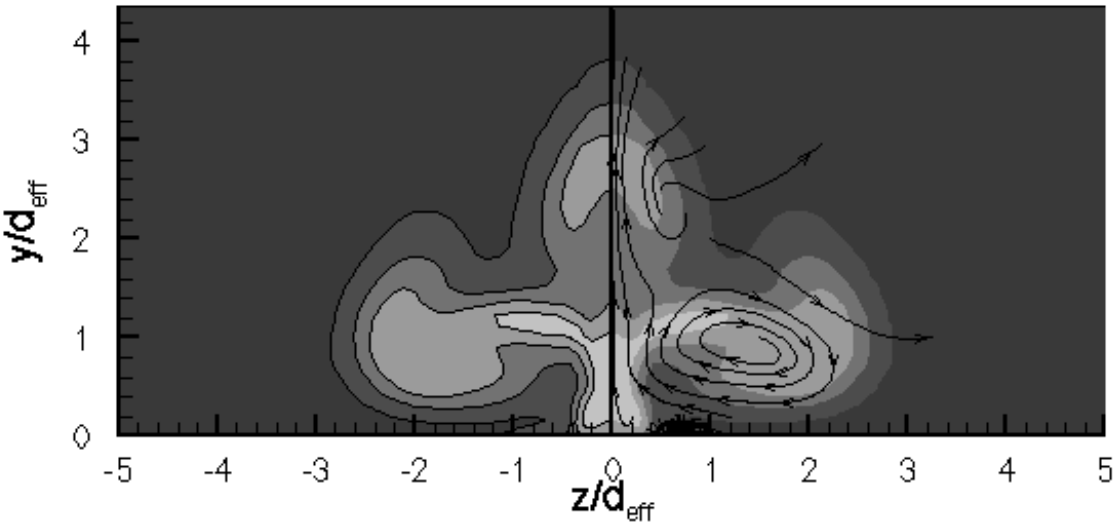

(g) Station 7, $x/d_{eff} = 8.00$

Figure 7.11 (Continued). Helium Mass-Fraction Contours (shaded) with Helium Mass-Fraction Contours (black lines on left) and Velocity Streamtraces (black lines on right) for Seven Different Crossflow Planes for the Nine-hole Injector Array.

semicircular shock weakens and dissipates in the boundary layer before it reaches the wall. On the inside, the high pressure band that marks the shock has three changes in curvature. Centered above each injector is a sharp increase in pressure, caused by the interaction of the injectant helium with the shock itself and by the resultant flow turning. (Notice on the left side of Figure 7.10 how the regions of higher pressure within the shock bands coincide with the upper reaches of the helium mass-fraction contours.) Similar pressure increases have been seen in other figures. Between the two helium plumes is a more moderate and gradual increase in pressure, the natural extension of the bow shock into the spanwise interplume channel.

The helium mass-fraction contours themselves are clearly visible on the left in Figure 7.10 and in Figure 7.11. At this early

stage in the streamwise development of the flow, very little penetration has occurred. Notice that once again the contours associated with the outer plume are not symmetric but have their greatest spanwise extent near the lower wall on the centerward side and near the top of the plume on the outside. The centerline plume is wider at the top than at the bottom, indicating that expansion has already begun.

The right-hand side of Figure 7.11 show the same mass-fraction contours coplotted with velocity streamtraces. Though little detail is visible at this point, the streamtraces originating within the centerline plume and on the centerward side of the outer plume are more vertical (i.e., show less horizontal expansion) than those of the outside of the outer plume. Thus there is evidence that the outer side of the outer injector experiences more spanwise expansion than either the centerward side of the same injector or the centerline injector itself. The coplotting of pressure with streamtraces in Figure 7.10 is also revealing. Notice that within the outer pressure contour of the bow shock many of the streamtraces have strong horizontal components, but above it they are all vertical. This indicates, as one would expect, that the bow shock forms a neat division between the flow influenced by the presence of the injectors and the undisturbed air of the freestream.

Station 2 is located midway between the first and second rows of injectors, in the region previously described as the interplume region. At this location the mixing area is quite complicated but also quite compact, so that enlargements are useful. Figures 7.12 and 7.13 provide such enlargements, and will be referenced along with Figures 7.9 through 7.11 The helium mass-fraction contours plotted in Figures 7.11 and 7.13 show that the innermost mass-fraction contours of the centerline plume become narrow and cease to exist as they approach the lower wall, driven by the adverse pressure gradients ahead of the second-row injector as described in the discussion of Figures 7.1 through 7.3. Above that level the centerline mass-fraction contours are smooth and rounded, suggesting that the

adverse pressure gradient that causes the helium to attenuate is not present at higher levels. The pressure contours in Figure 7.9 and 7.12 confirm that a small region of higher pressure exists at the wall itself, above which lower pressure reaches in a band outward from the centerline. This region of lower pressure coincides with a sharp increase in the concentration of centerline-injector helium, as one would expect. Comparison with Figure 7.1 shows that the low pressure region is part of the overall wake structure downstream of the first row of injectors, driven partly away from the centerline by the adverse pressure gradient ahead of the second-row centerline injector. Following the wake away from the centerline itself, one identifies a region of rather low pressure close to the lower wall, part of the wake region. Streamtraces in this low-pressure region are angled downward and inward, through the wake, and then turn up toward the low pressure region on the centerline. Above the region of low pressure on the centerline is a well-formed lobe of higher pressure, the recompression region shock/expansion theory predicts for an underexpanded jet. Within the lobe of pressure (centered approximately half an effective diameter above the lower wall) the streamtrace is nearly vertical, but at slightly higher points the flow begins to expand again. Figure 7.11 shows that the widening of the helium plume coincides with this turning of the streamtraces, as expected. The upper levels of the helium plume intersect the lower reaches of the high-pressure bow shock (as seen in Figure 7.10 on the left), and the pressure contours do show mild changes in curvature at the points of intersection, indicating a degree of interaction between the bow shock and the plume itself.

The bow shock itself has changed shape between the previous station and this one. Instead of two intersecting semicircles, it is now shaped like one quarter of a broad oval (in the half-plane, or one half a broad oval, considering symmetry), with no discernible indentation between injectors. This change identifies a blending of the pressure effects of the two separate injectors as the shock structure expands and propagates downstream, though their helium plumes are still

quite distinct. Indeed, pressure bands at the point of intersection of the two shocks are slightly wider than they are above the injectors themselves, creating a faint dip in the shock at the centerline. Once again the pressure decreases and the shock weakens before reaching the lower wall. The outermost plotted pressure contour, a somewhat arbitrary measure of shock penetration, crosses the centerline approximately two effective diameters above the lower wall and at its widest point reaches three effective diameters from the centerline.

The most important feature of the pressure field associated with the outer injectant plume is a region of rather low pressure, which reaches from the lower wall approximately three quarters of an effective diameter into the flow. It is clearly visible in Figures 7.9, 7.10 and 7.12. The low pressure region is not centered downstream of the center of the injector, but extends further to the outside than it does centerward. No doubt the asymmetry is the result of the channel of relatively undisturbed air that continues to flow between the outer and centerward injector and of the relatively high pressures created by the streamwise extension of the bow shock into this channel. (See Figure 7.6.) There is an indentation in the top of the outer injector's low pressure field, and above it a narrow, short extension of a higher pressure contour. That high-pressure extension in the middle of a low-pressure helium plume is a feature identified in a number of planes of Figure 7.6, and it will require considerable analysis. That analysis will begin with the following.

The low-pressure area that dominates the lower regions of the outer injectant plume likely has two causes. First is the expansion of the first-row injectant plume, which should have its greatest influence some distance above the lower wall at this point, as it does for the centerline injector. Second is the wake effect produced by the shelter the first-row injector provides for the flow just downstream of it. Because the low-pressure area encompasses regions of low and high helium concentration, it is likely that both processes contribute to the pressure field. (A theory supported by

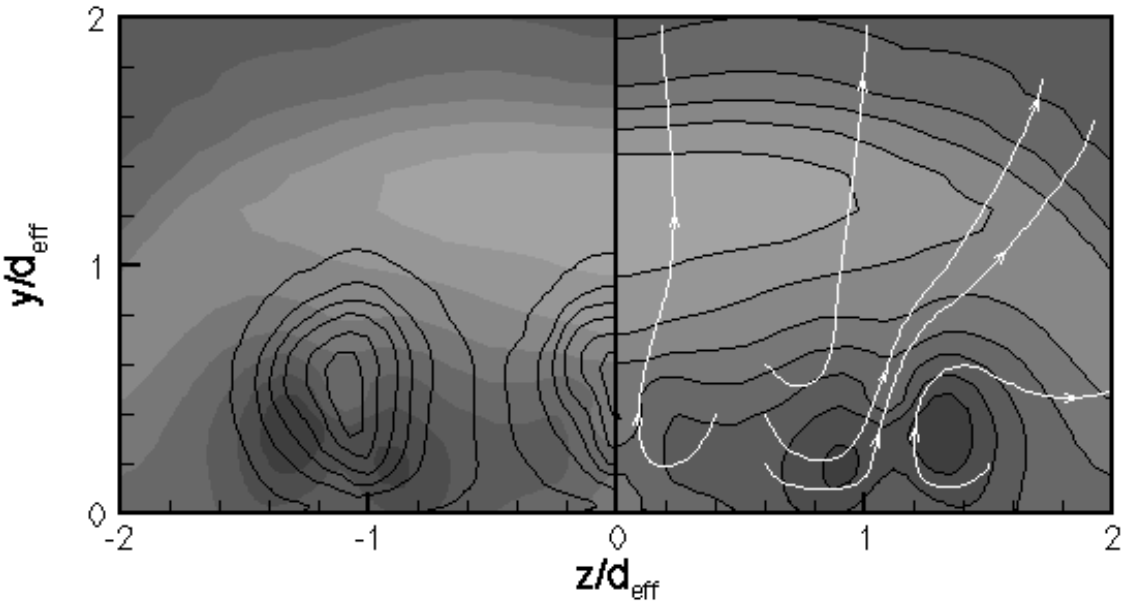

Figure 7.12. Enlargement of Pressure Contours (shaded) with Helium Mass-Fraction Contours (black lines on left) and Velocity Streamtraces (white lines on right) at Station 2, x/d_{eff}= 1.32.

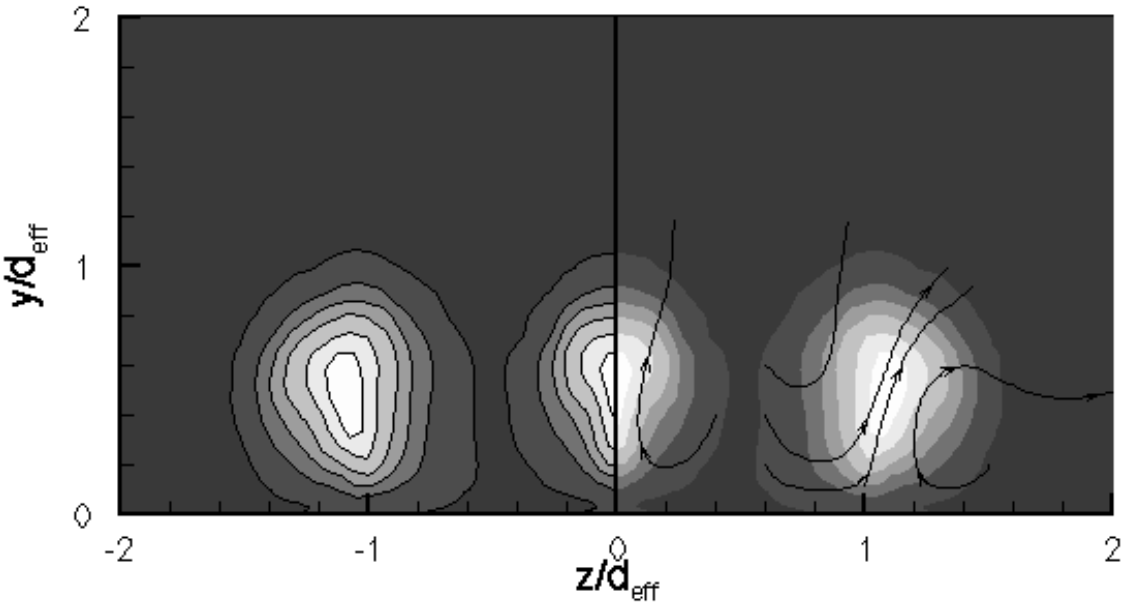

Figure 7.13. Enlargement of Helium Mass-Fraction Contours (shaded) with Helium Mass-Fraction Contours (black lines on left) and Velocity Streamtraces (black lines on right) at Station 2, x/d_{eff}= 1.32.

many of the figures presented and discussed above.) This low-pressure field extends toward the centerline as discussed above, but weakens somewhat in the interplume channel, influenced by the remains of the high-pressure system that dominated the interplume channel upstream. Above the low-pressure area are higher pressures caused by the upper remains of the bow shock, which cut through the helium plumes and the interplume channel and bend downward around the outside of the plume and the low-pressure area as discussed above.

Turning attention once more to helium mass-fraction contours, as seen in Figures 7.11 and 7.13, one notices an interesting pattern in the interaction of helium mass-fraction and streamtraces. All of the streamtraces originating between the centerline and outer helium plumes drop toward the lower wall before curving into one or the other of the plumes, indicating entrainment of air into the injectant plumes. Comparison with the pressure contours in Figures 7.10 and 7.12 shows the entrainment is driven by pressure gradients, with air drawn toward the wall and toward the center of the injectant plume by the low pressure region identified earlier. The uppermost streamtrace of the figures, having its origin at $y/d_{eff} = z/d_{eff} = 0.6$, does not behave exactly as the others. Originating in a region of higher pressure, it dips only slightly before turning upward into the bow shock. Careful observation of the left half of Figure 7.12 reveals that the outer helium plume extends slightly higher on this centerward side and overlaps a region of higher pressure. One possible explanation is that the helium in this portion of the plume interacts with the bow shock and is drawn upward with it, into the space being created by the upward movement of the shock-induced high pressure.

Closer to the lower wall, both Figures 7.12 and 7.13 show that streamtraces in the interplume channel near the outer plume are drawn sharply downward and away from the centerline, toward the near-wall region of the outer plume itself. Thus fluid is entrained along the bottom of the region of low pressure, and flows along the

wall toward the center of the low pressure, beneath the helium plume. On the outside of the plume air is also being entrained along the wall by the low pressure. In addition to the stream traces, the presence of entrained air can be identified in any of the Figures 7.10 through 7.13 by the lifting of all but the lowest-level helium mass-fraction contours off the lower wall. Indeed, the innermost contour remains approximately four tenths of an effective diameter above the lower wall at its lowest point.

The unique features of the pressure contours associated with the outer helium plume can be explained in the following manner: Air flowing inward from each side of the injectant plume has velocity primarily in the spanwise ("z", or horizontal in Figures 7.9 through 7.13) direction (at least when considering flow in the z-y plane. It also has a strong streamwise ("x") component.) When the inflowing air from each side of the plume collides with its opposite most of its spanwise velocity is lost. The sudden decrease in velocity would cause a sharp increase in pressure at the intersection point, were not the air streams able to turn and to flow vertically into the center of the low-pressure area. Indeed some increase in pressure is recorded in the contours at the intersection point, but the upward turning of the air streams no doubt relieves much of the pressure. As they turn they must displace some of the helium, which process itself tends to increase pressure along the path of the entrained streamlines in Figure 7.13. The effect is most noticeable at the top of the low-pressure area, where the helium pressure itself is higher and the pressure contour has an indention to indicate the higher pressure of the helium/air interaction. The second pressure contour has a very narrow band of elevated pressure that protrudes downward into the interaction area, suggesting that the interaction area itself is very narrow. Notice that the path of the entrained air indicated by the streamlines passes directly through the band of highest pressure. Another evidence of this entrainment path is the faint indentation visible at the bottom of the helium mass-fraction contours between the turning streamtraces, roughly $1.1d_{eff}$ from the centerline. Not

only does this data explain the higher pressures at the “notch” in the first-row helium plume in the lower planes of Figure 7.6, it explains the notch itself and establishes a pattern which, according to Figure 7.6, will probably be repeated downstream of the second-row injectors.

The streamlines in Figure 7.13 do provide a great deal of information about the shape of the helium plume at Station 2. Notice that the path is not exactly vertical, especially near the top of the helium plume. Instead, the entrained air bends outward, as does the rest of the helium plume at that location, passing through the weaker, outer edge of the bow-shock pressure region and avoiding the highest pressures, which lie higher and closer to the centerline. The path of the outermost streamline suggests the presence of a small vortex, which center would seem to be approximately one and a quarter effective diameters from the centerline and a little less than half an effective diameter above the lower wall. It exists at the junction between the inflowing fluid near the wall and the expanding, outflowing fluid at higher levels. This vortex is strengthened by the centerline injector, which presence strengthens the bow shock and raises the pressure above and centerward of the outer plume, leaving little opportunity for expansion other than on the outside of the plume, above the vortex. It is exactly through this quarter that the entrained air flows. The outer helium plume can then be divided into three parts: the entire lower portion, which is an entrainment region of low pressure, the outside upper portion, where the entrained air and helium curve outward to avoid the highest pressures associated with the bow shock above, and the upper/centerward lobe, where the fluid is drawn upward into the space created by the upward travel of the shock-induced high pressure system.

Given this understanding of the entrainment of air into the outer helium plume, the shape of the helium plume itself is now easier to explain. The indentations in the bottom of the inner contours are actually a two-dimensional representation of a three-

dimensional air pocket formed by the upturn of entrained air. It appears as a notch in both x=constant planes (Figures 7.10 through 7.13) and y=constant planes (Figures 7.6 and 7.7). The spanwise placement of the air pocket is in the center of the low-pressure region but not in the center of the helium plume, which results in the unequal tails of the contours on either side of the notch, as seen in Figures 7.6 and 7.7. The reason for the asymmetry of the plume itself is probably the asymmetric pressures that surround it. Higher pressures in the interplume channel centerward of the plume, especially closer to the leading edges of the injectors, drive and/or drove the plume outward.

Station 3 is $2.33d_{eff}$ downstream from the center of the first row of injectors and at the center of the second row of injectors. As seen in Figure 7.10, it is a region of complex pressure and helium patterns. The higher planes of Figure 7.6, shown in planes “c” through “e”, confirm that the large outer region of high pressure at Station 3 is still a part of the bow shock from the first row of injectors. Its shape here is nearly that of a quarter of a circle (a half a circle, considering symmetry) with a radius of approximately three effective diameters. The pressures within the bow shock are lower at this point, as it is beginning to dissipate. Once again the pressures that mark the shock weaken some distance above the wall.

Within the shock are the complex overlapping patterns of helium concentration and pressure that show the behavior of the second-row injector plumes and the continued downstream development of the first-row plumes. Though many of the patterns are present in Figures 7.11, they are most evident in Figure 7.10. Along the lower wall are two sets of small, high-pressure bubbles like the ones at Station 1 that mark the inflow of unexpanded helium from the injectors. The outer high-pressure bubble appears to have its center just less than one effective diameter from the centerline, a little to the outside of the injector center at $z=0.83d_{eff}$ but very well aligned with the innermost helium mass-fraction contours on the left side of Figure 7.10. The explanation lies in the fifteen degree inward

yaw angle of the outer, second-row injector, which causes the upstream end to extend further from the centerline than the injector's streamwise center. The off-center, high-pressure helium bubble observed in Figure 7.10 indicates the downstream penetration of the unexpanded helium from the upstream end of the injector past the bounds of the injector itself along the wall.

Above each high-pressure bubble is a small region of lower pressure as the injectant helium begins to expand. For the outer injector this lower pressure region is weak and very asymmetrical, with lower pressure on the outside and another, much larger region of high pressure almost adjoining the high-pressure bubble on the centerward side. This large high-pressure region dominates the channel between the centerline and outer plumes and is itself a part of the second-row bow shock. As discussed in connection with Figure 7.6 (particularly planes “a” and “b”), the second-row bow shock has its strongest point on the centerward side of the outer injectant plume, where the yaw angle of the injector provides a larger surface area and the inward displacement of the outer injector relative to that of the previous row reduces the sheltering effect of the first-row injectors. The shock itself is seen as a steep pressure gradient at the upper edge of the high-pressure region. Notice that the shock is not horizontal, but is slightly higher on the outer edge. This shape is a consequence of the three-dimensional nature of the shock itself. The upstream edge of the second-row injector is further from the centerline than any other point, owing to the yaw, and the path that follows the upstream edge toward the centerline moves steadily downstream as well. Therefore, the supersonic flow upstream encounters the injector first at the outside, allowing the outside edge of the shock to penetrate further into the flow at any streamwise station. Since the centerward edge of the shock has its beginning at the wall (like the outer edge) but further downstream than the outside edge, it will remain closer to the wall at every streamwise location.

The centerline plume has a small area of moderate pressure above the low-pressure expansion region, between $0.4d_{eff}$ and $0.6d_{eff}$ above the lower wall. Comparison with Figure 7.1 indicates that this moderate pressure is a part of the diffuse "bow shock" that forms on the leading edge of the second-row injector. Notice that the higher-valued contours of helium mass fraction surrounds all the pressure contours near the wall, indicating that the second-row injectant plume is instrumental to the pressure field in this region and penetrates nearly eight tenths of an effective diameter above the lower wall at this streamwise location. Just above the upper extent of the second-row injectant plume (roughly one effective diameter from the lower wall) is another area of elevated pressure. This region of high pressure is roughly semi-circular and rather clearly formed, with the highest pressure occurring near the intersection of the lower and upper bands of purer helium. See Figures 7.9 and 7.10. Figures 7.1 and 7.6 identify the crescent-shaped helium contours in this upper region as the remnant of the first-row centerline helium plume, driven upward and away from the centerline by increasing pressure ahead of the second-row injector, since the pressure is higher close to the lower wall. The high pressure that occurs at the point of intersection between the helium plumes has already been determined in the same figures to result from the interaction and turning of the two plumes. The lowest-level (outermost) helium contours that surround the centerline plume at Station 3 encompasses both the first-row plume and the fresher, second-row plume without distinction.

Within the contours of the outer injector plume at Station 3 lie the keys to the understanding many of the flow features considered problematic in the first two planes of Figures 7.6 and 7.7. Notice again the streamwise notches in the midvalue helium contours corresponding to the outer, first-row injector in Figure 7.7 planes "a" and "b". The data presented at Station 2 in Figures 7.9 through 7.11 and again in the enlargements, Figures 7.12 and 7.13 connect the notch in the helium contours with the inflow and rise of air from the

wall region on either side of the plume. Notice that the injectant helium from the second injector connects with centerward fork in the first-row plume, and that the first-row outer plume itself is forced outward, around the second injector. Notice also that the helium "ribbon" which extends from the outer tail is much narrower and lower-valued in the first and second-row portions of plane "a" of Figures 7.6 and 7.7 than in the corresponding portions of plane "b", which suggests that the helium plume is forced upward by the pressure rise associated with the second-row injectors and/or by its own vertical momentum. The helium mass-fraction contours in the outer plume at Station 3 in Figure 7.11 confirm this hypothesis by showing that the faint indentations visible at Station 2 near the lower wall have become significant notchs nearly half an effective diameter or more above the lower wall at this point. At the streamwise location shown at Station 3 in Figures 7.9 through 7.11, the fresh helium from the second-row outer injector exists as a mass completely separate from the high-level contours that remain from the first-row plume. Though the injector itself is angled centerward by fifteen degrees, the high pressures in the interplume channel drive the new helium outward, toward the low-pressure notch created by earlier entrainment. See the right-hand sides of Figures 7.10 and 7.11. The streamtraces shown in Figure 7.11 show that the outer parts of the new helium plume (near $z/d_{eff} = 1.0$) are being driven directly toward the highest part of the notch, where they will soon come into contact with the helium from the first-row plume. It is almost certain that the shape and position of the notch will be changed by the addition of the new helium stream.

The innermost contour of first-row helium in the outer plume has greatly changed shape between Station 2 and Station 3. The entrained air that created only a small indentation in the apple-shaped contour at Station 2 has now consumed the bottom half of the contour and formed a large, rounded vacancy in the center of the remaining portion. It is noteworthy that the centerward end of the curving contour is higher above the lower wall than the outer end,

even though plane “a” of Figure 7.7 shows that the centerward end of the contour remains close to the lower wall for a longer streamwise distance. The reason for the sudden change is probably the second-row bow shock, which is quite strong and directly in the path of the centerward end of the contour, forcing it to rise suddenly above the high-pressure field.

The most unique feature of the pressure field in and around the outer injectant plume at Station 3 is the presence of two distinct shocks. The outermost pressure contours have already been identified as the weak remnant of the first-row bow shock, but the second-row bow shock plays an important role as well. Figure 7.6 shows in planes “a” through “c” that the highest pressures of the second-row bow shock occur in the channel between the centerline and outer injectant plumes, with decreasing pressure through the outer plume itself then another high-pressure band on the outside where the second-row bow shock angles downstream. Station 3 of Figures 7.9 and 7.10 clarifies the matter by showing that an area of low pressure exists near the lower wall and just outside the second-row outer injector. It is almost completely surrounded by bands of higher pressure, most of which are parts of the second-row bow shock. Centerward is the region of highest pressure, corresponding to the strongest part of the shock and the interaction and turning of the fresh, high-pressure injectant helium. The left-hand side of Figure 7.10 shows a sharp decrease in helium mass fraction at the edge of this high-pressure region, suggesting very little penetration of second-row plume has occurred and confirming the streamtraces on the left side of the figure, which angle centerward and/or upward, around the high pressure channel rather than into it. Comparison with Figure 7.11 shows that some of these streamtraces are driven beneath the high pressure into the low-helium interplume channel, where they intersect streamtraces from the centerline plume, and the others move more vertically through the outer plume itself. Once within the first-row helium plume, these more vertical streamtraces bend outward, as at the previous station, but do not appear to wrap

around a vortex as they did upstream. The outward and downward path of the outermost streamtraces (where inflowing streamtraces existed at Station 2) suggest that the vortex identified upstream has been substantially weakened, if not completely destroyed, by the effects of the second-row injectors. There is still a region of elevated pressure at the intersection of the first-row helium mass and the vertical flow of entrained fluid, though it is weaker and less clearly formed than it was at the previous station. The most likely cause of this high pressure is the loss of vertical velocity that occurs when the entrained fluid interacts with the original plume. The elevated-pressure spot here is therefore at least similar to and probably an extension of the narrow high-pressure neck seen in the interaction region at Station 2, though it could also be strengthened by the formation of the second-row bow shock.

Notice that centerward of and just above the high-pressure bow shock and inward of and above the outer injector plume is a large region of lower pressure. According to Figure 7.6 plane "c", this low pressure is the downstream end of the wake region between the first and second rows of injectors, present at this streamwise location only above the beginning of the second-row bow shock and beneath the first-row bow shock (visible at this location in Figure 7.6 planes "d" and "e"). Between the two high pressure systems lies the upper/centerward lobe of the first-row helium plume, as discussed above. Herein lies a more complete explanation for the vertical velocity of the fluid in the upper/centerward lobe of the first-row helium plume. Careful examination of Figure 7.10 shows that the upper/centerward lobe lies sandwiched between the elevated pressures of the outer, downstream extension of the first-row bow shock on the outside and the high-pressure, second-row bow shock beneath, at the location of the low-pressure wake. In order to blend smoothly with the rest of the helium plume (which still has a strong horizontal component in its upper regions, as discussed above) the fluid within the lobe would have to develop a much stronger outward (horizontal) component, which would carry it away from the

low-pressure wake toward the high pressure of the entrainment region. Because this cannot happen, the upper/centerward lobe is forced to flow almost vertically, along the wake itself, in a path quite distinct from that of the rest of the helium plume.

Station 4 is located midway between the second and third row of injectors, 3.55 effective diameters downstream from the center of the first row. The state of the flow is in many ways similar to that at Station 2, except that at Station 4 the flow is influenced by all three rows of injectors, including the last row downstream. The centerline features a region of moderately low pressure near the lower wall, which Figure 7.1 identifies as the second interplume region. There is one triangular band of moderately low pressure that begins at the lower wall and ends in a point a little more than two tenths of an effective diameter above it. The pressure here is held above that of its surroundings by the subsonic flow identified in Figure 7.4, which allows upstream propagation of the third-row injectors' pressure field. Just at the upper edge of the wall-region pressure contour is a tiny area of lower pressure that extends to the centerline from the channel between the centerline and outer injectors. Figures 7.1 and 7.3 identify this lower pressure with the last, downstream vestiges of the second-row centerline plume's first major expansion, and Figure 7.6 plane "a" confirms that the low pressure region created by the centerline expansion does indeed connect, albeit weakly, with the general wake that exists between the second and third rows of injectors. Above the low-pressure expansion region is another, larger area of elevated pressure. This one is identified by two pressure contours, one a moderate-level contour that connects to the generally elevated pressures created by the bow shocks and overlaying the entire injector area like a blanket, and the other a higher-level pressure contour on the centerline within it (the latter being very small and only faintly visible in Figures 7.9). According to Figure 7.3, this area of elevated pressure is the downstream tip of the first recompression associated with the second-row, centerline injector. Careful examination of Figure 7.11 reveals that the bottom

of the second-row injectant plume, which passes through this near-wall region but remains above the wall itself, is elevated along the centerline, where pressures are highest, but that its outer edges trail lower where pressures are lower, suggesting that the upstream pressure influence of the third row of injectors is weaker away from the centerline.

The presence of reversed flow between the second and third rows of injectors fundamentally alters the analysis of data presented in the figures labeled Station 4. While the performance of the first row of injectors might be meaningfully discussed with little concern for the second row of injectors, the presence of reversed flow in the region between the second and third rows of injectors implies that the performance of the second row of injectors cannot be meaningfully discussed independently of the third row. (See Figures 7.2 plane "a" and 7.3 plane "a" for streamtraces identifying reversed flow.)

As discussed above, the midlevel contours associated with the second-row centerline plume have at their bottom edges a region of interaction with the reversed flow from the third-row centerline injector. Above the interaction region the second-row helium contours are surprisingly vertical, with no spanwise expansion at all. Indeed, the plotted streamtraces show the flowpath contracting as fluid rises along the centerline. Around one and a half effective diameters above the lower wall the helium contours suddenly branches outward like a mushroom, as the nearly vertical flow of helium from the second-row injector intersects the more expanded but still helium-rich mixture of the first-row plume. It is interesting to note that even this interaction does not cause substantial deviation of the streamtraces near the centerline from their vertical paths; instead, the centerline portions first- and second-row plumes merely move upward together. (See the streamtraces in plane "a" of Figure 7.2, which indicates that by this streamwise location the first-row plume has already adjusted to the more vertical path of the second-row plume and in the centerplane is almost indistinguishable from

it.) The pressure near the bottom of the intersection region on the centerline is relatively low, and a low-pressure region dominates the center of the well-expanded first-row plume, but the pressure becomes higher near and above the top of the helium mass-fraction contours in Figure 7.10. The pattern is explained by Figure 7.1, which connects the region of low pressure with the second expansion of the second-row centerline injector (following the basic pattern of expansion and recompression of an underexpanded jet) and the higher pressure above it with the last vestiges of the high pressure system created by the interaction and turning of the first- and second-row helium plumes. Notice the changes in curvature that occur in the pressure contours when they intersect the edges of the helium plume. Clearly there is an increase in pressure due to the presence of the plume. Notice also in Figure 7.10 that only within these contours of higher pressure do the centerline streamtraces begin to expand. Spreading of the outer edges of both the first-row and second-row centerline plumes is well underway, however, and all distinctions the lower-concentration contours once made between the separate plumes of the first two centerline injectors has been lost by this station. The joined c_{He}=0.25 contour is shaped rather like a lightbulb, with its widest point a little more than one effective diameter above the lower wall.

Higher above the centerline injectant plume, roughly three effective diameters from the lower wall, the weaker effects of the first-row bow shock can still be seen in pressure contours. Pressures within this bow shock are substantially lower than they were at the previous station, but the outermost contour in Figure 7.9, still forms an acceptable divider between the outer flow which is unaffected by the presence of the injectors and the inner flow, which is disturbed by them. This outer contour crosses the centerline approximately three and a half effective diameters from the lower wall, and at its widest point it reaches approximately four effective diameters from the centerline. Even more than at earlier stations, the higher pressures of the first-row shock weaken away from the centerline, so

that the innermost two contours exist only above the main mixing area and do not wrap around the sides. The peculiar, inverted-triangle appendage at the top of the contour near $y/d_{eff}=2$ can be identified in Figure 7.3 as a last remnant of the first-row bow shock, which is just intersecting the second-row pressure system at this location.

The dominating feature in the outer, lower part of the flow at Station 4 is the low-pressure area that exists downstream of the second, outer injector. Within the low-pressure region the processes that drive the flow are the same ones that created the flow features identified at Station 2. Air from either side of the injectant plume is drawn inward by the low pressure, intersects near the center of the helium plume, turns, and moves upward, producing the centerward notch in the outer helium mass-fraction contours and the lobe of higher pressure located just above it, as shown in Figures 7.10 and 7.11 and previously identified in planes “a”, “b”, and “c” of Figure 7.6. The larger, outer notch is similar to the one created in the first interplume region (shown at Station 2). Its shape is the consequence of a number of factors: first, the entrainment of air from the wall region on the outside of the injector into the plume itself, which reduces the helium concentration near the wall; second, the high pressure above the plume, which turns the rising fluid outward and bends the plume toward the horizontal; and third, the intersection of the first and second-row helium plumes, which creates another faint change in the curvature of the helium plumes roughly $1.2d_{eff}$ from the centerline. Once again the entrainment process is strong enough to keep higher concentrations of helium nearly four tenths of an effective diameter above the lower wall for half the width of the outer plume, despite the presence of the high pressure region above the plume.

(Though Station 4, at $x/d_{eff}=3.55$, is located slightly upstream of the unexpected behavior of the Mach contours seen in Figure 7.5, the proximity is close enough for a brief attempt at explanation. Considering the strength of the entrainment mechanism described

above and its influence on pressure and composition, particularly in the area roughly one effective diameter from the centerline and half an effective diameter above the lower wall (as seen in Figures 7.6 and 7.7), and considering the low helium mass fractions in the separating, supersonic band, it is likely that this flow turning mechanism is in some way responsible for the unexpected Mach number data. One possibility is that the entrained fluid, which is mostly air, accelerates as it is drawn inward.)

The vortex that earlier seemed to be destroyed by the second-row injectors has reappeared at this station, and seems at least as well-formed as it was at Station 2. The center itself is located very close to a local pressure minimum, as Figure 7.10 clearly shows, and lies just beneath the first-row portion of the outer helium plume (Figure 7.11). Its center is more than half an effective diameter above the lower wall and just less than one and a half effective diameters from the centerline. The streamtrace that marks the vortex makes two broad loops around the center, indicating the wide extent of its influence on the surrounding flow.

The band of slightly higher pressure that marks the path of the second-row bow shock wraps around both the vortex and the mass-fraction contours and extends in weakened form to the lower wall. Above the outer plume the bow shock pressure system becomes a stronger blanket of pressure that reaches from the outside of the outer injectant plume centerward through the channel between the plumes, until it connects with the high-pressure system above the centerline helium plume. The centerline high-pressure system has been previously identified with the interaction and turning of the second-row centerline helium plume with the first, and the distinction between the centerline interaction/turning pressure system and the bow-shock pressure system can best be made by careful examination of the shape of the pressure contours in Figure 7.10. The outer portions of the contours curve gently and uniformly, with the highest pressure and lowest position at the top of the channel between the centerline and outer plumes, as predicted by

plane “c” of Figure 7.6 and Station 3 of Figure 7.10 for the bow shock. Very near the point of intersection between the pressure contours and the mass-fraction contours of the centerline injector, the pressure contours change curvature drastically, with elevated pressures, greater penetration, and very little resemblance to the outer portions of the same curves. Notice that the pressure contours also intersect the mass-fraction contours of the outer injector, but without significant changes in curvature. The only logical conclusion is that there is a different mechanism responsible for the elevated pressure along the centerline, and Figures 7.1 and 7.3 identify it as plume interaction and turning.

The streamtraces of Figure 7.10 seem to show another vortex centered half an effective diameter from the centerline, at the center of the inner portion of the low-pressure wake. This smaller vortex is the product of many of the same forces that the outer one, namely, inflow along the wall from higher-pressure fluid in the interplume channel, followed by interaction with the opposing stream that turns the entrained air mixture upward, elevates the pressure, and forces the centerward again. Figure 7.10 suggests that fluid can escape the influence of this vortex and become part of the vertical flow at the centerline, a process that would seem to transport fluid from a region of low pressure into one of significantly higher pressure. Clearly this is a three-dimensional effect which cannot be completely explained with planar data alone. Perhaps the explanation lies with plane “a” of Figure 7.6, which shows that, just upstream of the present plane, pressures in the wall region were lowest along the centerline, and that streamtraces originating between the centerline and outer plumes do bend toward the lower pressures as they move downstream. In this case the apparent flow into higher pressure would be no more than an example of the danger of using two-dimensional plots to represent three-dimensional phenomena.

Figures 7.10 and 7.11 show that the upper/centerward lobe of the outer helium plume, which was first identified at Station 2, is perhaps more distinct at Station 4 than ever before. The flow forces

and mechanisms that created the lobe are still present, and serve to preserve and augment it. Notice in Figure 7.11 that the main path of flow that swirls around the vortex passes exactly beneath the upper/centerward lobe, much as it did at Station 2. Since the lobe is outside the vortex proper it is influenced mostly by the overlying pressure field, which is moving upward and creating beneath it an opportunity for vertical expansion. Notice that the streamtraces within the upper/centerward lobe do have a higher horizontal component than they did at Station 3, due to the stronger pressure field in the interplume channel centerward. Notice also the separation of the upper portion of the c_{He}=0.65 into two distinct contours, the tiny, higher one of which seems to be a part of the upper/centerward lobe while the larger follows the main plume outward toward the vortex.

Station 5 is located in the center of the last row of injectors, and the pressure field associated with it forms one of the most complicated plots of the entire set. Three sets of three-dimensional bow shocks, one from each row of injectors, along with wakes and plume expansion, contraction, and interaction create a thorough mess for the analyst. Nonetheless, an attempt will be made to decipher the meaning not only of the pressure field but also of the helium and velocity data as well.

The natural place to begin the analysis is on the centerline, where the most data is available, but the complexity of the near-wall flowfield near the centerline requires a certain amount of joint analysis. Figure 7.9 shows that the high pressure bubbles associated with both the centerline and outer injectors at Station 5 are connected to the larger band of “shock”-induced high pressure that dominates the interplume channel near the wall. Once again the word “shock” must be interpreted rather loosely, as Mach numbers are less than unity upstream of this entire injector region and proper shocks cannot form. Nonetheless a pattern of strongly elevated pressures exists in the channel between the two plumes, in a region of relatively low helium concentration. Notice that the outer

injectant plume follows a pattern similar to the one identified at the second row of injectors, lifted off the wall beyond the outer edge of this cross-section of the injector and apparently pointing outward, though the injector itself is angled centerward.

The pressure field associated with the centerline injector is substantially weaker than that of the outer injector and interplume channel, because, unlike the outer injector, the centerline helium plume is protected from the upstream flow by the sheltering effect of the other centerline injectors. As a result the centerline "bow shock" is much weaker in the third row (if it can be called a bow shock at all, given the subsonic flow upstream), the associated pressures lower, and the natural expansion of the injectant helium less restrained. Furthermore, the larger injection angle (forth-five degrees from the horizontal) of this row of injectors results in quicker penetration and a more eventful plane of data than the previous injectors produced. Less than half an effective diameter above the wall on the centerline is a tiny spot of relatively low pressure, which Figures 7.1 and 7.3 connect with the first expansion of the injectant helium. Just above the expansion should be a recompression, though there is no contour of higher pressure to identify it. Data presented in Figure 7.1 suggests that the expansion occurs just downstream of this plane, so that the large region of rather uniform pressure above the expansion encompasses both the upstream tip of the recompression and even fainter traces of the next, even more distant, expansion. Above the region of moderate pressure and near the tops of the helium mass-fraction contours is a large high-pressure system, as shown in Figure 7.9. Figures 7.1 and 7.3 associates this pressure rise with the interaction of the first and second-row helium plumes, which occurs well upstream but propagates downward through the pressure field. The interaction of the second and third-row helium plumes, while evident in the low-level helium contours of Figures 7.10 and 7.11 at this station, has yet to produce a significant impact on the pressure field. It may, however, contribute to the generally elevated pressures along the

centerline between one and two effective diameters above the lower wall.

The helium mass-fraction contours that outline the third-row, centerline plume are quite narrow throughout this figure, no doubt because the high pressures outside the injector near the lower wall discourage low-level expansion. Instead, Figures 7.10 and 7.11 show a strong vertical component of the streamtrace along the centerline. This centerplume streamtrace does not acquire a significant horizontal component until it reaches the mushroom-shaped part of the helium plume, which is still associated with helium from the previous rows of injectors and is connected to the third-row contour only by a narrow neck along the centerline. No doubt some of the plume's horizontal momentum has been carried downstream from other planes, but the primary driver is probably the large band of low pressure just outside the upper part of the centerline helium plume, which creates a strong pressure gradient encouraging spanwise expansion. The low-pressure band wraps around the entire injector region, breaking only at the centerline, and appears to be the remnant of the wake that formed downstream of the second row of injectors. (Notice that the wake remnant is considerably larger than plane "d" of Figure 7.6 suggests.)

The outermost (lowest-level) helium mass-fraction contour penetrates into this wake region and surrounds both the centerline and outer helium plumes. The second-level (c_{He}=0.25) helium contour curves almost without distinction around the two parts of the centerline helium plume (corresponding to helium from the current and previous rows of injectors) but connects to that of the outer injector only in one small region near the lower wall. It reaches approximately half an effective diameter from the centerline at its widest point and connects to the outer-plume contour less than two tenths of an effective diameter above the lower wall. Above the point there is a narrow but distinct channel of nearly pure air that separates the two injector plumes and serves to increase the surface area of both. The merging of the two plumes is essentially a new

feature of this row of injectors; at previous stations only the outermost (c_{He}=0.05) contours of the plumes have joined. One would expect the merging of the plumes to change significantly the entrainment behavior previously identified, a point that will be further addressed below.

The high-pressure system that appears on the centerline near the tops of the helium mass-fraction contours is quite broad, and it dominates the upper regions of the figure. While near the centerline high pressures extend to the lower wall and have been associated with the behavior of the centerline plumes, in the upper portion of the figure the high-pressure contours are a more general formation connected to the second-row bow shock. The first-row bow shock has weakened by this station and merged with the second-row shock, so that its effect is seen only at the sides in the outermost pressure contours, where it separates before dissipating near the wall.

Probably the most complex part of the flowfield at this station lies near the wall outward from the outer injector. It is a region of low but varied pressure, and the patterns at first seem to defy logic. Nonetheless, reason and understanding can be found in them through careful observation and comparison with other figures.

Just outside the outer injector is a column of rather low pressure. Though it appears beside the injector in this plane, Figure 7.6 plane “a” shows that the low pressure column lies downstream of the outermost, upstream end of the injector, and that it forms the beginning of a large downstream wake. The edges of several high-concentration helium mass-fraction contours run through or adjacent to the column at this point, lending credence to the theory that it is also a region of expansion for the outer injector. Streamtraces in Figure 7.10 show that the flow does have a strong horizontal component in the outer part of the low-pressure region, which further supports the expansion theory. Above and outside that region of low pressure is a nearly horizontal tongue of elevated pressure. While the pressure in this outer contour is considerably

weaker than that in the interplume channel between the centerline and outer injectors, the contour itself seems to have the proper shape, pressure, and position to represent the outward extension of the third-row bow shock (or the subsonic equivalent thereof), as Figure 7.6 plane “a” suggests. One interesting feature is the forked shape the shock acquires near its outer edge. The upper fork is simply the outward extension of the third-row bow “shock”, which happens to be roughly coincident with helium from the merged first and second-row plumes. Figure 7.10 shows that beneath this upper fork is a region of lower pressure which does not quite align with an area of lower helium concentration. Indeed, the data presented on the left side of that figure indicates that the lowest helium mass fractions align with the second, wallward fork of elevated pressure. The contours and streamtraces shown in Figure 7.11 identify this low-helium region as part of the second-row helium plume, which has been dissipated and driven away from the wall by the effects of entrained air and of interaction with the third-row helium plume. Entrainment of air from the outside of the plume and turning of the rising fluid continues at the present location, making this spot the location of the interaction and turning of two fluid streams, which penetrate the well-expanded helium plume and create the higher pressure through the familiar mechanism responsible for higher-pressure region within the helium plumes at Stations 2 and 4. Note that entrainment at this station, in the plane of the last row of injectors, continues strongly and the nearby vortex is well formed. This contrasts the behavior in the plane of the second row of injectors (Station 3), where the vortex was washed out and entrainment much less noticeable.

Worthy of particular notice is the outer extension of the outermost helium mass-fraction contours along the wall beneath the third-row bow shock. For the first time the notch of entrained air is lifted off the wall, and below it is a narrow, triangular region where helium-rich fluid flows outward from the main plume, as the outermost streamtrace in Figure 7.11 shows. While the origin of this

outward flow is something of a mystery, information presented in Figure 7.6 plane “a” suggests that the helium in the outer reaches of the outer flow has been drawn downstream from the second-row injectors, not outward from the third.

Another vestige of the previous rows of injectors is the low-pressure region located just outward from the third-row bow shock extension, roughly two effective diameters from the centerline in Figure 7.9. According to Figure 7.6 plane “a”, this simply represents the extreme downstream end of the wake region between the second and third rows of injectors, driven outward by the high pressures associated with the third-row bow “shock”.

The center of the vortex also coincides with the end of the upper c_{He}=0.65 contour, the innermost associated with the first and second-row outer plume at this location. As before, the elongated contour of swirling, high-concentration helium does not come into contact with the current injector's c_{He}=0.65 contour and consists solely of helium from previous rows of injectors, mixed with air. The outer tail of the contour is considerably lower than the centerward tail, owing to the lower pressures further from the centerline. The upper/centerward lobe identified at previous stations still exists, though it now encompasses the entire upper reaches of the outer plume. As at previous stations this lobe represents the portion of the helium plume that is not directly affected by the presence of the vortex and is not drawn into the swirling flow pattern.

Station 6 lies a little more than one effective diameter downstream of the last row of injectors, in a region dominated by a large wake, shown most clearly in Figure 7.9. The wake extends two effective diameters outward from the centerline and more than an effective diameter above the lower wall. Figure 7.10 shows that the vortex is still very well formed at this station, and that the outer edge of the low-pressure contours just encompass it. Outward from the vortex center is a fairly steep increase in pressure, caused by the presence of the third-row bow “shock”. Inward from the vortex core is the region of lowest pressure, nearly one and a half effective

diameters wide and roughly three-quarters of an effective diameter tall. The upper edges of all of these low-pressure contours are somewhat uneven, with higher pressures in the vicinity of the centerline and extending outward roughly two-thirds of an effective diameter from it. The higher pressures along the centerline are easily explained by Figure 7.1, which identifies them as the last, downstream remnants of the third-row centerline injector's recompression region. The jagged pressure contours away from the centerline at Station 6 are at least consistent with those in Figure 7.6 plane “b”, where they appear as streamwise extensions of high pressure. In the paragraphs below an attempt will be made to locate the cause of these pressure variations.

The most unique feature of the helium plume near the wall at Station 6 is that, for the first time, there is no division between the centerline and outer plume contours, including not only the outermost (lowest-level) contours but also those up to and including c_{He}=0.65. Instead there is a solid mass of helium-rich fluid that leaves the lower wall less than six-tenths of an effective diameter from the centerline. Notice that this distance is roughly four-tenths of an effective diameter smaller than the corresponding distance at Station 5, though the spanwise penetration of the outer contours is virtually unchanged. The reason for the joining of the two plumes is seen in Figure 7.7, planes “a” and “b”. The injectors of the last row are quite close together at their centers, and the outer injector is angled inward by thirty degrees, so that their downstream ends are even more closely spaced. Figure 7.6 plane “a” shows that the high pressure fields that form on each individual injector in the last row interact strongly enough to form a barrier upstream of the channel between the injectors and to prevent significant levels of upstream air from flowing between them. The helium contours in Figure 7.7 plane “b” reveal that the barrier exists even at that level, two thirds of an effective diameter above the lower wall. The lack of appreciable change in the spanwise placement of the outer contours (c_{He}=0.05 and 0.25) suggests that the merging of the third-row

plumes does not greatly affect the outer regions of the mixing area at this point, the helium in which is still largely that of the first and second-row plumes. However, the effect might be both noticeable and undesirable downstream. One of the undesirable consequences of the merging of these two plumes, already important at this streamwise location, is a great reduction in surface area of the high-helium plumes, as identified in Figures 7.6 through 7.11. While a narrowing of the interplume channel was identified at Station 5, at that location only the c_{He}=0.25 contours had merged, and they only a small fraction of an effective diameter above the lower wall. At Station 6 the c_{He}=0.25 contours are merged for one full effective diameter, and the c_{He}=0.65 contours themselves are connected for approximately eight tenths of an effective diameter. Clearly the reduction in mixing area is becoming more severe further downstream of the last row of injectors.

The upper edge of the wall-region c_{He}=0.65 contour is rather horizontal. There is a vertical spike of purer helium exactly along the centerline itself, where mixing of the helium from the last centerline injector is slower, but outward from the centerline mixing is quite a different story. Inflow of nearly-pure air from the outside of the plume, discussed above, brings large quantities of air into the heart of the plume itself and creates an upward flow of entrained air mixed with helium that has its strongest point just over half an effective diameter from the centerline. The mechanism that drives this upward flow is exactly the same as was present downstream of each previous row of injectors: The low-pressure wake downstream of the outer injector draws air inward along the lower wall from the sides. At some point, previously the center of the plume, the air collides with another stream of fluid and is forced to turn upward, through the helium plume. Where the pattern was seen at previous stations the outer helium plume was separate from the centerline plume and air flowed inward from both sides. Here the centerline and outer plumes are joined together and air can be entrained from the outside only. Instead of a counter-flowing stream of air the

inflowing fluid meets the helium plume itself, which by symmetry has no opportunity for spanwise expansion or displacement, and is forced to turn upward, raising the pressure slightly along its path. The streamtraces in Figure 7.11 illustrate the phenomenon.

Continuing now with a close look at the bottom of the combined helium plume, one can see in Figures 7.10 and 7.11 that the outer mass-fraction contours, corresponding to c_{He}=0.05 and 0.25, have much the same shape as at the previous station. Their notch of entrained air is larger and more rectangular, due to the low-pressure wake that draws in air from the outer regions. There is still a thin layer of helium along the lower wall below the notch, as outlined by an c_{He}=0.25 contour, but careful examination of the streamtraces in Figure 7.11 suggests that the flow within this layer is directed centerward, opposite its direction at Station 5. So it is that even within this near-wall layer of purer helium is an entrainment region. The lower layers of the entrainment region send air into the joined plumes of both third-row injectors, as discussed above. From there they are turned upward and expelled through the nearly horizontal top of the inner helium contours, at which point they travel almost directly upward until turned outward by high pressures close to the centerline.

Turning attention to the outer plume, the upper reaches of the outer entrainment region, close to and within the c_{He}=0.45 contour that surrounds the vortex, feed fluid (mostly air) directly into the stream that flows around the vortex. As at Station 4, this inflowing stream largely coincides with the path of highest helium concentration. The swirling contours of purer helium flow that actually surround the vortex have changed somewhat from the previous station. The upper/centerward lobe is more strongly formed than before, caught as usual above the influence of the vortex. The inner helium contours themselves are elongated and thin and more horizontal, as mentioned above. Notice the tiny c_{He}=0.65 contour separate from the larger one, more than two effective diameters from the centerline. According to Figure 7.7

plane “c”, this represents the purest part of the second-row outer plume, which, unlike the lower-level contours, has not blended with the third-row plume.

Returning to the centerline, one notices a large region of moderately low pressure beginning approximately one effective diameter above the lower wall, marking the upper end of the purest part of the wake discussed above. Streamtraces in Figure 7.10 suggest one driver of the elevated pressure to be the interaction and turning of entrained air with the outer helium plume, which occurs only a fraction of an effective diameter from the centerline at a position identified by Figure 7.9 as a local pressure maximum. Another driver of the elevated pressure is identified by Figure 7.1, which shows the region of moderate pressure to be coincident with the most downstream reaches of a recompression of the third-row centerline plume. The top of the moderate-pressure region coincides with the center of a second set of helium contours, which connect to the center wall-region plume by a thin, low-concentration helium column on the centerline. Figure 7.1 shows that this upper plume is composed of helium from all three injectors, and the high pressure system above it is shown by the same figure to be the downstream propagation of the high pressures created by the interacting and turning of the first and second-row centerline plumes. As at previous stations this high-pressure region is connected to the bow shocks, though the shock structure is quite unusual at this location. High pressures along the centerline within the helium plume are the result of flow turning, discussed above. Outward from the centerline the third-row bow shock produces high pressures that curve downward around the wake to the lower wall. Notice in Figure 7.9 that significantly higher pressures (relative to the surrounding fluid) reach the lower wall itself at this point, perhaps a consequence of the stronger pressure field associated with the third row of injectors. Above and outward of the third-row bow shock are the remnants of the second-row wake, beyond which the second-row bow shock still exists. The first-row bow shock is not identifiable at this location.

The centerline c_{He}=0.25 contour has changed little from the previous station, except that at Station 6 it is more thoroughly merged with the outer plume's corresponding contour, as discussed above. The vertical penetration of the helium plume has increased at this station to nearly three effective diameters, and the high pressure region above it extends beyond the upper edge of the figure. Throughout most of the plume the lower pressures near the centerline retard expansion. Only near the top of the plume is an increase in horizontal spreading observed as the streamtraces in Figure 7.10 curve outward away from the high pressures on the centerline. Likewise, the outer plume has expanded only a fraction of an effective diameter vertically or horizontally since the previous location.

The plots labeled “Station 7” complete this set of figures by presenting data from the plane x/d_{eff}=8.00, two effective diameters downstream of the previous plane and three and a third effective diameters downstream of the center of the last row of injectors. Downstream of the injection region flow properties change much more slowly, and data in this plane is expected to closely resemble data from Station 6. Indeed, many features of the two sets of figures are strongly similar.

The helium mass fraction contours have changed little, as Figure 7.11 shows, with perhaps the most noticeable change being the (rather predictable) decreased helium concentration at Station 7. At this station no contour higher than c_{He}=0.65 appears, whereas at the previous station values as high as c_{He}=0.95 were identifiable. Additionally, the size of the helium plume has increased. At this station the center plume reaches a height of approximately three and a half effective diameters, an increase of half an effective diameter from the previous station, and the outer plumes achieves a half-width of three effective diameters, again an increase of half an effective diameter. The remnants of the third-row plumes remain merged on the centerline, have begun to lift above the lower wall, and have contracted considerably, as the established entrainment

process continues to draw air toward the center of the plume and the large, strong vortex pulls helium outward and away. (See the streamtraces in Figure 7.11.) Under the influence of this vortex the upper edge of the third-row helium contours are remarkably horizontal, suggesting that the vortex, while aiding mixing, may be retarding penetration. Even the upper/outer lobe, the portion of the outer helium plume that has at other stations remained relatively uninfluenced by the presence of the vortex, appears to be following a downward path, though not necessarily a spiral one. The underside of the outer helium plume still turns inward and under at its end, a development identified in upstream figures and probably influenced by the vortex.

The upper portion of the center plume itself is taller than at Station 6. Helium concentrations are lower, and the innermost contour is completely separate from the lower helium plume. This is in contrast to Station 6, at which the same contour was connected to the wall-region flow by a thin plume along the centerline. The shape of this contour has not changed, however, from that of an inverted horseshoe. The outermost contours have changed shape, being much more directly connected to those of the outer branch of the helium plume.

Though at first glance the pressure field in Figure 7.9 may seem simple, it is still quite significant. Beneath the broad arch of pressure that marks the remnant shocks (now completely blended) is a large region of low pressure, which occupies an area roughly three effective diameters in height and half-width. Pressures are lowest in this wake away from the centerline, near the center of the vortex, and higher on the centerline near the wall, where entrained air encounters the helium plume and turns upward, as the streamtraces in Figure 7.10 reveal. The low pressure contour just above the wall near $z/d_{eff}=1$ is disrupted by a pair of tiny spots of elevated pressure barely visible in Figure 7.9 but present in Figure 7.6 plane “a” as a long, thin spike of higher pressure beginning just upstream of the present location. Figure 7.10 identifies a small but intense vortex

located just above the lower wall at the same location which is almost certainly responsible for the local pressure increases. (In Figure 7.10 the streamtraces that mark the vortex are so tightly wound as to appear as a large, white dot at the wall.) Though the exact mechanism responsible for the elevated pressure is not certain, one possibility is that the small, lower vortex impedes the progress of fluid being entrained into the helium plume, raising the pressure as momentum is lost. A third, less clearly formed vortex exists more than two effective diameters above the lower wall and less than one effective diameter from the centerline. The driving forces of this vortex appear to be the low pressure and vertical momentum of the centerline flow coupled with the high pressures above and outside the centerline plume. The result is streamtraces which bend first centerward and down toward the wake, then upward, outward, and down again. The effect of this vortex on both the pressure field and the helium distribution appears to be negligible at this location, though the downward movement of the outer (i.e., not centerward) portion of the vortex may be in part responsible for the downward turn of the ends of the upper, centerline plume.

One additional figure has been chosen to provide insight into the flow field at Station 7. Figure 7.14 shows stagnation (or total) pressure normalized by the freestream value, with the familiar contours of helium mass fraction overlaid on the left. Clearly there is a significant loss of stagnation pressure as a result of injection. The innermost contours of stagnation pressure, corresponding to the greatest losses, are almost indistinguishable in shape and position from the helium mass-fraction contours. The one exception is the small contour of higher stagnation pressure that exists on the centerline near the top of the innermost helium mass-fraction contour. This probably is evidence of helium from the third row of injectors, which has not yet experienced the mixing, turning, and other mechanisms responsible for creating the stagnation pressure losses. Notice that moderate losses of stagnation pressure extend beyond the helium plume itself, particularly in the vertical direction.

To put Figure 7.14 in context and to show the streamwise development of the stagnation pressure field, Figure 7.15 is a similar plot of stagnation pressure and helium mass fraction, taken this time from the measurement plane. The scale of the figure is the same as in Figure 7.14, though the range of the vertical axis has been increased to more completely capture the expanded flowfield. Qualitatively this figure resembles the previous one, with stagnation pressure ratios approaching unity outside the helium plume and plunging as low as 0.25 or lower within it. Clearly these are significant losses, of the same order as those within the boundary layer. Unfortunately, some degree of stagnation pressure loss is inevitable in any injection scheme, and specific meaning can only be assigned to these losses through direct, exact comparison with similar injection schemes.

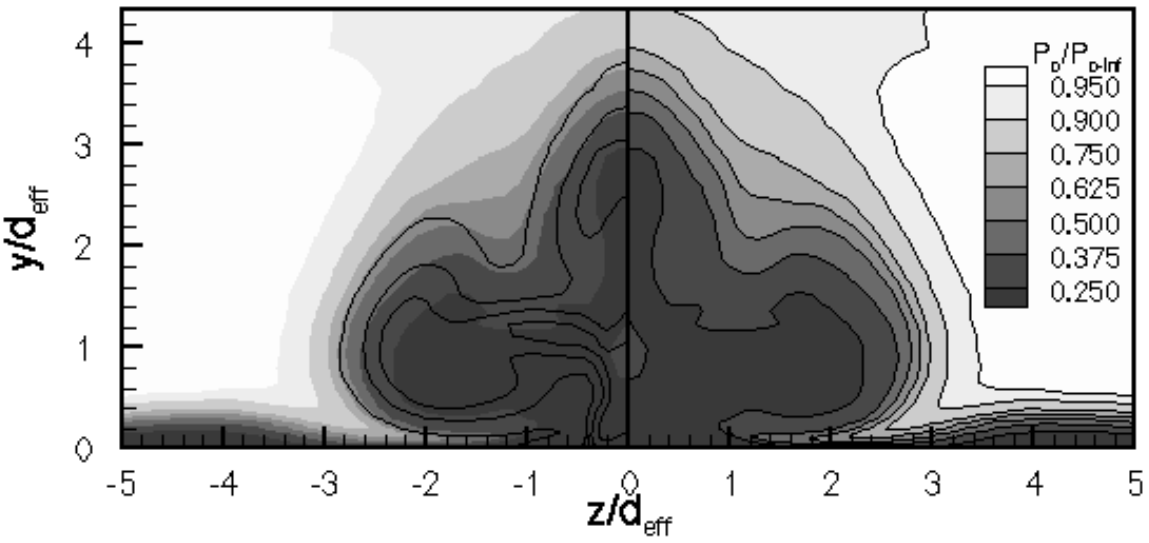

Figure 7.14. Total Pressure Normalized by the Freestream Value at Station 7, x/d_{eff}=8.00, for the Nine-Hole Injector Array. Black lines on the left are helium mass-fraction contours.

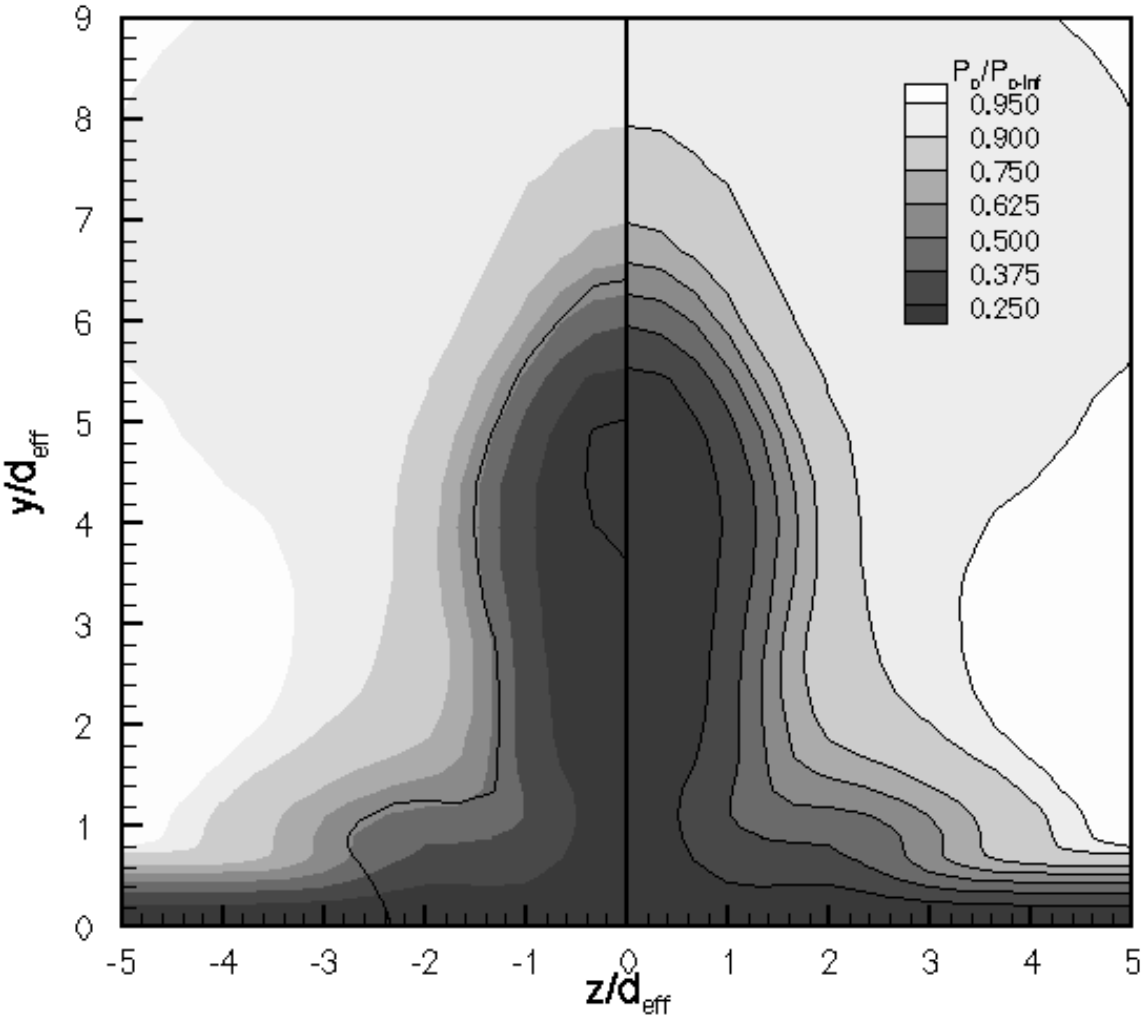

Figure 7.15. Total Pressure Normalized by the Freestream Value at Measurement Station, x/d_{eff}=43.0, for the Nine-Hole Injector Array. Black lines on the left are helium mass-fraction contours.

Wall Conditions

With these figures we reach an end to the flow analysis portion of this chapter. The pattern of behavior of the nine-hole injector array has been established and the most important mechanisms in its function have been identified. Though the locations and strengths of the various vortices may vary slightly downstream, and the degree and location of entrainment and its effect on the pressure and

helium fields may change, the essential points have been made for the understanding of flow behavior. The one remaining task is that of interpreting the effect of these flow structures upon the structure of the injector itself, that is, upon the wind tunnel wall into which the array is set. To this end the following figures present data representing conditions on the lower wall. Figure 7.16 contains pressure and helium mass-fraction data, both plotted with the same contour levels as seen elsewhere in this chapter. Shaded pressure contours occupy both the upper (mirrored) and lower (calculated) portions of the figure. Black lines in the upper half outline pressure contours, while those in the lower half represent helium mass-fraction contours.

In this figure the injector ports are clearly visible, identified both by the white high-pressure contours and by the densely-packed lines of helium mass fraction. The static pressure of the injectant

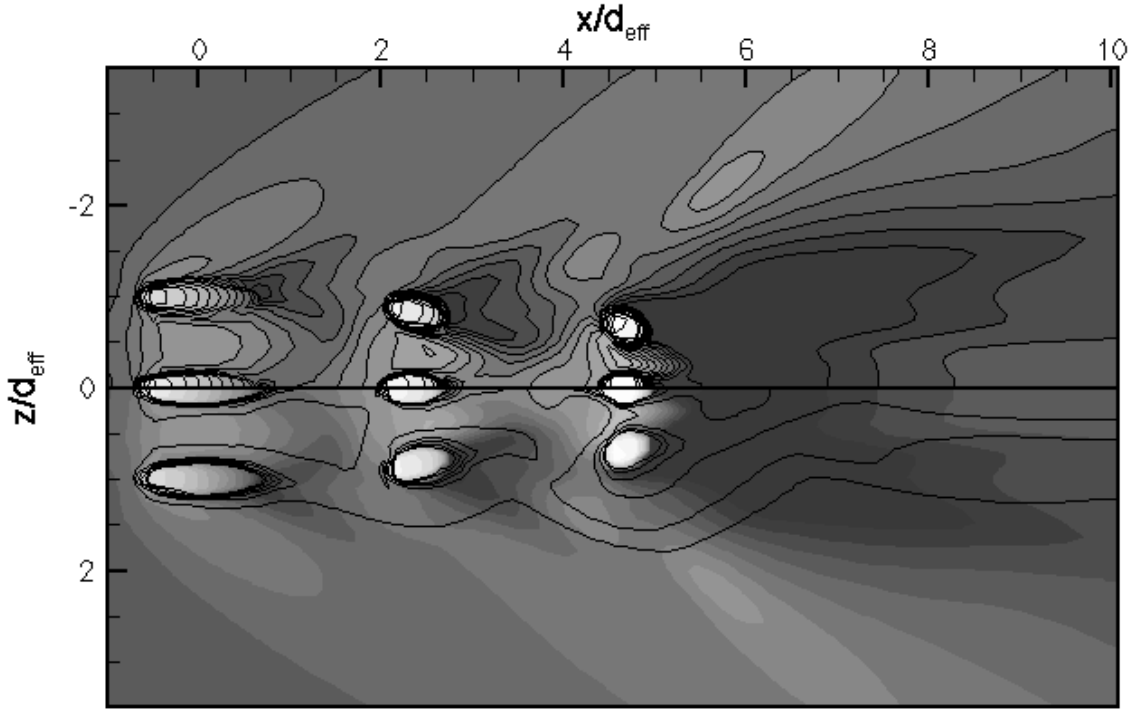

Figure 7.16. Pressure (shaded contours) and Helium Mass Fraction (black lines on lower half) on the Lower Wall in the Injector Region of the Nine-Hole Injector Array.

helium far exceeds even the stagnation pressure of the freestream fluid, a situation necessary for the satisfaction of the test conditions. Aside from the pressure within the injectors themselves, the highest wall pressures occur between the centerline and outer injectors of the respective rows of injectors, reflecting the interaction of bow shocks identified earlier in the chapter. Pressures are especially high between the injectors of the third row, where interaction is strongest. Also unique about the third row is that significant concentrations of helium can be seen to leave the injector ports and travel along the walls, both upstream and downstream of the injectors. This feature, too, is a consequence of the interaction of the respective pressure fields of the centerline and outer third-row injectors, which lead to reversed flow upstream and a large, low-pressure wake downstream. (Notice the lower wall pressures in the wake indicate a loss not only of static pressure but of total pressure as well.) This wake is several times larger than those downstream of the other outer injectors but does display the same forked shape. This increase in pressure near the center of the downstream ends of the wakes is evidence of the important flow entrainment mechanism discussed earlier. It first forms downstream of the first-row, outer injector and appears downstream of each subsequent row, even disrupting the weak pressure "footprint" of the curving bow shocks.

Figure 7.17 returns to the lower wall with heat transfer data. The calculations of this flowfield were made using the assumption of constant-temperature walls, an approximate but appropriate option. Under the assumption of isotropic walls, the heat transfer necessary to maintain the specified wall temperature can be easily plotted to indicate potential thermodynamic dangers to the combustor hardware. The data presented below represents heat transfer to the fluid, not the wall, so that positive heat transfer indicates transfer of energy into the fluid, i.e., loss of thermodynamic energy by the wall, and negative heat transfer indicates energy gained by the wall and lost by the fluid.

The largest transfer of energy, by at least an order of magnitude, occurs within the injector ports themselves, where cold, high-velocity helium absorbs energy from its surroundings, including the wall. A similar amount of energy is absorbed just downstream of the last row of injectors, in a region previously identified as one of high velocity and one with a high concentration of fresh (and therefore cold) helium. Weaker contours of positive heat transfer, that is, energy lost from the walls to the flow, occur downstream of the second row of injectors and outward from the third, also locations identified in Figure 7.8 with higher velocities. Even milder streaks of elevated heat transfer and similar ones of negative heat transfer parallel the centerline downstream of the injectors, and may be related to the small, wall-bound vortex identified at Station 7 above. The background for all these contours is weakly positive, indicating that small amounts of energy must be transferred from the wall to the fluid to maintain the specified fluid temperature at the wall. Small, low-magnitude contours of negative heat transfer do exist in regions where the flow velocity is low. The most significant of these contours occur between the centerline and outer injectors of the first and second rows. The third row does not have such a contour, perhaps because the injectant plumes interact and accelerate immediately. Additional, smaller contours of negative heat transfer (i.e., heat loss to the wall) occur at flow turning points in the entrainment regions downstream of each row of injectors and along the centerline where velocities become small. Small though they are, these contours of heat loss are perhaps the most significant of the plot, as they identify locations of potential thermal stress in a higher-enthalpy flow. Particularly significant is the fact that many of them lie in regions of strong mixing, where in a reacting flow combustion might elevate wall temperatures further.

Figures 7.18 and 7.19 are the last in this series and show skin friction drag on the lower wall. Skin friction is a measure of wall shear stress, and has real meaning only on surfaces. That is to say, the plotted skin friction values are meaningless within the injectors

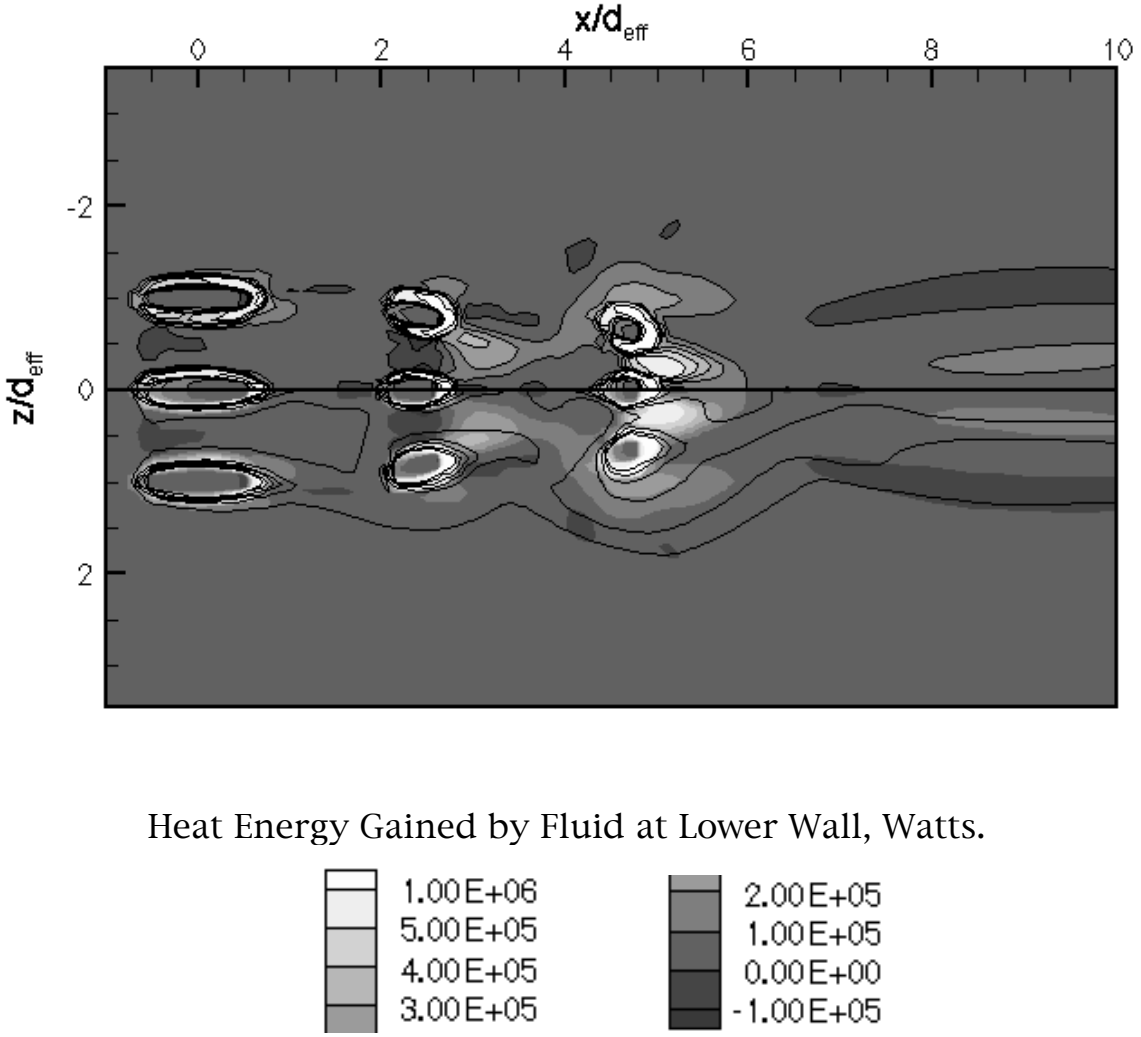

Figure 7.17. Heat Transfer Contours for the Nine-Hole Injector Array.

themselves. Figure 7.18 provides a general examination of skin friction, and the discussion will begin with that figure. The highest skin friction values surround the spanwise and downstream edges of the injectors in very narrow bands, products of the shear forces at work between the inflowing helium plumes and the surrounding fluid. Additional high levels of skin friction appear between the centerline and outer injectors of each row but downstream of the injectors themselves. This phenomenon is an indication of the higher velocities, and therefore higher velocity gradients, present in the channel between columns of injectors. It grows stronger at the

downstream ends of the injectors where velocities are highest. (See Figure 7.8.) Skin friction downstream of the first, most widely spaced row of injectors is hardly elevated above the freestream, but levels increase downstream as the injectors become closer and interact more strongly. Skin friction downstream of the third row of injectors is on the same order as that at the edges of the injectors themselves, further evidence that the close spacing between the injectors of the third row substantially alters the local flow. Skin friction is also elevated in the spanwise shock extensions, though the value is much closer to the freestream than to the levels downstream of all but the first row of injectors. Low values of skin friction appear at the upstream ends of the spaces between the injectors of each row, reflecting lower velocities (specifically, smaller velocity gradients) caused by adverse pressure gradients. Separation appears in this figure as contours of zero skin friction ahead of each row of injectors, with the contours ahead of the second and third rows occupying most of the wake regions. Reversed flow exists where the skin friction coefficient becomes negative, and is shown more clearly in Figure 7.19. Notice that the extent of the separated and reversed flow at the wall itself is much larger than previous figures have revealed. The large wake downstream of the third row of injectors is not marked by such extremes of skin friction as are present in the injector region itself, perhaps because the flow accelerates more quickly and uniformly here. This downstream region is marked by occasional spots of higher or lower skin friction, the products of flow entrainment and turning mechanisms identified in this chapter. (Again see Figure 7.18.) Flow turning and the resultant deceleration lead to decreases in skin friction along the centerline just downstream of the third row of injectors and again roughly one effective diameter out from the centerline, both regions previously identified with low velocities and strong flow turning. Conversely, the tiny, surface-bound vortex visible at Station 7 of Figures 7.10 and 7.11 increases both the local velocity and the magnitude of the

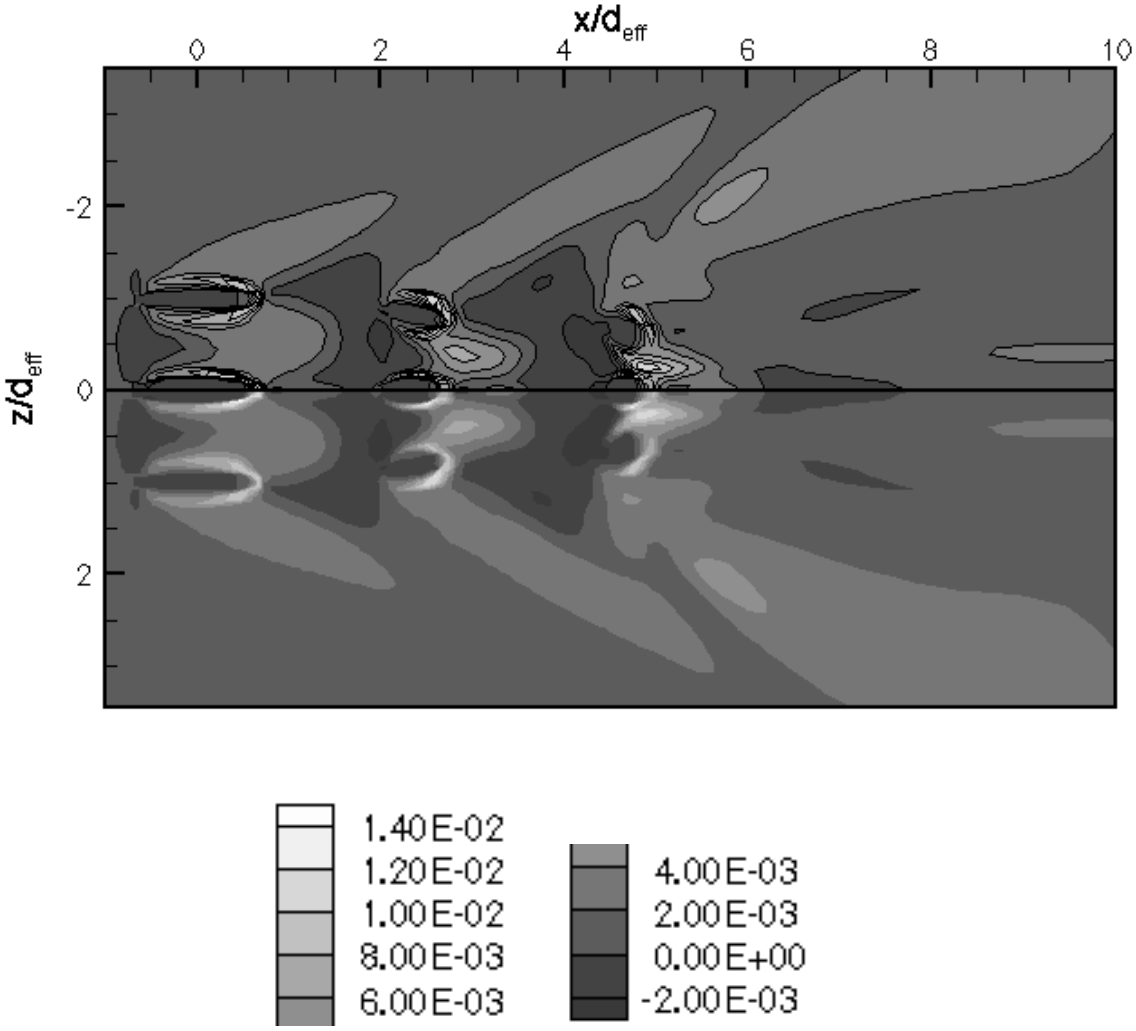

Figure 7.18. Skin Friction Contours for the Nine-Hole Injector Array.

velocity gradients, and likely causes the narrow bands of higher skin friction outward from the centerline near the downstream edge of the figure. Thus the wakes, plume interactions, entrainment, and vortices identified as primarily responsible for the pattern of mixing in the fluid are also responsible for the pattern of energy and forces on the injector wall.

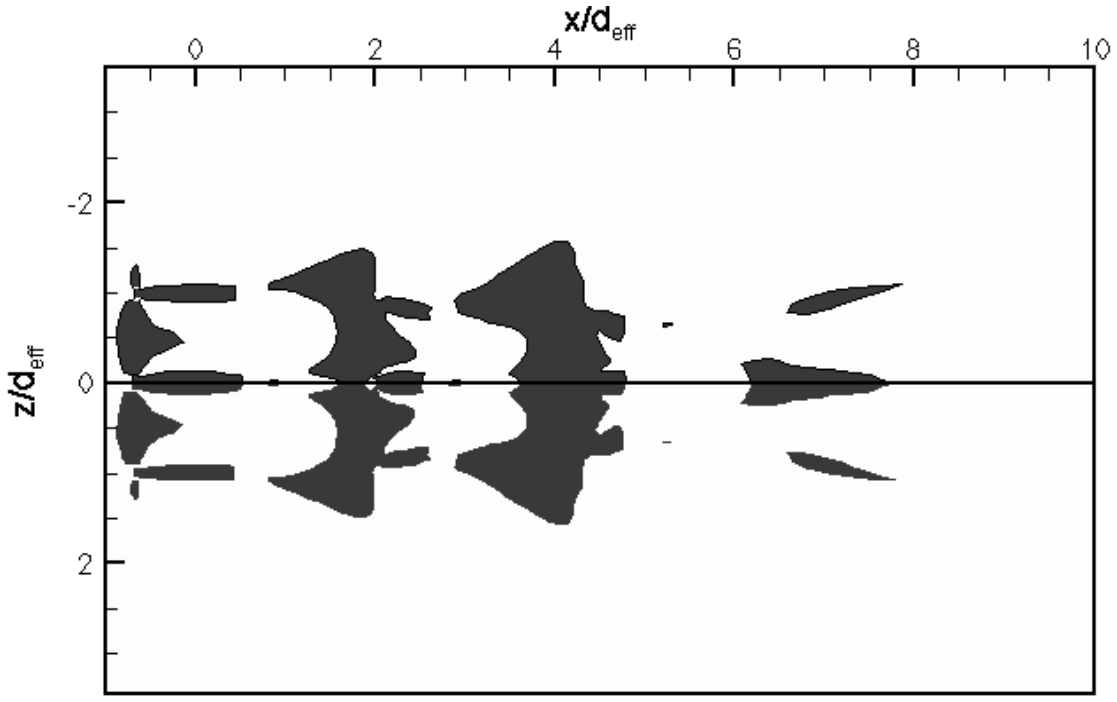

Figure 7.19. Skin Friction Coefficient on Lower Wall for the Nine-Hole Injector Array. Black corresponds to negative values, white to positive.